EFFECT OF THERMO-MECHANICAL TREATMENT ON STEREOLOGICAL ASPECT OF W-Ni-Fe ALLOYS

By

Sanjib Kumar Rout

DEPARTMENT OF MATERIALS AND METALLURGICAL ENGINEERING

Indian Institute of Technology Kanpur

FEBRUARY, 2002

EFFECT OF THERMO-MECHANICAL TREATMENT ON STEREOLOGICAL ASPECTS OF W-Ni-Fe ALLOYS

A Thesis Submitted

In Partial Fulfillment of the Requirements

For the Degree of

Master of Technology

by

Sanjib Kumar Rout

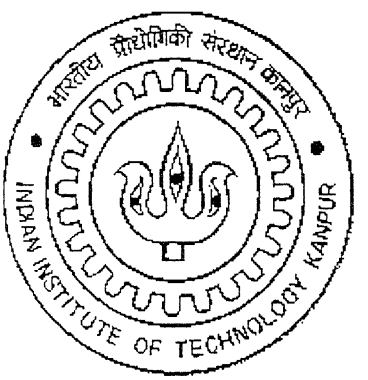

DEPARTMENT OF MATERIALS AND METALLURGICAL ENGINEERING

INDIAN INSTITUTE OF TECHNOLOGY, KANPUR

FEBRUARY 2002

CERTIFICATE

It is certified that the work contained in the thesis entitled "**Effect of Thermo-Mechanical Treatment on Stereological Aspects of W-Ni-Fe Alloys**" by **Sanjib Kumar Rout (Roll No. Y010632)**, has been carried out under our supervision and to the best of our knowledge this work has not been submitted elsewhere for a degree.

Dr. A. Upadhyaya
Assistant Professor
Department of Materials and
Metallurgical Engineering.
Indian Institute of Technology,
Kanpur.

Dr. A. Tewari
Assistant Professor
Department of Materials and
Metallurgical Engineering.
Indian Institute of Technology,
Kanpur.

ABSTRACT

The current work investigates the processing of 90W-7Ni-3Fe alloys through cold swaging and heat treatment. The research closely looks at the microstructural evolution in these alloys swaged and heat treated in different condition. Tungsten based alloys, because of their high temperature strength and hardness, are used in various kinds of applications, such as radiation shielding, high momentum penetrators and inertial systems. As far as the penetrator application is concerned the materials are subjected to high temperature deformations. One of the ways to further improve the mechanical properties (toughness and strength) is thermo-mechanical treatment. In this work, three ordnance grade W-Ni-Fe alloys containing 90, 93, and 97 wt% tungsten were (cold)- swaged stage wise to up to 96% reduction in area. This is the first time ever that these alloys have been swaged to such a large degree of reduction without any intermediate anneal treatment. The reported literature and industry has hardly exceeded 45% swaging. In a long-rod penetrator, the objective is to impart micro structural anisotropy selectively in the principal stress direction so as to promote localized shear band formation and consequent self-sharpening penetrator. In another set of experiment the swaged alloys were subjected to heat treatment at 500, 900, and 1400°C for 1h in reducing atmosphere. Extensive quantitative microstructural analysis was done on the swaged and heat-treated samples for volume fraction, grain size and contiguity. A unique feature of these measurements is the measurement of the effect of orientation on Sv (surface area/volume) of the tungsten-matrix and tungsten-tungsten interface.

Table of Contents

		Page no.
List of Figures		v
List of Tables		ix
Acknowledgements		x
Chapter 1.	INTRODUCTION	1
Chapter 2	BACKGROUND	4
2.1	Tungsten Heavy Alloys	4
2.2	P/M Processing of W-Ni-Fe Alloy	15
2.2.1	Solid State sintering	17
2.2.2	Liquid Phase Sintering	21
2.3	Post Sintering Heat Treatment	33
2.4	Mechanical Working of Tungsten Heavy Alloys	37
2.5	Thermo-Mechanical Processing	41
2.6	Mechanical Properties of W-Ni-Fe Alloys	51
2.6.1	Static Mechanical Behaviour	51
2.6.2	Dynamic Mechanical Behaviour	56
2.7	Microstructural Characterisation	63
2.7.1	2D Measurements	64
2.7.2	3D Measurements	69
2.8	An Overall Summary	72

Chapter 3. SCOPE OF PRESENT WORK 73

Chapter 4. EXPERIMENTAL PROCEDURE 76

4.1. Materials 76

4.2. Density Measurements 76

4.3. Swaging Operation 77

4.4. Heat Treatment Procedures 76

4.5. Metallography 78

4.6 Mechanical properties 81

4.5.1. Macro hardness Measurements 81

4.6.1 Micro hardness Measurements 81

4.7 Quantitative Metallography 82

4.7.1 Microstructure Evolution 82

4.7.2 Contiguity 82

4.7.3 Surface Area per unit Volume (*Sv*) 83

4.7.4 Grain Size Measurements 83

Chapter 5. EXPERIMENTAL RESULTS 84

5.1. Density Measurements 84

5.2. Microstructure Evolution 84

5.3. Surface Area per unit Volume of W-Matrix Interface 95

5.4. Volume Fraction and Grain size 95

5.5. Contiguity 101

5.6. Macro-Hardness 104

5.7. Micro-Hardness 104

Chapter 6. DISCUSSION 111

6.1. Quantitative Analysis of Microstructures 112

6.2. Analysis of Surface Area per unit volume (*Sv*) of W-matrix Interface. 112
6.3. Macro-Hardness Measurements 113
6.4. Micro-Hardness Measurements 113
6.5. Contiguity and Grain Size Measurements 114
Chapter 7. CONCLUSIONS 116
REFERENCES 117

List of Figures

Figure

2.1. Optical Micrograph of typical 95% tungsten heavy metal alloy [1].

2.2. Flow Chart for typical Fabrication of Tungsten Heavy Alloy Penetrator [1].

2.3. Fe-Ni Equilibrium diagram [2].

2.4. Ternary phase diagram of W-Ni-Fe alloys [3].

2.5. Effect of Ni to Fe Ratio on Impact Energy of W-Ni-Fe alloy (93%W) [7].

2.6. The Effect of Contiguity on UTS and Elongation of W-Ni-Fe alloy [7].

2.7. Optimum Values of Room temperature strength and fracture elongation and their correlation with contiguity factor of tungsten heavy alloy [6].

2.8. Tungsten heavy alloy parts (machined) used in aviation and radiation shieldings [6].

2.9. Three sphere sintering model. (a) Original point contacts. (b) Neck growth. (c) and (d) pore rounding [11].

2.10. The process associated with classic liquid phase sintering, giving the main microstructural changes [13].

2.11. The classic stages of liquid phase sintering involving mixed powders which forms liquid on heating [13].

2.12. Microstructure of W-Ni-Fe alloys in (a) solid-sate sintered (1400°C, 1h) and (b) Liquid phase sintering conditions (1500°C, 1h) [14].

2.13. The grain size, grain shape and volume fraction changes in W-3.5Ni-1.5Fe at sintering temperature of (a) 1475°C, (b) 1490°C and 1580°C [15].

2.14. The variation of sintered density, hardness, tensile strength and elongation with respect to sintering temperatures [15].

2.15. The influence of atmosphere change (from hydrogen to argon) upon strength, elongation [18].
2.16. Typical sintering cycle for tungsten heavy alloy [14].
2.17. Optical micrograph of swaged sample 30% swaged sample [6].
2.18. Optical micrograph of swaged sample 80% swaged sample [6].
2.19. The influence of cold, warm and hot deformation on grain and sub grain structure and on deformation and fracture mechanisms [24].
2.20. Variation of hardness, UTS, yield strength and % of elongation of cold swaged heavy alloys with respect to annealing period at 700°C [22].
2.21. Mechanical property variation with respect to cold deformation [22].
2.22. Schematic description of microstructural development during solid state sintering and liquid phase sintering [26].
2.23. Schematic representation of the penetration of a melt layer along a deformed boundary between original tungsten grains [26].
2.24. Effect of aging temperature and deformation levelon elongation and UTS of 92.5%W heavy alloy [25].
2.25. Effect of temperature and strain rate on Yield stress of W-Ni-Fe alloy [31].
2.26. True strain fracture in tensile stress vs deformation temperature [31].
2.27. Shear-stress and shear-strain curves of W-5Ni-3Fe at different strain rates [39].
2.28. Effect of cross speed and test temperature on Ductility and strength of 90W-7Ni-3Fe alloy [35].
2.29. Application of tungsten heavy alloy as kinetic energy penetrators and ammunitions [6].
2.30. Penetration behaviour of (a) depleted uranium and (b) WHA penetrator [14].
2.31. Schematic diagram showing penetration of ideal tungsten heavy alloy penetrator [31].
2.32. Shear band formation in 90W-7Ni-3Fe alloy [14].
4.1. Schematic diagram of rotary swaging.
4.2. Schematic diagram showing orientation of test lines for quantitative micro structural measurements.
5.1. As-received microstructure of 90W-7Ni-3Fe alloy.

5.2. As-received microstructure of 93W-4.9Ni-2.1Fe alloy.
5.3. As-received microstructure of 97W-2.1Ni-0.9Fe alloy.
5.4. Microstructure of 37% swaged 90W-7Ni-3Fe alloy.
5.5. Microstructure of 70% swaged 90W-7Ni-3Fe alloy.
5.6. Microstructure of 91% swaged 90W-7Ni-3Fe alloy.
5.7. Microstructure of 96% swaged 90W-7Ni-3Fe alloy.
5.8. Microstructure of as-received 90W-7Ni-3Fe heat treated at 500°C.
5.9. Microstructure of as-received 90W-7Ni-3Fe heat treated at 900°C.
5.10. Microstructure of as-received 90W-7Ni-3Fe heat treated at 1400°C.
5.11. Microstructure of 37% swaged 90W-7Ni-3Fe heat treated at 500°C.
5.12. Microstructure of 37% swaged 90W-7Ni-3Fe heat treated at 900°C.
5.13. Microstructure of 37% swaged 90W-7Ni-3Fe heat treated at 1400°C.
5.14. Microstructure of 70% swaged 90W-7Ni-3Fe heat treated at 500°C.
5.15. Microstructure of 70% swaged 90W-7Ni-3Fe heat treated at 900°C.
5.16. Microstructure of 70% swaged 90W-7Ni-3Fe heat treated at 1400°C.
5.17. Microstructure of 91% swaged 90W-7Ni-3Fe heat treated at 500°C.
5.18. Microstructure of 91% swaged 90W-7Ni-3Fe heat treated at 900°C.
5.19. Microstructure of 91% swaged 90W-7Ni-3Fe heat treated at 1400°C.
5.20. Microstructure of 96% swaged 90W-7Ni-3Fe heat treated at 500°C.
5.21. Microstructure of 96% swaged 90W-7Ni-3Fe heat treated at 900°C.
5.22. Microstructure of 96% swaged 90W-7Ni-3Fe heat treated at 1400°C.
5.23. Variation of *Sv* (Surface area per unit volume) with orientation of test lines for as-received 90W-7Ni-3Fe.
5.24. Variation of *Sv* (Surface area per unit volume) with orientation of test lines for 37% swaged 90W-7Ni-3Fe.
5.25. Variation of *Sv* (Surface area per unit volume) with respect to orientation of test lines for 70% 90W-7Ni-3Fe.
5.26. Effect of volume fraction of tungsten particle on the amount of tungsten content.
5.27. Effect of heat treatment temperatures on the grain size variation of as-received 90W-7Ni-3Fe Alloy
5.28. Effect of heat treatment temperatures on the grain size variation of 37% swaged 90W-7Ni-3Fe Alloy

5.29. Effect of heat treatment temperatures on the grain size variation of 70% swaged 90W-7Ni-3Fe Alloy

5.30. Contiguity variation with heat treatment temperatures.

5.31. Variation of Contiguity with orientation of test lines for as-received 90W-7Ni-3Fe Alloy.

5.32. Variation of Contiguity with orientation of test lines for 37% Swaged 90W-7Ni-3Fe Alloy.

5.33. Variation of Contiguity with orientation of test lines for 70% swaged 90W-7Ni-3Fe Alloy.

5.34. Effect of heat treatment temperatures on Macro hardness of 90W-7Ni-3Fe Alloy.

5.35. Effect of heat treatment temperatures on Micro hardness of W-particle for 90W-7Ni-3Fe Alloy.

5.36. Effect of heat treatment temperatures on Micro hardness of matrix for 90W-7Ni-3Fe Alloy.

List of Tables

Table

2.1. Comparison of fibrous alloy after first stage deformation and material swaged by 30%.

2.2. Mechanical properties of representative tungsten heavy Alloys.

2.3. Contiguity for 92.5% W Alloy.

4.1. Composition and processing techniques of W-Ni-Fe Alloy used.

5.1. Density measurements.

5.2. % Amount of deformation on swaging.

5.3. Sv data for W-matrix interfaces.

5.4. Sv data for W-W interfaces.

5.5. Grain size data for not heat-treated and heat treated 90W-7Ni-3Fe Alloy.

5.6. Contiguity values for 90W-7Ni-3Fe alloys.

5.7. Macro hardness values.

5.8. Micro hardness values.

Acknowledgments

I would like to express my deep gratitude to Dr. A. Upadhyaya and Dr. A. Tewari for their expert guidance, support and encouragement through out my graduate studies at Kanpur. Their leadership was immeasurable help to my early identification of an industrially significant area of research.

I gratefully acknowledge the help received from Mr. Sachan, Dr. Mungole, Mr. Soni and Rajan for providing me with guidance and letting me benefit from their experience during the experimental work.

My time at the P/M lab was enriched by the interaction with my fellow students. I am thankful to Shankar, Maya, Kausik, Chiradeep, Amit, Anirban and Pampa. Many of them are my close friends. I hope to keep for life.

I must acknowledge the support provided by my beloved parents, brother and sister. I would not have come this far without their unconditional love and support. This thesis is dedicated to them.

Last but not the least, I extend my special thanks to all the staff of Materials and Metallurgical Department and Advanced center for Materials Science, for their unconditional help.

Sanjib Kumar Rout
IIT, Kanpur
February, 2002.

Chapter 1

INTRODUCTION

Tungsten heavy alloys have been linked to powder metallurgy processing since 1930's. Tungsten Heavy alloys are a class of material that contains 80-90 wt% W. They generally exhibit a dual phase microstructure, where principal phase being mainly pure tungsten in association with a binder phase containing transition metals (Ni, Fe, Cu, Co) having dissolved tungsten. Tungsten grain it self is brittle and addition of transition metals make these alloys ductile in nature. The basic advantage of these alloys is that they have high density, high UTS, moderate ductility, good machinability, good corrosion resistance and thermal conductivity. Application of these alloys includes radiation shielding, mass balancing, inertial systems and high momentum penetrators. As a whole tungsten heavy alloys have a wide range of mechanical property variation, especially hardness, UTS, ductility, which makes the alloy unique in the field of powder metallurgy. However the present research mainly focuses on the processing of W-Ni-Fe alloys. These heavy alloy microstructures comprise of two phases, the refractory tungsten phase (B.C.C) and other lower melting matrix phase (F.C.C). because of refractoriness of tungstenLiquid phase sintering is the only mechanism to produce these heavy alloys. However in order to get the desired properties of the as sintered alloy one should control the sintering temperature, sintering atmosphere depending upon composition. The properties of these alloys are very much sensitive to processing and are degraded by residual porosity, impurity segregation, interfacial embrittlement and inter-metallic phase formation. Nickel to iron ratio also is an important factor for deciding the mechanical property. However the mechanical property of W-Ni-Fe alloy can be improved through thermo-mechanical processing in such a way that this alloy is the best alloy to be used for application mentioned above. The change in mechanical property is interdependent on various factors like, powder characteristics, sintering time, temperature, atmosphere, chemistry and post cycle treatments. Few researches have been carried out on post-sintering treatment like quenching of the sintered alloy in some way can improve % of elongation and UTS. This can be reasoned in a way that during quenching the interfacial segregation of impurity element can be reduced, as

compared to annealed and sintered parts. Vacuum treatment has also been suggested for improving the mechanical property as it avoids the occurrence of hydrogen embrittlement.

Different thermo-mechanical treatment has been discussed in various literatures. One of the ways to improve the UTS and yield strength is through cold working and annealing, but hardness value has often-negative effect of this treatment. The heavy alloy when solid state sintered after cold working show better mechanical property, but not that much better as compared to the material liquid phase sintered after mechanical working. The liquid phase sintered material shows better mechanical property due to refined microstructure through recrystallization, stress induced boundary migration and melt penetration into the fine-grained material. Also few research have been performed on primary reduction by extrusion followed by multiple secondary reduction by swaging with intermediate anneals and introduction of intermediate cold swaging to hot rolled and hot swaged specimen. Some time aging treatment of this alloy partially improves the hardness value over a certain range of temperatures due to the precipitation within the W grains, but above a certain temperature the negative effect takes place. The tungsten content has a marked effect on tensile properties of these alloys. The maximum UTS was obtained at 93% W. As far as the penetrator application is concerned, the high momentum penetrator desires high toughness in combination with ductility and strength as they are subjected to high temperature and high strain rate. DU and WHAs have been successfully used for this application. Though the penetrator performance of DU alloys is more efficient than the WHAs, but due to its environment hazards they are of limited use. Research has been carried out on failure mechanisms of these materials under dynamic compression tests.

However this work mainly aims about, keeping the same volume fraction of W, the mechanical property like toughness in combination with strength can be improved through swaging and heat-treating at 500, 900 and 1400°C. Chapter 2 gives the background for our studies. This includes introduction about tungsten heavy alloy, powder metallurgy processing of W-Ni-Fe alloys, post sintering heat treatments, mechanical working, mechanical properties relating to thermo-mechanical processing. Finally different aspects of microstructural characterization.

In chapter 3 scope of our present work is discussed. This includes reason for thermo mechanical treatment of W-Ni-Fe alloys, effect of thermo mechanical treatment on mechanical properties and microstructure evolution.

Chapter 4 describes in detail the experimental procedures. It includes sample preparation, density measurements, mechanical working (swaging), heat treatment procedures and quantitative analysis of microstructures through stereo logy for Vv, Sv measurements and contiguity determination. Chapter 5 deals with the experimental results. Chapter 6 and 7 consists of discussion and conclusions, respectively.

Chapter 2

BACKGROUND

2.1 Tungsten Heavy Alloys.

Tungsten is a vital industrial material with a rich history that spans over several centuries. It is one of the heaviest metals, having the same density as gold. The most characteristics of this metal are its very high melting point temperatures(3420°C) which exceeds over all other metals. This characteristics of tungsten metal is due to very strong inter atomic cohesion of metal and accounts for its great strength at elevated temperatures with low co-efficient of thermal expansions. It also exhibits outstanding thermal properties, which makes it attractive to be useful over a broad range of applications. However for some special applications, its electrical and thermal conductivity, sensitive towards oxidation and very poor workability are quite unsatisfactory. So these limitations of tungsten have led to the development of two-phase alloy, where the useful properties of tungsten are combined with those of additives.

The term tungsten heavy alloys are used for a group of two-phase composites, based on W-Ni-Fe and W-Ni-Cu. They are characterized by their high density and a novel (unique) combination of high strength and ductility. Tungsten is the main element of these alloys (typically present in the range of 90 to 98 wt%) and the reason for their high density (between 17 to 18.5 g/cm3). The additives serves as a binder phase and holds the tungsten grain together which makes the alloy ductile and workable. A typical microstructure is shown in Figure 2.1, which consists of spherical bcc tungsten grains embedded in a tough fcc metallic matrix.These above properties gives rise to many applications for this family of materials spanning over a wide range of consumer, industrial and government applications which includes:

- Damping weights for computer disk drive heads
- Balancing weights for ailerons in commercial aircraft, helicopter rotors, and for guided missiles
- Kinetic energy penetrators for defeating heavy armor
- Fragmentation war heads

- Radiation shielding, radioisotope containers, and collimation aperatures for cancer therapy devices
- High performance lead-free shot for water fowl hunting
- Gyroscope components
- Weights in premium golf clubs for improving consistency in response
- Electrical contacts

***Fabrication*:**

Heavy alloys are fabricated by conventional P/M technique. Figure 2.2 shows the flow chart for a typical fabrication process of tungsten heavy alloy penetrators.

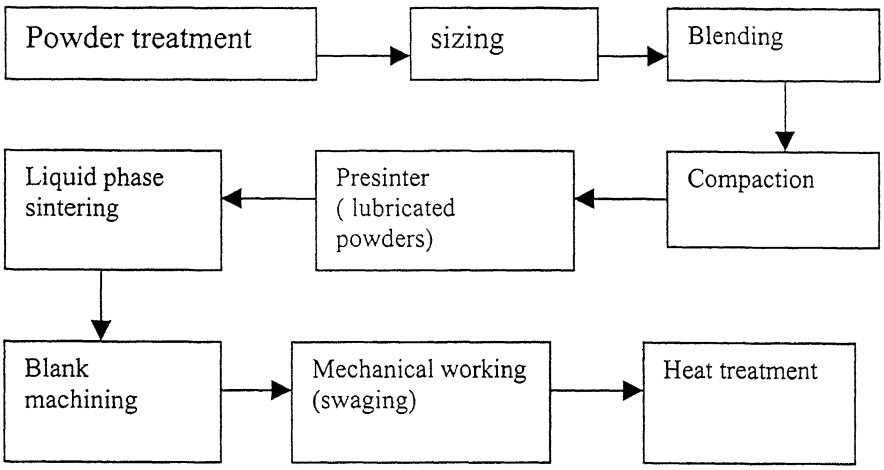

Tungsten heavy alloys are typically formulated from elemental powders with mean particle sizes in the range of 1.5 to 7 μm. Blend homogeneity is essential for microstructural uniformity and predictable sintering to full density. They are commonly processed to full density by solid-state sintering or liquid phase sintering in H_2 atmosphere. Liquid phase provides a superior means of densifying pressings in which a microstructure consisting of spheroids of nearly pure tungsten in the binder phase of transition metals plus dissolved tungsten forms via Ostwald ripening. Post sintering processes plays an important role in improving the mechanical properties of these alloys. Impurity segregation and embrittlement of interfaces is controlled by using pure powders and post sintering heat treatments that quench from high temperatures. Hydrogen embrittlement is controlled by changing gases within sintering cycle; using vacuum anneals as post-sintering heat treatments or using the

vacuum as the sintering atmosphere. The sintering atmosphere plays a vital role in controlling the residual porosity.

During sintering on cooling a significant amount of tungsten remains in solid solutions depending on the binder composition and cooling rate. The solubility is highest in W-Ni alloys (typically 40 wt%), making the alloy low ductile in nature but addition of Cu, Fe depress it to lower values (typically 20 to 25 wt% W) resulting a tough and ductile binder matrix.

Depending on the binder composition heavy alloys can be classified into two main groups:

(a) W-Ni-Fe alloys: this group of alloys generally contains nickel: 1-7 wt%, iron: 0.8 –3 wt% and are ferromagnetic in nature. These alloys exhibit excellent strength /ductility combinations and can be cold worked to a reductions of 70% without intermediate annealing. Higher addition of iron causes a significant matrix strengthening effect and improves high temperature strength. Figure 2.3 shows the binary phase diagram of Ni-W. Figure 2.4 shows the ternary phase diagram of W-Ni-Fe alloys. The equilibrium phase diagram shows the lowest melting temperature for the matrix phase is near 1435°C. For W-Ni-Fe system, it has been seen that at 1435°C a congruent melt forms and it gives a ternary eutectic system. But in practice, due to mixing of powders the melt formation occurs at 1465°C. From the nickel iron binary phase diagram it has been seen that melt forms at above 1452°C, which is the melting point of nickel. In W-Ni-Fe system tungsten grains are embedded in Ni-Fe matrix. The solubility of W in the matrix is low. But due to increase in nickel content in the system the solubility of tungsten increase, which is harmful in respect of mechanical property. The formation of different intermetallics depends upon Ni to Fe ratio in the system. The possibility of formation of intermetallics is minimum when the nickel to iron ratio is 7:3. Nickel to iron ratio plays an important role in the selection of W-Ni-Fe alloys for specific applications. Typically Ni to Fe ratio ranges between 1:1 and 4:1. Various research have been carried out in variation of nickel to iron ratio on the mechanical properties of W-Ni-Fe alloys. The mechanical properties of un worked alloys depends upon the nickel to iron ratio. Avoiding the formation of brittle intermetallic phases at the interfaces is the most important factor that should be considered in selecting the nickel to iron ratio. The work reported in

[1] reveals that an intermetallic phase of Fe_7W_6 forms at low Ni to Fe ratios, where as at ratios higher than 4:1, Ni_2W, NiW and Ni_4W intermetallic phases form. Extensive studies have been performed on the effects of the Ni to Fe ratio on the mechanical properties of tungsten heavy alloys. Among the various Ni to Fe ratios studied, 7:3 and 8:2 are frequently used, with a large number of investigations using 7:3. The selection of Ni to Fe ratio of 7:3 effectively prevents the formation of brittle intermetallic phases. Caldwell [4] has argued that it is possible to use higher or lower Ni to Fe ratio and to achieve high mechanical properties by using proper heat treatment. Ni to Fe ratio higher than either 7:3 or 8:2 can significantly improves mechanical properties if proper heat treatment is performed to control the precipitation of brittle intermetallic phases. This study involved W-Ni-Fe alloys (93%W) with a series of Ni to Fe ratio ranging from 0.5 to 30; heat treatment involved vacuum annealing and vacuum annealing followed by quenching. The results clearly shows that following vacuum annealing and quenching, the optimum Ni to Fe ratio is 6 to 10 and that mechanical properties are higher than those following vacuum annealing only (Figure 2.5). Similar results were also obtained in the work of Spencer and Mullendore [5], in which they found that quenching significantly improve properties.

(b) W-Ni-Cu alloys: members of these groups are nonmagnetic and exhibit higher electrical conductivity. Nickel: 1-7 wt% and copper: 0.5 –3 wt% with nickel to copper ratio ranging from 3:2 to 4:1 are used for this alloys. It experiences lower strength and ductility as compared to W-Ni-Fe alloys. Generally low heating rates are required to obtain full density due to low melting point of copper.

Properties

The principal phase in tungsten heavy alloy is nearly pure tungsten, which shows that the physical properties of the material should be very close to that of elemental tungsten. Though it comprises of high melting point metal, tungsten heavy alloys are limited in service temperatures by nature of the transition metal binder phase and formation of intermetallics. Even under ambient conditions, oxidation alone may impose a temperature ceiling of ~ 300°C to 400°C. A mechanically worked

tungsten heavy alloy results in noticeable strain aging at ~ 300°C in as short a time as a few hours resulting in altered properties. The ultimate limit on service temperature is imposed by threshold of formation of a liquid phase, which can occur in some W-Ni-Fe alloys as low as ~ 1450°C. As a whole thermal properties are determined by the tungsten phase and service temperature limitations are determined by the binder phase. Tungsten heavy alloys are sensitive to hydrogen embrittlement.

The main advantage of tungsten heavy alloys over pure tungsten is their ability to be machined to complex geometries using common metal working tools and techniques. They tend to form short chips on machining. The exceptions are alloy containing low tungsten content, which forms continuous chips, and require more attention to chip breaking. The machining characteristics of tungsten heavy alloy resemble those of super alloys. So tungsten heavy alloy possess high elastic stiffness and cutting forces are higher than for most metal cutting operations, thus requiring carbide tooling, rigid support, and adequate spindle torque.

Due to difference in both chemistry and melting point of the tungsten phase and the binder content tungsten heavy alloys are not readily weldable. However brazing of tungsten heavy alloy to dissimilar metals is possible using copper or commercial brazing alloys based upon copper, nickel and silver. Generally the mechanical properties of joints are lower due to formation of inter metallics [1].

As far as the environmental hazards is concerned tungsten heavy alloy offers minimum toxicity providing them an incentive for their selection over other common high density materials such as DU. Among all the applications, tungsten-based alloys have attracted considerable interest for defence applications, specially those requiring high densities, such as kinetic energy penetrators. In order to achieve as high a kinetic energy as possible, high-density materials are critically required. Considering various factors like density, availability, cost and properties, only two density materials (i.e., depleted uranium (DU) and tungsten heavy alloys) have been developed and used in the application of kinetic energy penetrators. DU alloys are currently the most widely used and suitable material for long rod kinetic energy penetrators. However because of increasing environmental concerns and political pressures related to contamination that results from residual low-level radiation of DU materials, finding suitable substitute for these alloys has become increasingly necessary. As a result, tungsten based alloys have been developed and used as long rod kinetic energy penetrators.

Contiguity of the microstructural surfaces plays an important role in deciding the mechanical properties of the material. Contiguity represents the average fraction of surface area shared by one tungsten grain with all neighbouring tungsten grains. Figure 2.6 shows the effect of contiguity on elongation and UTS of W-Ni-Fe alloys. It depicts that with increasing in contiguity of the microstructural surfaces the mechanical properties gradually decreases. Because the W-W contact area acts as the main centre for load application. When the material is strained under application of some load the W-W contact area acts as the major weak point for crack nucleation due to its brittle nature. Figure 2.7 shows the optimum value of room temperature strength and fracture elongation and their correlation with the contiguity factor for tungsten heavy alloys. With increasing tungsten content the contiguity of the tungsten grain increases. From the figure it is clear that for high tungsten content the elongation is zero and UTS is about 400 Mpa. So with high tungsten content the fracture easily occurs due to increase in tungsten amount. So in order to get the best combination of properties, contiguity should be optimum keeping the same volume fraction of tungsten.

Apart from the better mechanical properties there are other attributes which makes the heavy alloys a versatile product, which are as follows:

- The high modulous of elasticity (much higher than steel)
- Excellent vibration damping characteristics
- Good machinability
- High absorption ability for X-rays and γ-rays
- Good thermal and electrical conductivity
- Low electrical erosion and welding tendency
- Good corrosion resistance

Figure 2.8 shows how tungsten heavy alloy parts can be machined and used in aviation and radiation shieldings.

Recent advances

Recent efforts have focused on improving the strength and hardness of heavy alloys at the expense of ductility, which requires strengthening through alloying additions and microstructural control. The effective alloying addition includes Ta, Mo, Re, which have total solubility in tungsten and high solubility in matrix. As a

result it gives grain size refinement with improved strength and hardness. Addition of Cr, V, Nb should provide improved strengthening effect, but these also have densities lower than the tungsten, thus even though the strength and hardness are increased the theoritical density is lower. On the other hand, Re is a high density alloying addition that proves very effective in tungsten heavy alloy system due to its small atomic size as compared to tungsten.

The present research concentrates on W-Ni-Fe alloys containing 90, 93, 97-wt% W with nickel to iron ratio of 7:3.

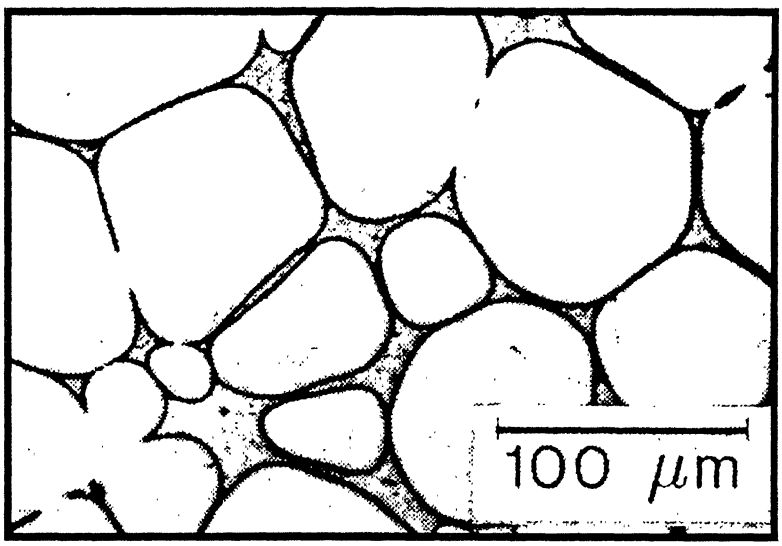

Figure 2.1. Optical micrograph of typical 95% tungsten heavy metal alloy [1].

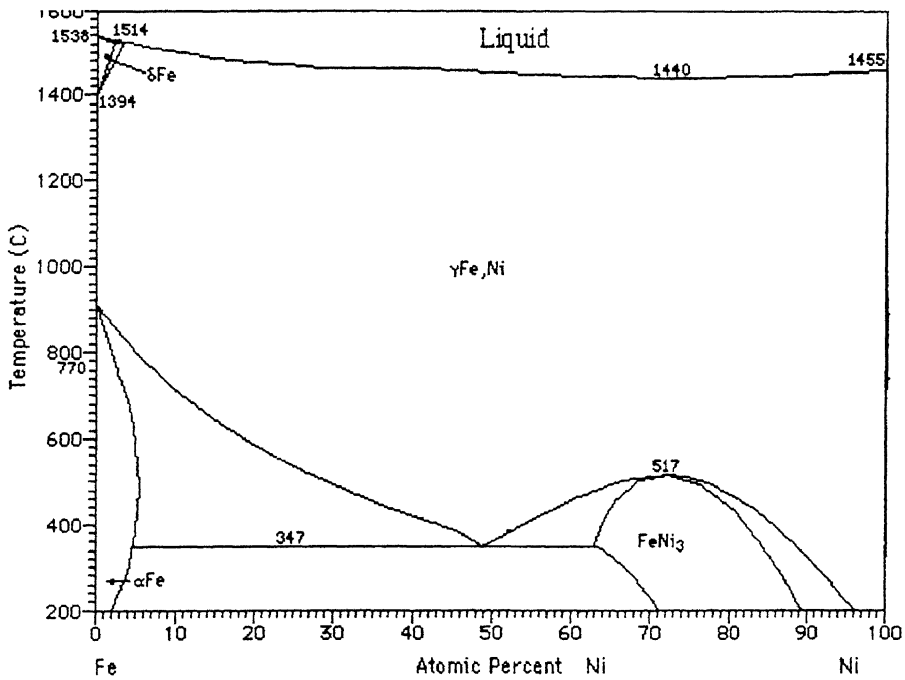

Figure 2.3. Fe-Ni Equilibrium diagram [2].

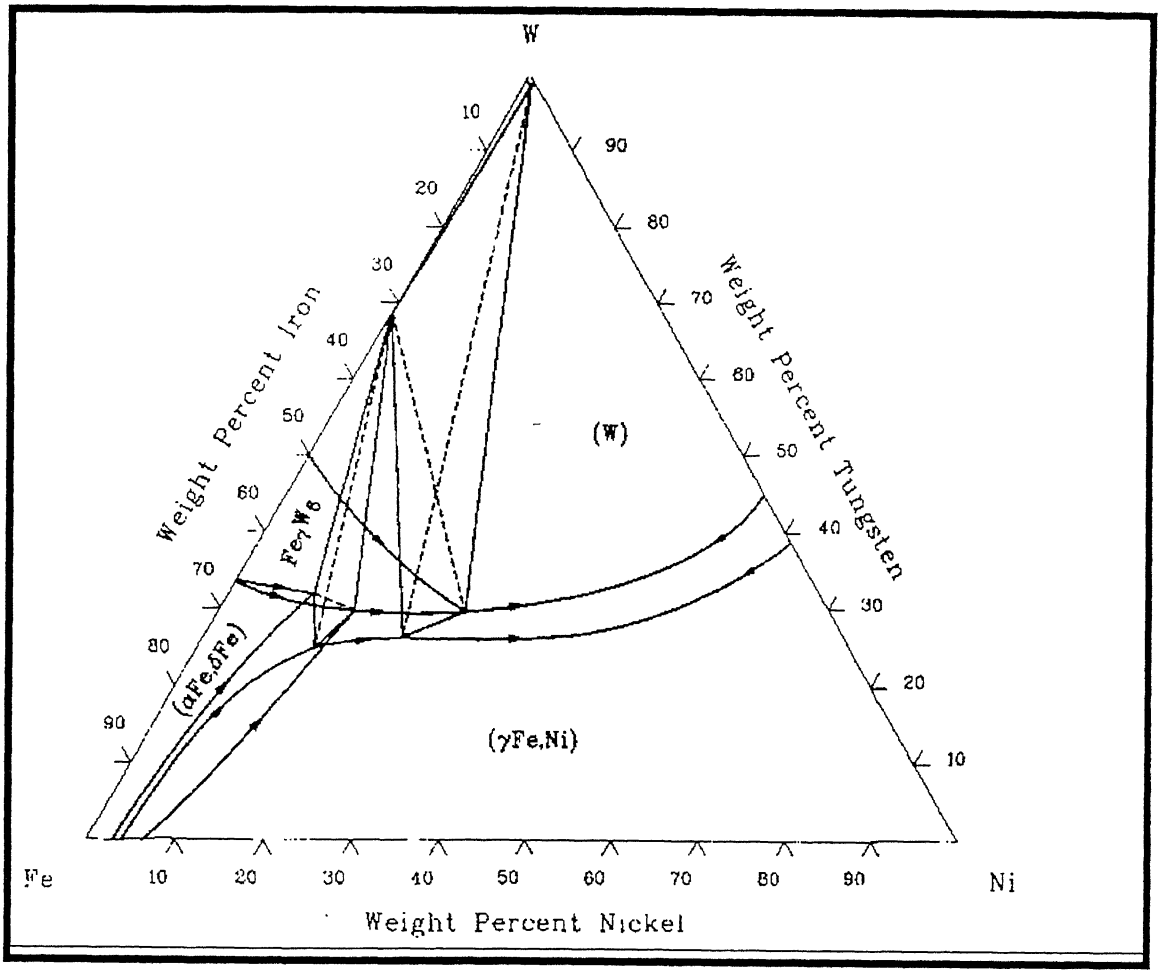

Figure 2.4. Ternary phase diagram of W-Ni-Fe alloys [3].

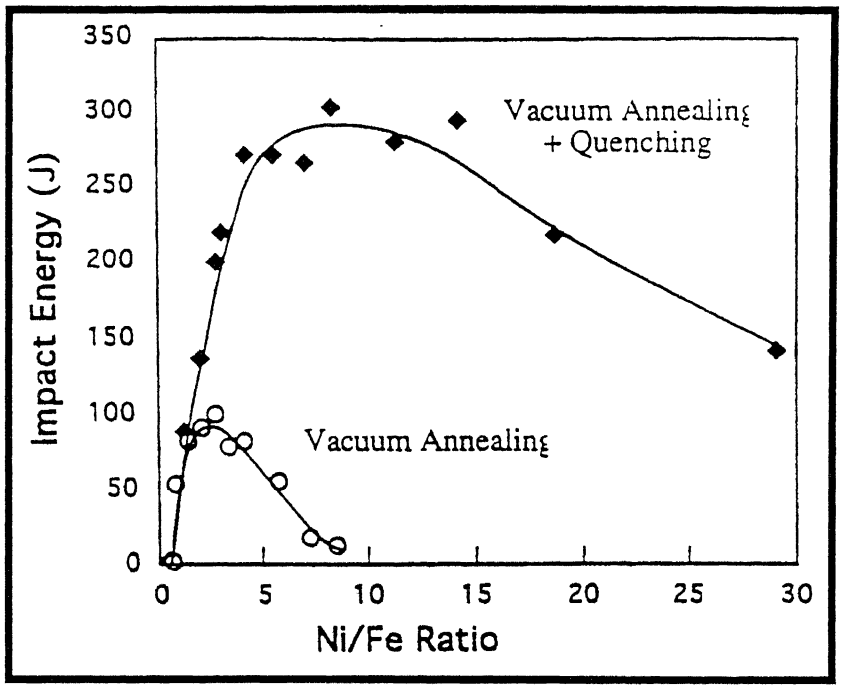

Figure 2.5. Effect of Ni to Fe ratio on impact energy of W-Ni-Fe alloy (93%W) [7].

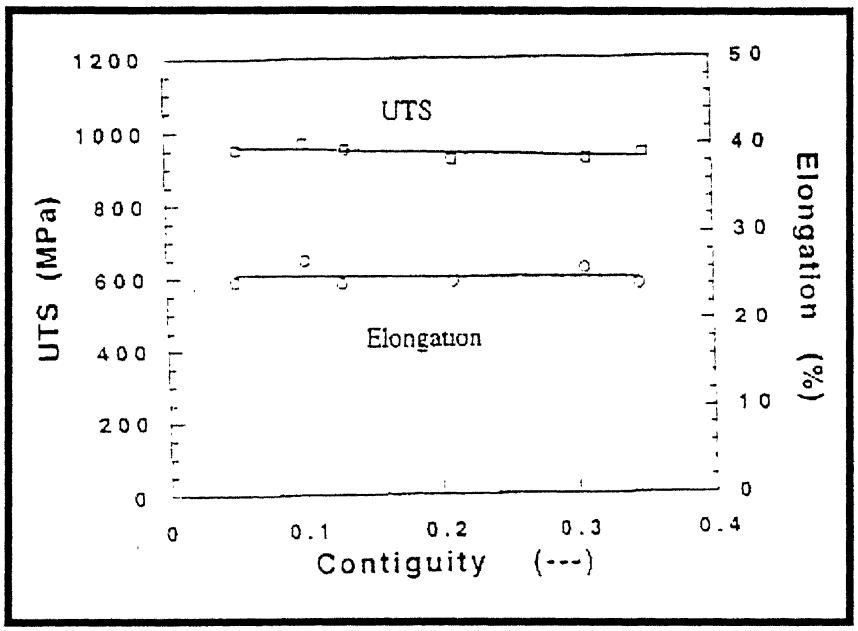

Figure 2.6. The effect of contiguity on UTS and elongation of W-Ni-Fe alloy [7].

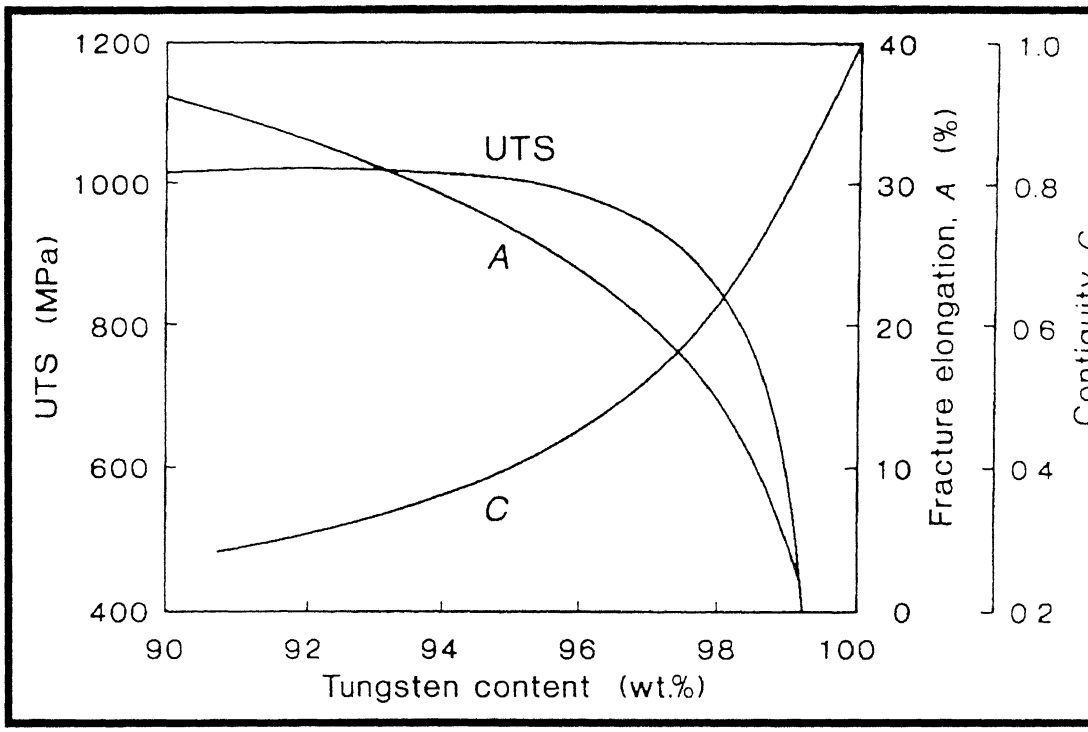

Figure 2.7. Optimum values of room temperature strength and fracture elongation and their correlation with contiguity factor of tungsten heavy alloy [6].

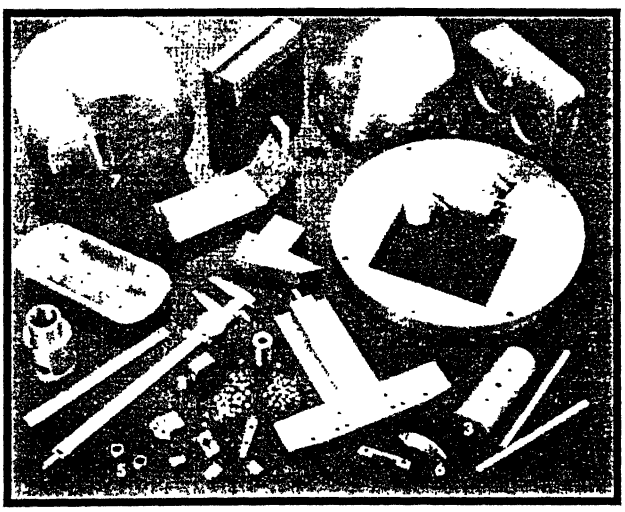

Figure 2.8. Tungsten heavy alloy parts (machined) used in aviation and radiation shieldings [6].

2.2 P/M Processing of W-Ni-Fe alloys

Powder metallurgy (P/M) is the study of the processing of metal powders, which involves fabrication, characterization, and conversion of metal powders into useful engineering components. P/M method is one of the most modern methods known for fabrication of metal components. For the last few decades powder metallurgy methods is the most promising and emerging field to produce materials with novel properties which cannot be produced by any other technique.

The P/M processing strategies includes application of pressure, deformation and heat to the powders. As a result of which the powders gets shaped to a desired component with improved properties. The powder metallurgy manufacturing process can be considered to be consists of three basic steps:

a) powder mixing
b) powder compaction
c) consolidation or sintering

Metal powders can be produced by physical, chemical and mechanical methods. Both elemental powders are produced in substantial quantities by the process named 'atomization'. In this process a stream of molten metal is broken up into droplets which are rapidly quenched to powder by high velocity jets of either water or gas. Powders of high purity are produced electrolytically. The behaviour of powder during the subsequent consolidation process is determined by both particle and bulk properties. A powder is characterized, therefore, not only by chemical composition but also particle shape, size and surface chemistry and in bulk by compressibility. Powders are blended to meet the required specifications and mixed with a lubricant usually a metal stearate, which aids compactions. The compression of the powder in the closed die reduces the voids between the particles.

The pressed compact is given a thermal treatment named sintering under a protective atmosphere or in vacuum, during which the lubricant is evaporated and porosity is reduced by metal transport involving surface and volume diffusion. This leads to chemical bonding of the particulate. The driving force for sintering in the total energy systems. This occurs by the formation of interparticle bonding and removal of solid-vapour interfaces. As sintering proceeds, the original inter-connected porosity is reduced, closed pores are formed, and the overall shrinkage is controlled to ensure the

final dimensions of the compact come within the required engineering tolerances. Variation on the foregoing process is made to meet particular product requirements.

Advantages of P/M

The development of P/M is due to its great advantage over other methods like casting stamping or machining and avoids casting defects such as blow holes, shrinkage and inclusions [30]. P/M is the best methods, which provides the requirements for strength, wear resistance or high operating temperatures. Processing of refractory metals and alloys falls in this group. P/M alone can produce alloys made from metal insoluble in each other, which is not possible by ordinary methods.

P/M also make it possible to obtain metals and alloys of high purity (uncontaminated by material from furnace lining or by oxidation), unlike metal produced by conventional processes.

The major advantage of P/M is to provide finished parts without machining. It not only saves time but also provides high material utilization (>95%). Above all the advantages of P/M can be summarised as follows:

- Metal powders are high purity materials
- Close dimensional tolerances can be maintained
- High volume process with excellent reproducibility
- Quality control is inherent in this process
- Low labour input
- Machining is eliminated or reduced
- Scrap losses are eliminated or reduced
- Segregation is avoided
- Controllable porosity and density can be precisely controlled
- Complex immiscible metals
- Complex shapes can be produced
- High material utilization (~98%)

Disadvantages P/M

The disadvantages of powder metallurgy which make its use restricted should be mentioned along side its advantages. The main draw back of P/M is high cost of

high purity metal powders. During processing the impurities may restrict the mechanical properties of final product. Porosity plays an important role in restricting the use of P/M products. Because during processing the pores present inside cause oxidation not only on the surface of the material but also on the entire product. Porosity also decreases the thermal and magnetic properties of the material. If blend of two materials with large difference in density are used for P/M processing then problem of segregation may occur. In many cases depending upon the system used, shrinkage or expansion occurs after sintering. So special care should be taken during processing to get the required specifications of end products. But inspite of all the limitations the role of P/M is more and more [8]

Sintering fundamentals

Currently several processing methods are being used for processing of W-Ni-Fe alloys, such as sintering (solid state sintering and liquid phase sintering), arc casting, electron beam melting, swaging, hot extrusion, hot explosive consolidation, chemical vapour deposition and powder injection molding, mechanical alloying [9]. Apart from these hydrostatic extrusion is also being investigated as a technique for making high performance tungsten based alloys. Recently low pressure, plasma spraying and vacuum plasma spraying have emerged as two promising consolidation techniques, which have successfully used for producing high density, W-Ni-Fe alloys. However as a result of high melting point of tungsten, sintering particularly liquid phase sintering, remains as the preferred approach for consolidation of tungsten based alloys.

Sintering is the process of bonding together of particles at high temperatures. It can occur at temperatures below the melting point of major constituents. Generally the bonding occurs due to the growth of cohesive necks at the particle contacts.

2.2.1 Solid State Sintering

The driving force for solid state sintering is excess surface free energy. Sintering is a complex process and for any given metal and set of sintering conditions there are likely to be different stages, driving forces and material transport mechanisms associated with this process.

Different stages of solid state sintering

One of the basic aspects of sintering is that it usually takes place at a constant temperature (or at least a major part of it) and the time is varied to achieve certain result. Consequently, it becomes useful to attempt to describe the stages of sintering in terms of their relative order with respect to time. Solid state sintering is divided into six stages [10]

1. Initial bonding among particles
2. Neck growth
3. Pore channel closure
4. Pore rounding.
5. Densification or pore shrinkage
6. Pore coarsening.

***Interfacial bonding among particles*:**

Bonding involves diffusion of atoms leading to the development of grain boundary. It is the bonding that imparts high degree of coherency and integrity to the material. In fact the grater the original density of the material, the greater the amount of contact area and potential grain boundary area. No densification and no dimensional change take place in this stage. If green density is higher, initial bonding is also higher. This stage of sintering does not lead to any dimensional change of the material. Bonding in this stage imparts high degree of coherency and integrity to the material, which is extremely important. This can be proved by the achievement of high strength and hardness even after relatively short exposures to elevated temperatures.

Neck growth:

It is the second stage of sintering and is related to the first stage of initial bonding The newly formed bond areas are called necks. Material transport takes place through the necks without any shrinkage. The curvature changes but not the center-to-center distance. This does not affect the continuity of porosity, porosity remains same. This stage greatly increases the strength of the compact but does not involve any densification.

Pore channel closure:

This stage represents the major changes in the nature of the porosity in the sinter mass. Continued neck growth can cause pore channel closure. Major changes in nature of porosity means, porosity >10% called interconnected pores and porosity <15-10% are called closed or isolated pores.

Pore rounding:

Pore rounding may be considered to be natural consequences of neck growth. If morphology of pore changes then, it become rounded and can be applied to both for interconnected and closed pores. Long time holding leads to spherical pores. More rounded pore results into more toughness. This stage of sintering is illustrated by the idealised three-sphere models in Figure 2.9.

Densification or pore shrinkage:

Sufficient time and temperatures are required for densification, depends upon single or multicomponent system. In single component system densification is equivalent to porosity shrinkage. In multi-component system, the situation is somewhat complicated. Sometime growth increases, some times shrinkage decreases.

Pore coarsening:

In this stage no change in volume, only grain coarsening takes place. Porosity remains same; number of pores will change. This stage is not desirable in sintering, which decreases the mechanical property. Isolated pores are very difficult to remove. In many case this microstructural change is analogous to the precipitate coarsening which occurs during severe over ageing of conventional age-hardening alloys [8].

Sintering mechanisms

The various structural changes that take place during sintering obviously depend upon mass transport to and from various regions within the powder compact. A net decrease in free energy must be associated with sintering if these structural changes are to occur spontaneously. In a simple material this decrease in free energy is associated with a decrease in the total surface area (and therefore surface energy) of the compact. All of the basic structural changes, such as neck growth, pore rounding; etc., lead to reduced total surface area within the compact.

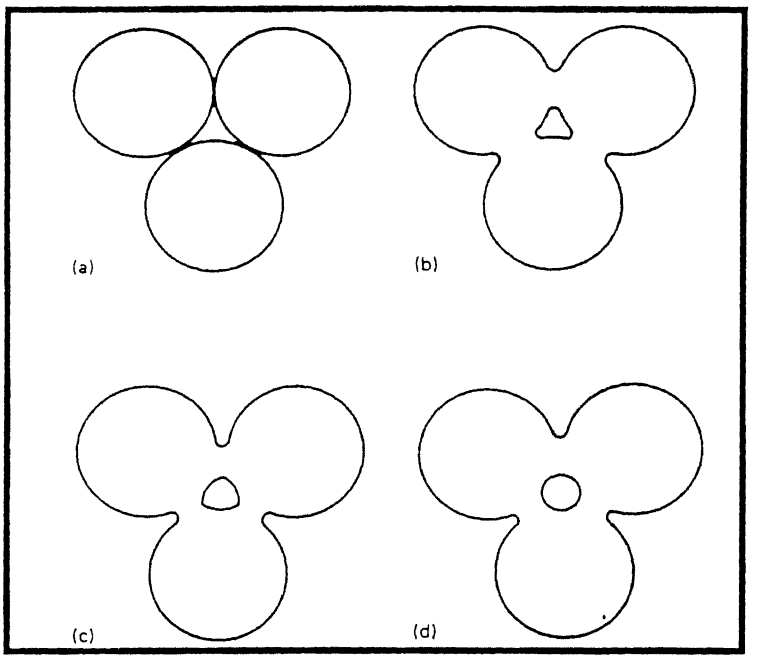

Figure 2.9. Three sphere sintering models. (a) Original point contacts. (b) Neck growth. (c) and (d) Pore rounding [11].

Thus it is not surprising to find that the greater the original surface area the larger the driving force for sintering- i.e. compacts of fine powders sinter faster than compacts of coarse powders [8]

Transport mechanisms determine how mass flows in response to the driving force for sintering. The total mass transport can be summation of many stages. They are

1. Evaporation and condensation
2. Diffusion mechanisms:
    - Surface diffusion
    - Grain boundary diffusion
    - Volume/bulk/lattice diffusion.
3. Nabarro-herring mechanisms
4. Plastic flow (creep mechanisms)

and occurs through the formation of inter particle bonds brought about by atomic motion at the sintering temperatures.

Limitations of solid – state sintering

As a whole solid-state sintering occurs in solid state, the diffusion rate is slow compared to the other sintering process. When we are considering the theory of solid state many assumptions have been made to simplify the situation. But in actual process, these assumptions may not valid, which results into a serious problem in predicting the process. Sintering generally considers about the spherical size of powders, but in actual practice the powders are non-spherical in nature with wide particle size distributions. Compaction repacks the particles, collapses large pores, and enlarges the particle contact but may introduce new defects. Most of the bonding takes place prior to the holding time at maximum temperatures. Again the assumption of isothermal conditions may not be valid for most of the models. Actually, the compact faces very dynamic situations, with gradients introduced by thermal stesses and atmospheric interactions. In many cases the gradients have a significant effect on the sintering process.

2.2.2 Liquid phase sintering

Liquid phase sintering is characterized by the presence of one or more than one liquid phase throughout or in part of sintering cycle. The formation of liquid

phase sintering usually increases the sintering rate. Various forms of liquid phase sintering have been practiced since as early as 4000B.C, largely in fabrication of pottery and glass-bonded ceramics, such as porcelain [12]. The tungsten heavy alloys (W-Ni-Fe, or W-Ni-Cu) in the 1930s provided an important theoretical basis of the process. Today, liquid phase sintering, including dental porcelains, cemented carbide cutting tools, automotive connecting rods, and refractory ceramics. Liquid phase sintering offers many advantages compared to the conventional solid state sintering. Higher sintering rate is one of them. Other advantages are a high material utilization (>95%), near-net-shape fabrication, high productivity and superior control over the microstructures, which results into better properties. So above all a higher production rate can be achieved as compared to conventional processes. Because of these above advantages around 70% of sintered products are made from the liquid phase sintering [13]. We know that mass transfer rate through the liquid is much higher than the solid. The capillary attraction due to wetting liquids results rapid compact densification without the need for an external pressure. The liquid also aiding to the rapid rearrangement of particles by reducing the friction. The liquid phase present in the system facilitates packing and high compact density.

In dual phase system (W-Ni-Fe , WC-Co, TiC-Ni) it is possible to form low melting phase. Where it is the first requirement as the liquid must form a film around the solid phase. Wetting is defined by the equilibrium of surface energies given by

$$\gamma_{SV} = \gamma_{SL} + \gamma_{LV} \cos(\theta)$$

Where γ_{SV} = solid vapour surface energy

γ_{SL} = solid liquid surface energy

γ_{LV} = liquid vapour surface energy

and θ is wetting angle

The basic criteria is solid must be soluble in the liquid and the liquid film provides a surface tension force to aid densification. Densification rate is much higher in Liquid phase sintered material as compared to solid-state sintered material. Dihedral angle plays an important role during sintering, it is the angle which represents the balance between interfacial energies and surface energy ratio, and can be estimated from following equation.

$$\gamma_{SS} = 0.5\,\gamma_{SL} \cos(\Phi 2)$$

Where $\Phi$is the dihedral angle

If Φapproaches zero, then there is no defined ratio for surface energies. Densification proceeds through 3 stages

1. Rearrangement
2. Solution reprecipitation
3. Grain coalescence.

Sintering Mechanisms

1. **Rearrangement**: it involves large-scale bulk movement of particles within the liquid phase, which causes rearrangement and densification. Liquid flows through the pores and displaces solid particles into the centre of compact. Some gas may bubble out through the liquid phase. Increasing the amount liquid phase leading to greater densification enhances particles movement. Wetting of solid particles by liquid phase is necessary. The driving force may be expressed in terms of surface energies/tensions, the greater the decrease in free energy the better is the driving force for densification. Most WHAs densify to full density before the onset of liquid formation. Once the melt formation takes place, it subsequently wet the W-grains by means of capillary action called rearrangement.

2. **Solution re-precipitation**: This stage promotes the particle motion associated with the first stage. Solution reprecipitation occurs if the solid particles have limited solubility in the liquid phase. This stage also leads to densification, but at slower rate. The solubility of particles in the liquid phase increases by increasing the convexity (smaller size particles). Material transport by melt and subsequently reprecipitation on the coarser W-grains occurs called reprecipitation or Ostwald ripening mechanisms. (Figure 2.10)

3. **Grain coalescence**: In the last stage grain coalescence takes place. After dissolution no more liquid remains for second stage. In case of dihedral angle >0, interface (solid-solid) is still stable. The elimination of pore is not high, so

densification rate is very slow. But in this stage, there is an overlap of second stage possible. So amount of densification may be due to secondary accommodation.

If wetting of particles by the liquid phase is incomplete then there may be some solid particles in contact rather separation, which lead to skeleton type of structure after densification. On the other hand if the amount of liquid phase is more than sufficient then it may lead to "Sweating". So for proper densification the amount of liquid phase and their separation of solid particles through liquid phase should be controlled properly. So finally all these stages of liquid phase sintering leads to full density compact and micro structural modification.

Figure 2.11 shows the classical stages of liquid phase sintering involving mixed powders which form liquid on heating [13].

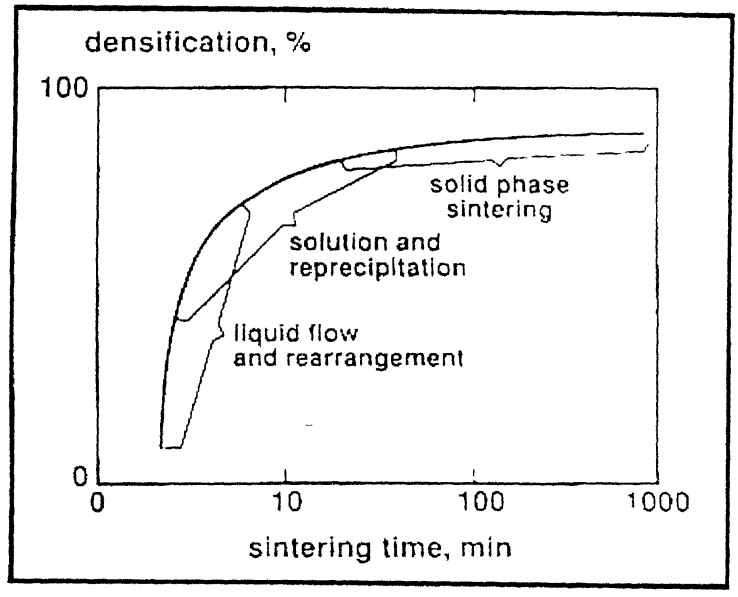

Figure 2.10. The process associated with classic liquid phase sintering, giving the main microstructural changes [13].

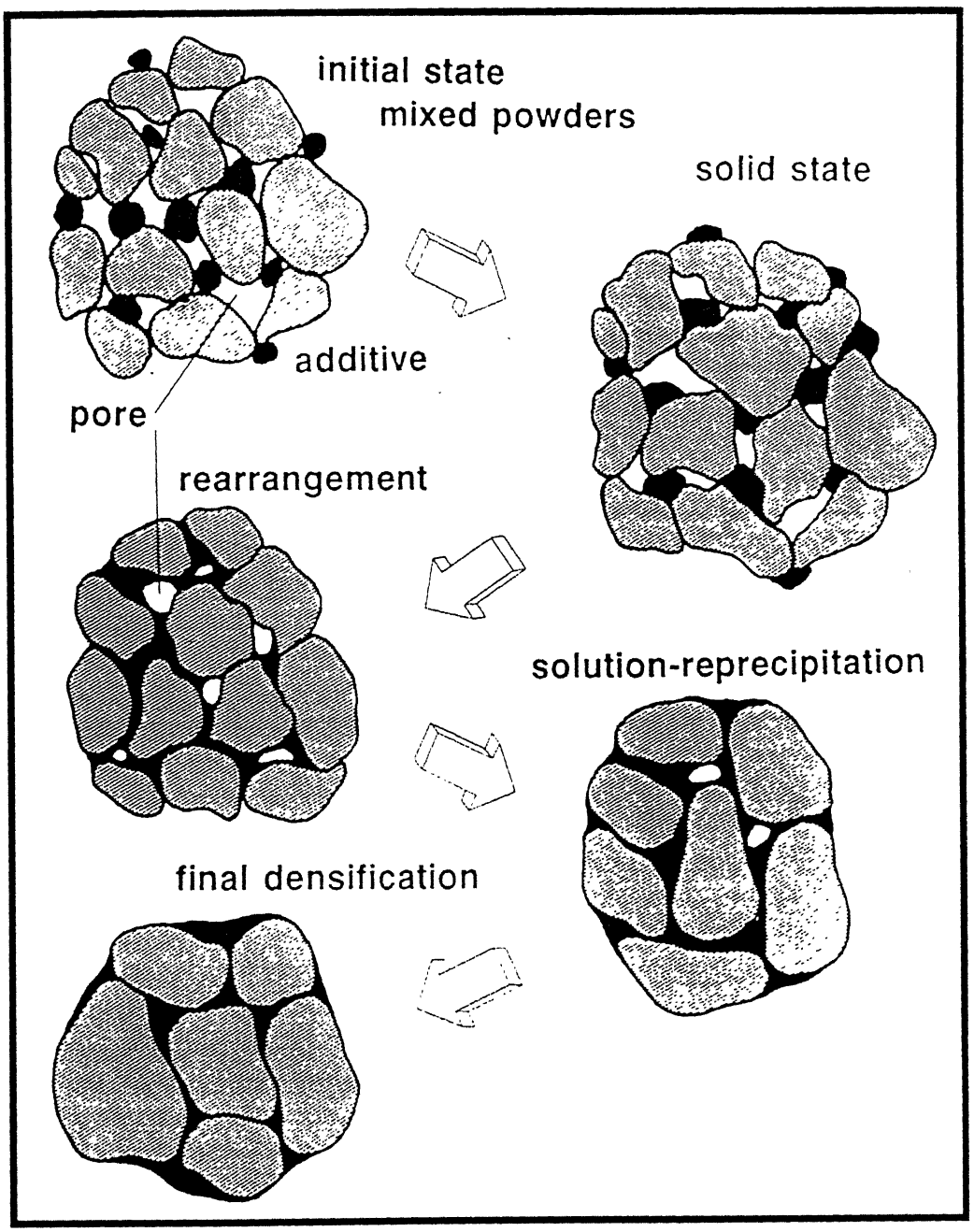

Figure 2.11. The classic stages of liquid phase sintering involving mixed powders which forms liquid on heating [13].

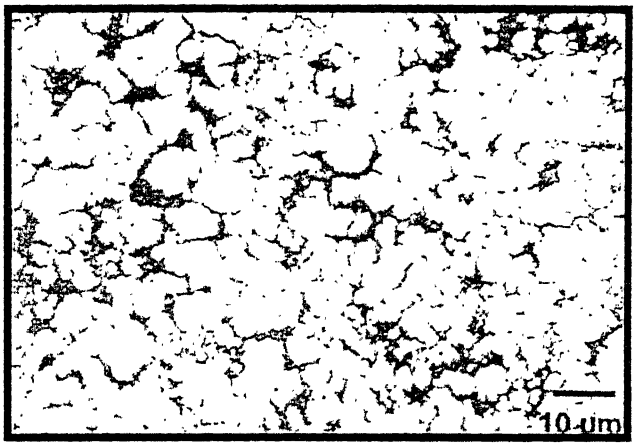

(a)

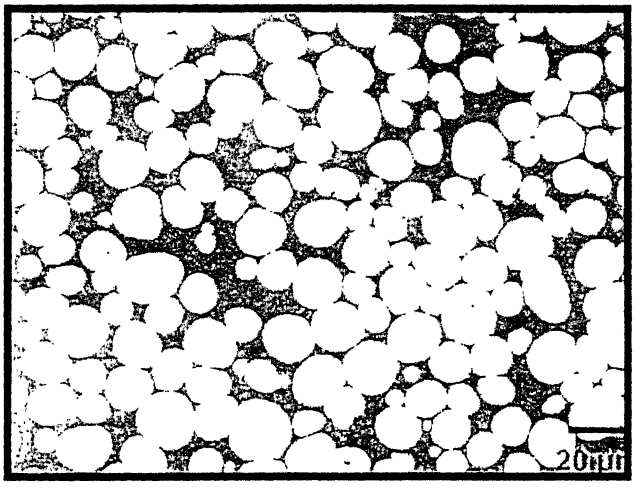

(b)

Figure 2.12. Microstructure of W-Ni-Fe alloys in (a) solid-state sintered (1400°C, 1h) and (b) Liquid phase sintered conditions (1500°C, 1h) [14].

Microstructure of W-Ni-Fe Alloys.

A typical microstructure of W-Ni-Fe alloys produced by liquid phase sintering consists of spheroidized tungsten particles embedded in a Ni-Fe matrix. The particles are nearly pure tungsten with a body-centered structure (BCC). There are two discrete interfaces present in tungsten heavy alloys. The first is boundary between tungsten and matrix. The second is interface between the tungsten particles. These two interfaces have significant effect on fracture behavior of W-Ni-Fe alloys. The fracture features of these alloys are characterizes by

- Tungsten grain cleavage;
- Matrix failure;
- Tungsten-tungsten grain intergranular grain boundary separation;
- Tungsten-matrix separation

The tungsten-tungsten interfaces are generally weakest inorder to initiate fracture at the tungsten-tungsten interfaces. The proportion of tungsten separation depends on the contact area between tungsten grains, which is related to grain size and tungsten concentration. The deformation mechanism of these alloys generally depends upon the bond strength of tungsten-matrix interfaces. If the tungsten-matrix interfaces are strong the fracture mode is dominated by the tungsten cleavage and if they are weak the fracture feature is dominated by the separation between tungsten particles and the matrix as well as the limited tungsten cleavage.

Effect of Sintering Condition

W-Ni-Fe alloys exhibit unique combination of high strength, density and ductility. Their mechanical properties especially ductility is more sensitive to sintering condition. Numerous research have been done on the effect of sintering temperature, sintering time and sintering atmosphere on the mechanical properties of tungsten heavy alloys. Processing condition affect porosity, densification and grain growth, all of which eventually affects the final mechanical property.

The work reported in [16] states that as sintering temperature increases the grain size and volume fraction of matrix also increases while the contiguity decreases. The trend is shown in Figure 2.13. The high sintering temperature results in the high solubility of tungsten in matrix, which in turn leads to more matrix phase. On the other hand high sintering temperature leads to high diffusivity of tungsten in the

matrix phase, which leads to faster tungsten grain growth rate. More over high sintering temperature leads to decrease in dihedral angle. A low dihedral angle corresponds to a lower contiguity. As a result microstructure changes with the changes in sintering temperature. Strength and hardness decrease while ductility increases to a maximum and then decreases with increasing sintering temperature (Figure 2.14) [15]. At higher sintering temperature, there are few but large tungsten grain, more matrix and consequently greater mean free matrix path. As a result, the dislocation slip paths in the matrix are long and there fore less work hardening is present, which leads to lower strength and hardness. On the other hand the increase in ductility is attributed to the more matrix, long dislocation slip paths, less work hardening and low contiguity. At higher temperature the formation of large tungsten grains leads to initiation of larger crack at the tungsten tungsten interfaces which ultimately lead to decrease in ductility. It has been observed that sintering strength and ductility of tungsten heavy alloy decrease over given sintering time period [17]. Churn and German reported that pore coarsening due to prolonged sintering leads to significant degradation of mechanical properties [18]. The mechanism of pore coarsening is similar to that of tungsten grain growth by Ostwald ripening and pore coalescence. The initial distribution of particle sizes and particle packing is the primary reason for pore coarsening, which leads to an inhomogeneous distribution of pore sizes. As a result the larger pore grow at the expense of smaller pores due to difference in their chemical potential. The influence of sintering time on the microstructure and mechanical properties of W-Ni-Fe alloys containing 95%W With Ni to Fe ratio 7:3 were studied [16]. The results show that with increasing sintering time the tungsten grain contacts flatten and tungsten contiguity decreases. The tensile strength and grain size exhibit maximum values with 90 minutes of sintering.

Figure 2.13. The grain size, grain shape and volume fraction changes in W-3.5Ni-1.5Fe at Sintering temperature of (a) 1475°C; (b) 1490°C and 1580°C [15].

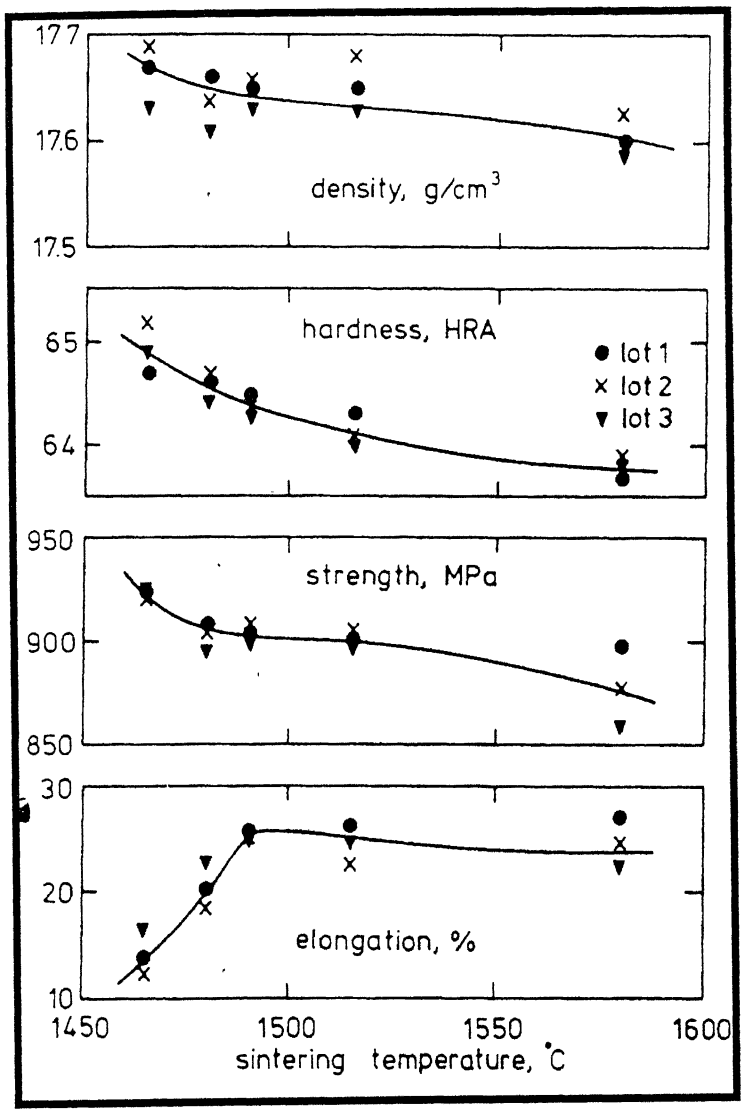

Figure 2.14. The variation of sintered density, hardness, tensile strength and elongation with respect to Sintering temperature [15].

Sintering atmosphere has significant effect on the density, residual porosity and there fore on mechanical properties of sintered alloys. It is well established that porosity greater than 0.5% originating from entrapped gas or solidification shrinkage drastically degrades the mechanical property. Further more the elimination of pores is dependent upon the solubility and diffusivity of the entrapped gas in the matrix since in an enclosed pore the gas atoms must dissolve in the matrix and then diffuse out to the surface of the sintered alloys. If solubility of entrapped gas in the matrix is negligible, such as the case of argon and nitrogen in many metallic interfaces, densification will be hindered as surface energy effects are balanced by compression of gas inside pores. To that effect hydrogen is widely used as sintering atmosphere due to its combination of high diffusivity and slight solubility in most matrices of tungsten heavy alloys. In addition to that hydrogen produces reducing effects that are associated with the decreasing residual oxygen content in the sintered alloys. On the other aspects the hydrogen may embrittle tungsten alloys by segregating to the tungsten and matrix interfaces. German and Churn [18] have successfully implemented an approach, which involves using hydrogen in the first stage of sintering followed by an inert or vacuum atmosphere (Figure 2.15). Maximum ductility and strength were observed in the samples sintered 30 minutes in hydrogen followed by 10 minutes in argon. Some of the research have been carried out in [14]. Figure 2.16 shows the typical sintering cycle for tungsten heavy alloy. For high tungsten alloys (>90%) switching of sintering atmosphere from hydrogrn to argon was effective in preventing hydrogen embrittlement but for low tungsten alloys in situ formation of water vapour occurs which drastically reduces the ductility of the alloy. So the generic approach is to use dry-wet hydrogen combination along with argon to avoid gas pores and hydrogen-embrittlement.

Another alternative approach in liquid phase sintering is to sinter alloys under vacuum conditions. Vacuum sintering provide greatest densification rate, resulting in near full density. Sintering in a vacuum eliminates the pore gas pressure effective, giving rapid and complete densification.

Scanning auger electron microscopy has been used to examine the distribution of impurity elements on the fracture surface of W-Ni-Fe alloys. On the interphase boundaries between the fcc Ni-based matrix phase and the tungsten particles, segregation levels of phosphorus have been observed in as-sintered, furnace-cooled specimens. The phosphorus is homogeneously distributed but at fracture surface the it

adheres preferentially to the matrix phase. High temperature heat treatment at 1350°C followed by water quenching reduces significantly the phosphorus segregation and improve the degree of cohesion across the boundaries [19].

Pre sintering

It is the pre-processing step before sintering, which exhibits better mechanical properties as compared as sintered specimen [20]. The hypothesis says that impurity elements like O, C, P, K, are much concentrated at the inter phase boundaries for without pre-sintered material, so their ductility is very poor, since the strength of boundaries are weaker than that of Tungsten particles. While loading (charpy impact testing) the separation of boundaries occurs before the material starts to deform.

2.3 POST SINTERING TREATMENTS

In the present research post-sintering treatment refers to cold working and post sintering heat treatments. Post sintering treatment is often offered inorder to eliminate residual hydrogen and there by prevent hydrogen embrittlement, homogeneously redistribute any impurity present and prevent the formation of intermetallic phases at the tungsten-matrix interface [21].

Cold working particularly swaging is the major strengthening method that is used for tungsten heavy alloys. As a result of cold working the strength is increased but toughness and ductility is decreased [22].

Kohno and Mayama [20] showed that the mechanical properties of W-3.5Ni-1.5Fe could be much improved by post sintering treatments and the sample content impurity elements like C, P, and K.

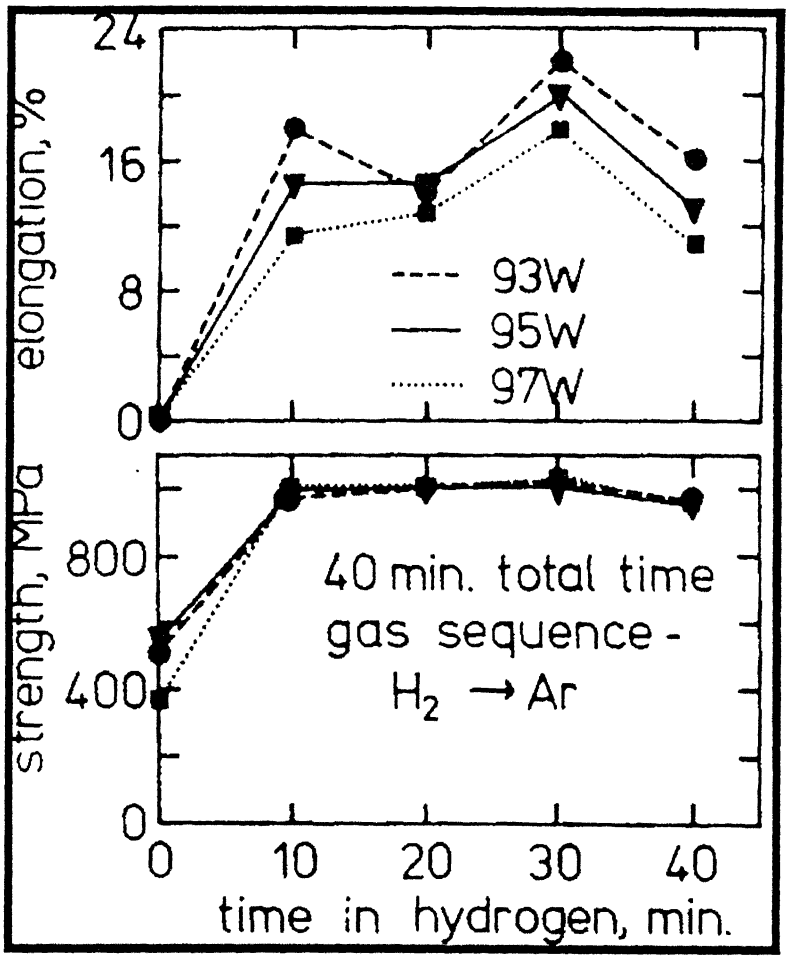

Figure 2.15. The influence of atmosphere change (from hydrogen to argon) upon strength and elongation [18].

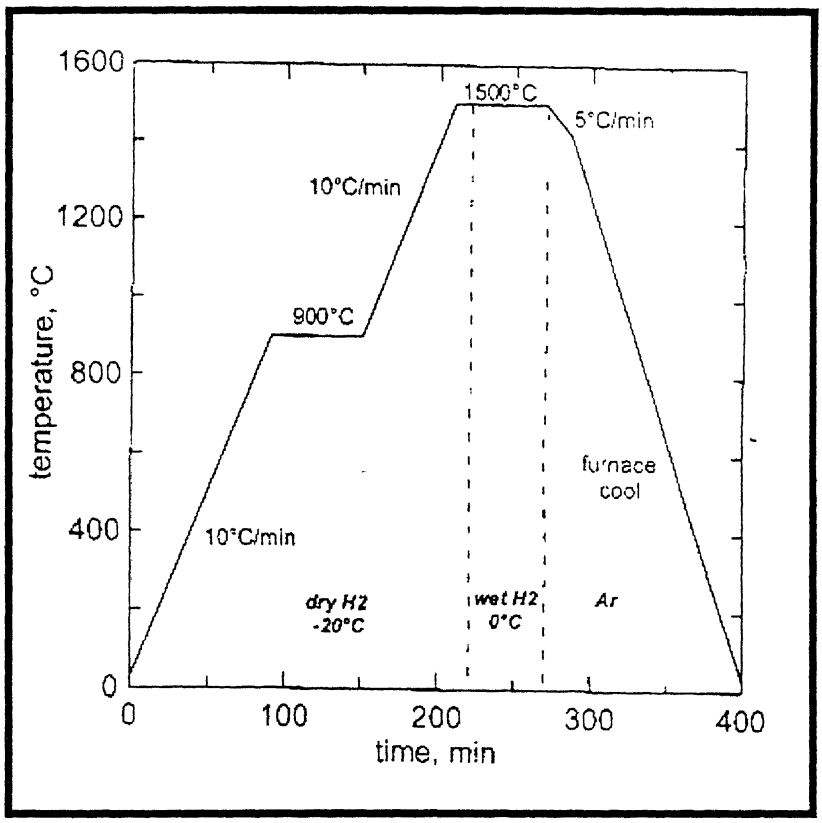

Figure 2.16. Typical sintering cycle for a tungsten heavy alloy [14].

Water Quenched Sample

This process shows heating at 1150°C for 60 mins in Ar and subsequent quenching into water, showed improved mechanical properties as compared to as sintered one.

Furnace Cooled Sample

Heating the specimen at 1150°C for 60 min. in Ar and subsequent furnace cooling gives better mechanical properties as compared to sintered specimens. The specimen which were furnace cooled from 1150°C , however show poorer ductility and toughness as compared to quenched one and it seems that the poorer mechanical properties of sintered specimen that were furnace cooled from 1150°C are due to interfacial segregation of impurity elements in the matrix phase which is made possible by keeping the samples at high temperature and their segregation is reduced by quenching. If it is compared that in the cases of annealing the property is intermediate between as sintered and water quenched. Then one can easily interpret that there may be the percent of dissolution of impurities in the matrix phase is intermediate between other two conditions.

Vacuum Treated Sample:

Yoon et al. [23] described about the enhancement of mechanical property (UTS, % elongation) by vacuum treatment of W-Ni-Fe alloys. First he compacts were pre sintered at 950°C for 1 h and sintered at 1400°C for 1 h in flowing H_2 atmosphere. Then the sintered specimen were heat treated under vacuum at a temperature between 400°C, and 1000°C for various times. The heating and cooling rates were similar to that of sintering treatments.

They found that the heat treatment in the hydrogen leads to decreased mechanical property, which shows that hydrogen embrittlement occur in WHAs, which drastically reduces the %elongation. As the matrix content is lowered all the hydrogen assumed to be contained mainly inside the matrix, but the strong embrittling effect of H_2 in the alloy is removed by treating in vacuum due to diffusion of H_2 from the matrix interface. For relatively small specimens of 2 mm in radius the embrittlement effect can be removed in short times at temperatures above 600°C. For larger specimens, the required heat treatment time will increase in proportion to the square of their lineal

dimension. So for a longer specimen the practical approach may be heat-treating in the temperature range of 800 to1000°C.

2.4 Mechanical Working

The importance of metal in modern technology is due, in large part, to the ease with which they may be formed into useful shapes such as tubes, rods, and sheets. Useful shape may be generated in two basic ways:

- By plastic deformation process in which volume and mass of metal are conserved and the metal is displaced from one location to another.
- By metal removal or machining process in which material is removed in order to give it required shape.

However in this research major emphasis is given to plastic deformation process that is swaging. Swaging is a mechanical deformation technique of reducing or shaping the cross-section of rods or tubes by means of repeated impacts or blows. The swaging process consists of dies, which are given the requisite external shape. These dies intermittently hammer the stock to produce the deformation. This hammering action, besides producing the necessary shape, ensures good surface qualities, better grain structure and higher tensile strength. It is very simple and can be carried out by unskilled operator.

Most sintered alloys have some residual porosity in as-sintered condition. Different pressure working process (extrusion, pressing, forging, rolling etc.) is used to decrease porosity. Mechanical working of powder metallurgy materials not only leads to consolidation of materials but also change the structure and sub structure of materials, which implies change in grain size and variation of substructure as well. During plastic deformation process not only pores but also segregation of impurities are also changed. Plastic deformation is also used for hot and cold powder pressing. Final mechanical properties of powder metallurgy materials depends upon the grain size, dislocation substructure, deformation texture, porosity and segregation of impurities [24]. Figures 2.17 and 2.18 shows the microstructure of swaged specimens.

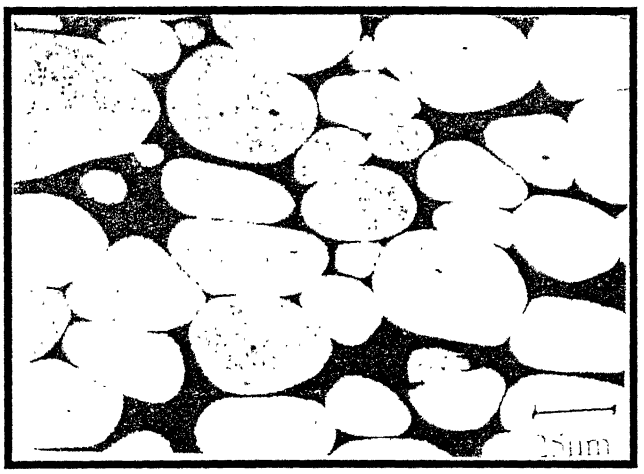

Figure 2.17. Optical micrograph of 30% swaged tungsten heavy alloy [6].

Figure 2.18. Optical micrograph of 80% swaged tungsten heavy alloy [6].

It was assumed that for commercially pure metals cold deformation temperature corresponds to the temperature T< 0.4Tm, warm deformation corresponds to 0.4Tm< T< 0.6Tm and hot deformation to T>0.5Tm. Here Tm is the melting point. The temperature ranges of cold, warm and hot deformation shall be determined by the evolution in the deformation process of grain structure and dislocation substructure and depends on the values of characteristics deformation temperature, and recrystallization temperature. Characteristic deformation temperature is the temperature below which crystal lattice resistance to dislocation movement (Peierls-Nabarro stress) becomes significant. An approach to fundamentals of hot, warm and cold deformation has to be developed not in connection with the necessity of metal heating or cooling but on the basis of structural changes on the deformation process.

Hot deformation is the plastic deformation above dynamic recrystallization temperature. During hot deformation equiaxed grains with low dislocation density and low internal stresses level are formed in the metal. It is often used for primary working of cast metal and sintered powder billets. But during such deformation it is impossible to succeed in forming small-grained structure and also in forming cellular grain structure. When the equilibrium is reached between the process of strain hardening and softening, and grains size is determined by the temperature and degree of deformation. Hot plastic deformation produces fine-grained metal with little variation in grain size. At lower temperature deformation may be warm or cold. Recrystallization is not observed in warm and cold deformation processes; rather initial equi axed grain after plastic deformation becomes non-equiaxed. Figure 2.19 shows the influence of cold, warm and hot deformation on grain and sub grain structure.

For anti-armour kinetic energy penetrators the primary driving force for the advancement of tungsten heavy alloy has been focused on the production of fibrous microstructure in the material. Some of the research has been carried out on the determination of mechanical properties of mechanical worked material [25]. Mechanical deformation of up to 20-30% has been found to be useful for the development of successful penetrator.

Deformation kind	Hot deformation	Warm deformation	Cold deformation
Deformation temperature	$T > T_r$	$T^* < T < T_r$	$T < T^*$
Grain and dislocation structure	equiaxed grain structure, low dislocation density $\rho<10^6 \div 10^8 cm^{-2}$ 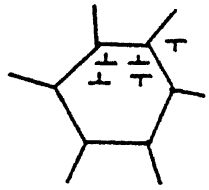	non-equiaxed grain structure, cellular dislocation structure $T<0.8T_r$ $T>0.8T_r$ 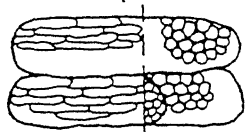 non-equiaxed cells equiaxed cells	non-equiaxed grain structure, random dislocation structure (dislocation forest) $\rho>10^8 \div 10^{10} cm^{-2}$ 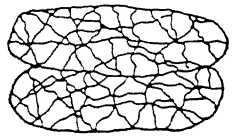
Strain hardening	low or zero	grows rapidly with increase of deformation to the ε_c, than grows slowly, $\varepsilon_c \sim \sigma_{ef}^2 \cdot d$	grows rapidly and monotonically with the increase of deformation degree to fracture
	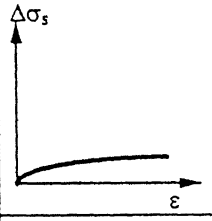	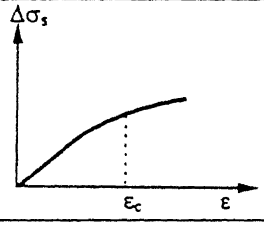	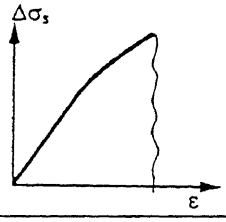
Fracture mechanism	ductile	ductile or quasibrittle	brittle or quasibrittle
Activation energy of plastic deformation	activation energy of self-diffusion	activation energy of dislocation movement	activation energy of dislocation movement

Figure 2.19. The influence of cold, warm and hot deformation on grain and sub grain structure and on deformation and fracture mechanisms [24].

Beyond this the strength decreases. But M.C. Hogwood et al [25] found that in creating fibrous microstructure careful selection of process parameters permits the use high deformation up to 90% to be achieved without the need for remedial heat treatment.

Table 2.1 : gives the comparison of fibrous material after first stage deformation and material swaged by 30%.

Alloy Condition	0.2% Proof Stress Mpa	UTS Mpa	Elongation (%)
90% Reduction	1430	1530	2
30% Swaged	1195	1210	11

2.5 THERMO-MECHANICAL PROCESSING.

The development of high strength materials, coupled with good formability, has always been the aim of material scientists. The demand for such a combination has increased considerably during the last few decades because of ever increasing applications in the areas of space, deep sea and high pressure technology. Alloying, mechanical working, heattreatment, grain size control and nuclear irradiation's are some of the techniques, which may be taken recourse to individually or in combination for this purpose. Individually each one of them has strengthening effect. Inorder to attain enhanced properties; various combinations of these unit operations may be adopted advantageously. Thermomechanical treatment is one such combination. As the name suggests, it is a combination of mechanical working followed by heat treatment.

Cold Working and Annealing

Srikanth and Upadhyaya [22] reported about the effect of cold working followed by annealing at 700°C for varying periods of 90W-7Ni-3Fe heavy alloys. Cold swaging without any intermediate annealing was carried out on a specimen, which was earlier sintered in hydrogen so as to undergo 25,35 and 50% reductions in the area of as received rods. Both as received and swaged rods were annealed at

700°C for varying periods namely 30 to 120 min., which was further tensile, tested. Figure 2.20 shows the various mechanical properties variation after annealing of as received and cold worked heavy alloy samples. In the case of as received samples the hardness value increase with increasing annealing period, up to 60 min. and later decreases, where as ultimate tensile strength increase with increasing annealing period and then decrease followed by an increase. For all the cold worked samples hardness value decrease with increasing annealing period due to phenomena of recovery, where as for all the cold worked samples the ultimate tensile strength values initially increase with annealing period and remain almost constant up to 60 min followed by a subsequent increase. The variation of percentage elongation with respect to annealing period also shows a qualitatively similar trend to that of ultimate tensile strength variation. Figure 2.21 shows that, the hardness value increases with increase in percentage of cold deformation for any annealing period. For any fixed annealing period, percentage elongation increases with increase in degree of cold deformation. On the other hand for zero and 30 min annealing period, these values initially decrease with increase in degree of cold working followed by an increase. For 60 and 90 min annealing periods ultimate tensile strength and yield strength generally increase with increase in degree of cold working.

The basic reason for increasing ductility as a result of annealing after cold working is that during cold working increase in dislocation density occurs resulting in increased strength as compared to as-received alloys and on further annealing easier diffusion of hydrogen atoms takes place from dislocation network there by increasing its ductility.

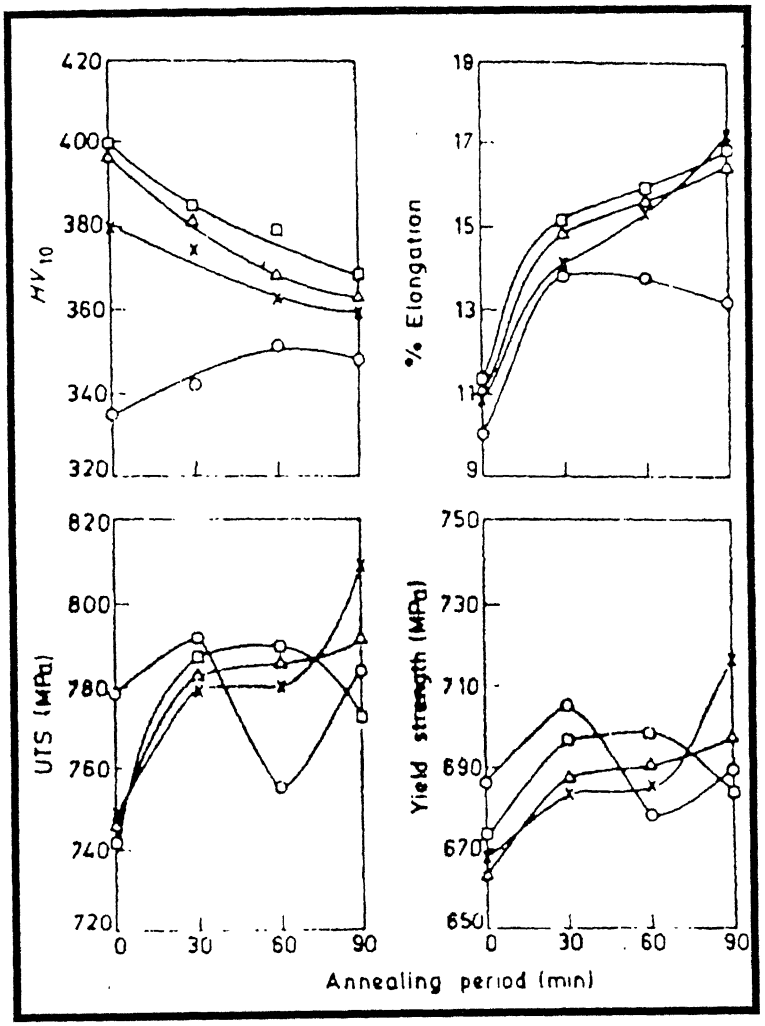

Figure 2.20. Variation of hardness, UTS, yield strength and % elongation of cold swaged 90W-3Fe-7Ni alloys with respect to annealing period at 700°C. Cold reduction(o) 0%. (x)25%, (∇) 30%, (□) 50% [22].

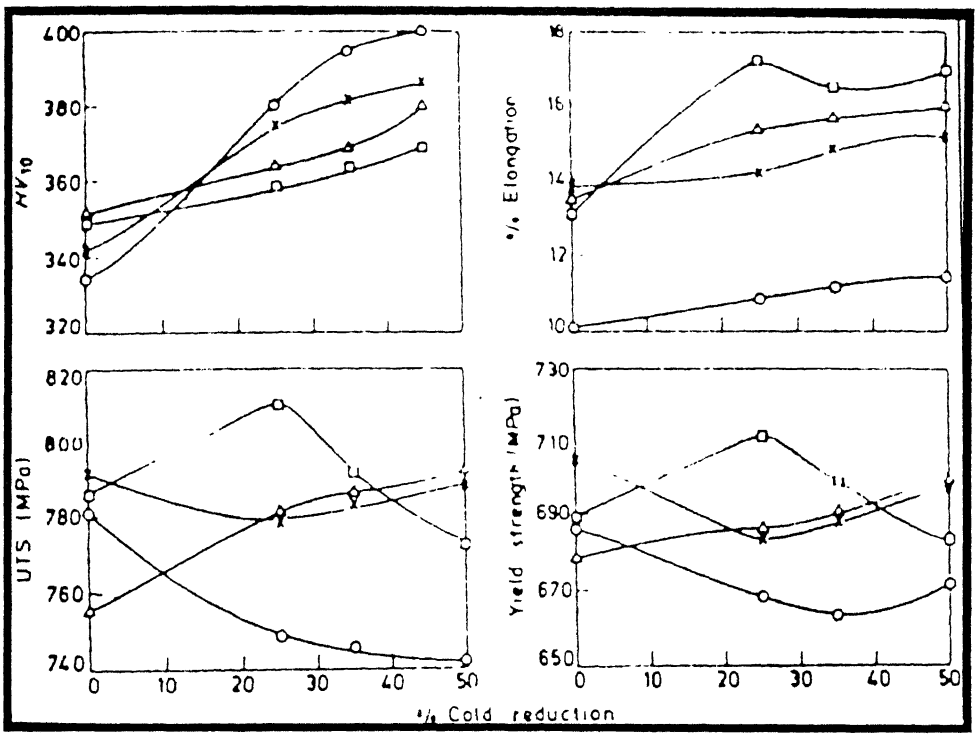

Figure 2.21. variation of hardness, UTS, Yield strength and % elongation of differently annealed 90W-7Ni-3Fe alloys with respect to degree of cold reduction. Annealing period (min). (X) 30, (∇) 60, (□) 90 [22].

The results shows that hardness values of worked and annealed heavy alloys increase with increase in degree of cold work. This may be due to stored energy associated with the cold worked specimens.

Micro Structural Influence on Degree of Cold working.

A narrow inter-particle distance between tungsten spheroids is observed with increase in degree of cold working, which leads to the increase in the ultimate tensile strength. The increase in ductility with increase in annealing period for the cold worked alloys appears to be related to easier diffusion of hydrogen atoms from the dislocation network, as sintered atmosphere contains hydrogen. Finally they have concluded that the strength and ductility levels increase with extent of cold working at any set of annealing period.

Cold Worked and Solid State Sintered

Mitkov and Kaysser [26] prepared 90W-7Ni-3Fe alloys by liquid phase sintering at 1470°C in flowing dry H_2. The sintered samples were given a height reduction of 5 to 50% and solid state sintered at 1420°C for 3 min. During solid-state state sintering of cold deformed W heavy alloy new grains form at contact areas and the interior of original W grains.

In sample reduced by 15 %, new recrysrtallized grains of diameter around 6 μm are formed, however as incase of 50% reduced samples recrystallized grains are formed mostly at contact areas, between original W grains. The microstructure that has 25% forged sample and solid state sintered for 3 minutes and 40 minutes. In case of prolonged heating (40minutes) the recrystalliozed grains grow into the interior of original W grains forming new grain boundaries, and which are wavy shape in nature.

Cold worked and liquid phase sintered

Muginstein and Rosen [27] studied about tungsten heavy alloy of same composition 90W-7Ni-3Fe, which was cold worked, and heat-treated for periods of 20 to120s. Their main aim was to refine the microstructure, which leads to enhanced strength and ductility. All the microstructures signify about the disintegration and further recrystallization of the elongated grains. At 40s of heating penetration of liquid matrix start to take place causing very small disintegration of elongated grains. On further increasing time period of heating all the elongated grains divides into

small-recrystallized grains at 50s. In case of 60 and 70s of heating the micrographs results into a homogenous microstructures of small rounded grains, but there may be slight grain growth for 70s. 120s of heating damaged the specimen by melting the centre part partially. Since in all the above cases temperature was almost constant and the variation is due to time period. Figure 2.22 shows a schematic representation of micro structural development during solid state sintering and liquid phase sintering.

Liquid film penetration during Liquid Phase Sintering.

The penetration mechanism of thin liquid films along the boundaries is not yet clear. However it was observed that penetration reduces the grain size instead of usual grain coarsening. After liquid phase liquid phase layers replaced sintering initial boundaries. So it suggests that specific boundary energy is smaller than twice the surface energy before deformation, but it is larger after deformation.

Figure 2.23 shows a model where a liquid film of approximately 1 micrometer penetrates along prior grain boundaries. At the top of the penetrating liquid film, material with high dislocation densities dissolves in the melt, diffuses along the melt layer and precipitates at solid/liquid interfaces, which are not part of contact areas [26]. Here it was reported that varying the type and amount of solute atoms added could change the rate of chemically induced liquid film migration. This was observed during prolonged liquid phase sintering. The detachment of grain from poly crystalline materials areas requires the penetration of melt along the grain boundaries. The detachment also requires sufficient cross-sectional area during grain movement and a certain spherodization of grains at triple junction and at the nodes of four adjacent grains. However Mitkov and Kaysser have not mentioned about the influences of mechanical properties during liquid phase sintering of cold worked alloys. So it is my hypothesis that due to formation of new grains at contacts areas and in the interior of original single crystal tungsten grains the hardness increases gradually with increase in tungsten content, but to get the strength in combination with hardness we have to optimize the time and temperature of heat treatment.

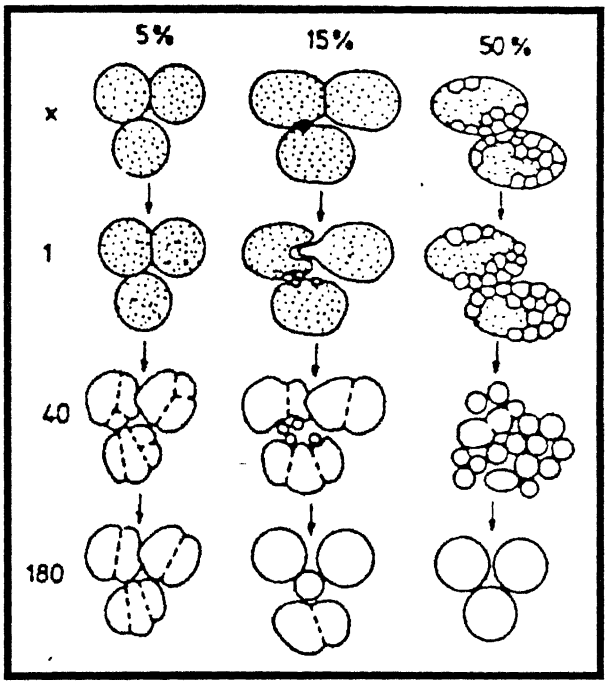

Figure 2.22. Schematic description of microstructural development during solid state sintering and liquid phase sintering at 1470°C for 1. 40, 180 min [26].

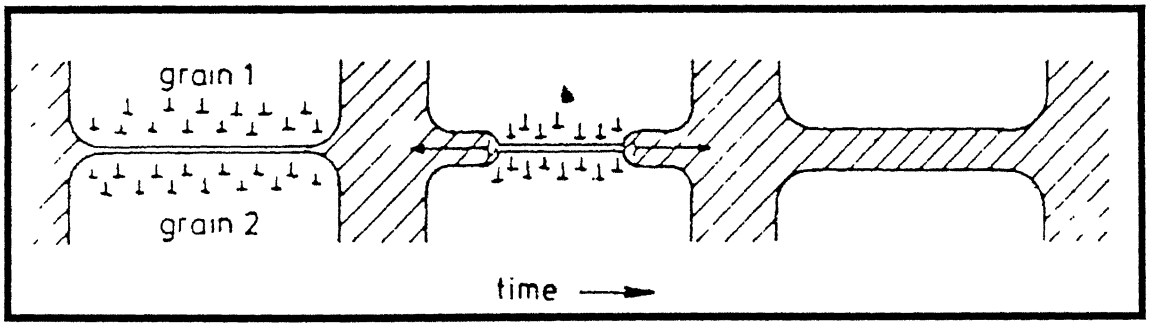

Figure 2.23. Schematic representation of the penetration of a melt layer along a deformed boundary between original tungsten grains [26].

Primary reduction followed by multiple secondary reductions

Leonard and Magness [28] who performed thermo-mechanical study which consists of primary reduction by extrusion, followed by multiple secondary reductions by swaging with intermediate anneals for WHAs containing 93 and 96% W composites. In this process total reduction was achieved. The sample was preheated to 1000°C before extrusion. The combination of strength and ductility developed in two TM processed alloys represent significant improvement over those found in conventionally processed alloys.

Table 2.2 shows that 96% W TM processed alloys show better combination of strength and ductility as compared to 93 % W. Higher density alloys usually have lower ductility than lower WHAs due to smaller volume fraction of the ductile matrix.

Application of intermediate cold swaging to hot rolled and hot swaged specimens.

93W-4.9Ni-2.1Fe heavy alloys were prepared by liquid phase sintering. The sintered specimens were subjected to hot rolling and hot swaging. The hot rolling and hot swaging operation were performed immediately after annealing at 1150°C for 30 min in flowing argon atmosphere [29]. The ratios of hot rolling and hot swaging operation were up to 50 and 60% respectively. It is clearly seen that the W/W grain boundaries in cyclically heat-treated specimens were replaced with W/matrix interfaces by matrix penetration into W/W grain boundaries, as compared to as sintered specimens, the matrix penetration is due to the thermal stresses caused by co-efficient of thermal expansion difference between matrix phase and tungsten grains. During hot swaging process, the thermal stresses due to the co-efficient of thermal expansion difference as well as the mechanical stress caused by the applied stress are concomitantly introduced into W/W grain boundaries. Matrix penetration arises due to thermal stress but promoted by mechanical stress. The matrix penetration in case of hot rolling process is more dominant as compared to hot swaging process. Because the co-efficient of thermal expansion is larger than that of W grains. During hot rolling when the W/W grain boundaries were parallel to the rolling direction the matrix was partially penetrated. Generally the W/W grain boundaries can be replaced with the strong W-matrix interfaces by the application of tensile stress. So as a result of which the application of both mechanical and thermal stresses to the materials may be reflected in the mechanical properties of W heavy alloy.

Alloy Chemistry and Processing History	Hardness Rc	Yield Strength MPa	UTS MPa	Tensile Elongation %
93%W TM-Processed	48	1447	1640	13
93W-4.9Ni-2.1Fe Swaged 8% RA	39	1075	1157	14.7
93W-4.9Ni-2.1Fe Swaged 18% RA, Aged	44	1272	1344	5.2
93W-4.9Ni-2.1Fe 80% RA by Extrusion	43	1227	1496	3.3
96%W TM Processed	45	1399	1454	15
93W-4.9Ni-2.1Fe Swaged 18%RA	41	1116	1197	13.4
96W-2.8Ni-1.2Fe Swaged 12% RA	40		1103	5.9

Table 2.2. Mechanical Properties of Representative WHAs [28].

During hot swaging process, the thermal stresses due to the co-efficient of thermal expansion difference as well as the mechanical stress caused by the applied stress are concomitantly introduced into W/W grain boundaries. Matrix penetration arises due to thermal stress but promoted by mechanical stress. The matrix penetration in case of hot rolling process is more dominant as compared to hot swaging process. Because the co-efficient of thermal expansion is larger than that of W grains. During hot rolling when the W/W grain boundaries were parallel to the rolling direction the matrix was partially penetrated. Generally the W/W grain boundaries can be replaced with the strong W-matrix interfaces by the application of tensile stress. So as a result of which the application of both mechanical and thermal stresses to the materials may be reflected in the mechanical properties of W-heavy alloy.

For development of high strength and toughness fibrous microstructures in W-Ni-Fe alloys for kinetic energy penetrator application, it has been usual practice to produce a microstructure of ellipsoidal tungsten grains in a matrix phase by imparting mechanical deformation levels up to 30%. The research also says that the processing routes for producing fibrous microstructures in such alloys can be utilised for producing exceptional mechanical properties, like tensile strength levels in excess of 1700 Mpa, elongation to failure of 15% and toughness values four times that of existing tungsten penetrator alloys. Figure 2.24 shows the variation of UTS and Elongation with respect to ageing temperatures. Here the alloys have been swaged to three stages of deformation (30, 90, 95%). The figure demonstrates that the strength levels achieved from new materials are some 300Mpa higher than that can be achieved from swaged materials. That is at low ageing temperatures there is progressive reduction in strength levels. It is thought that this ageing behaviour is due to precipitation of Ni and Fe within the tungsten grains which causes hardening while at higher heat treatment temperatures there is softening due to dislocation rearrangement and the coarsening of intergranular precipitates. Also there is tendency for growth of precipitates on the tungsten-tungsten grain boundaries. Some of the research have been carried out about the ageing treatment of W-Ni-Fe alloys [30].

2.6 Mechanical Properties of W-Ni-Fe Alloys

The mechanical properties of tungsten and tungsten alloys have long been of interest. These properties are often used to glean valuable information about the quality of prior processing, and are important tool in assessing the overall calibre of the final product. In fact the bond strength between tungsten and matrix critically influences mechanical properties of W-Ni-Fe alloys.

2.6.1. Static Mechanical Behaviour

Static mechanical behaviour refers to application of load with low strain rates generally ($< 10^{-2}\ s^{-1}$).

K.O.Zamora *etal*, [31] studied about the influence of temperature and strain rate on the strength and ductility of high W content W-Ni-Fe alloys (93.5and 95.5 %W). The strain rate was 10^{-4} per sec to 10^{-1} per sec and static in the temperature range of 300 to 1000°C and they found that almost the same behaviour of mechanical property as described earlier. Fractographic evidence shows that the progress loss of ductility at high temperature is due to the beginning of W-matrix interface, which is attributed to the existence of the segregation induced W matrix interfacial phenomenon [31]. Figure 2.25 corresponds to the variation yield strength for 2 WHAs as a function of temperature and strain rate (a) 93.4 %W (b) 95 % W .

At 500°C the curve shows an inflection, perhaps linked to the condition of the mechanisms, controlling the kinetics of plastic deformation of composites. Below 200°C, the increase in yield strength is probably linked to the low temperature plastic regime W, controlled by the pearls stress of its screw dislocations. Figure 2.26 shows the true stress-true plastic strain curves of 95% WHA at 200°C at three different strain rates. At intermediate strain rate the yield strength nearly surpasses the yield strength at high strain rate. WHA also display static strength age hardening at a regular temperature interval, which shows the dynamic strain aging takes place when the static loaded specimens are used for a long time at different temperatures.

There is a correlation between fracture surface appearance and the ductility levels, because fracture strength determines the ductility. At 300°C the ductility is more than twice than the room temperature, which is due to concurrent dynamic strain

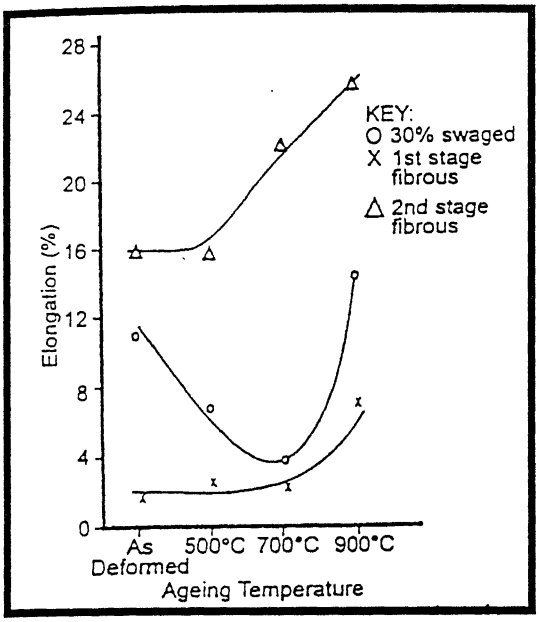

(a)

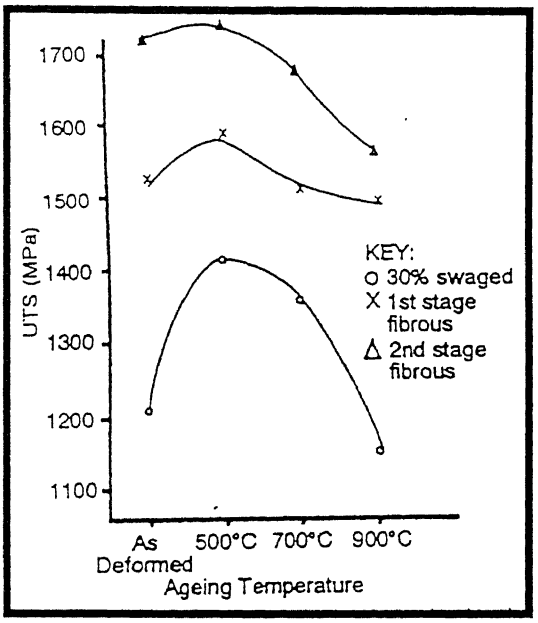

(b)

Figure 2.24. (a) Variation of % of elongation and (b) UTS as a function of ageing of temperature [25].

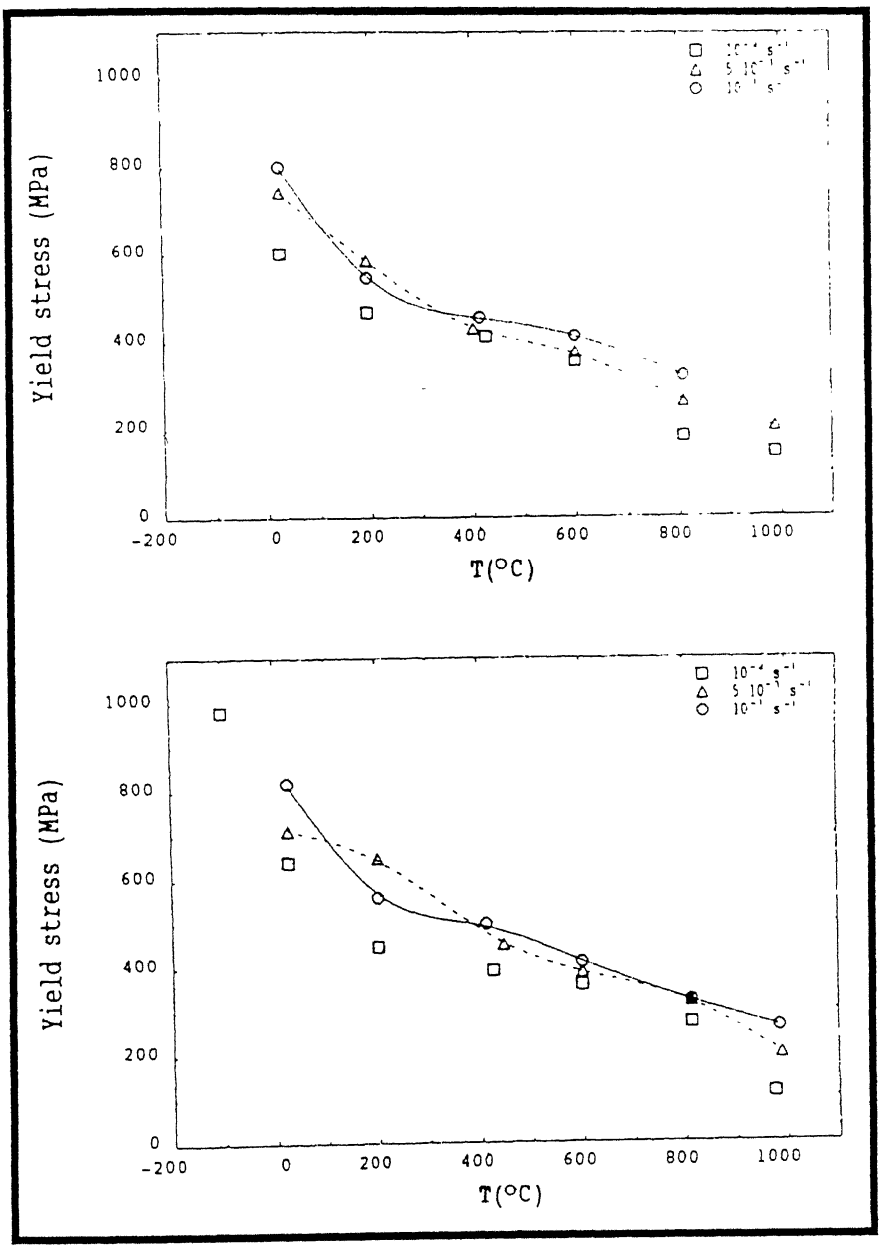

Figure 2.25. Yield stress (ϵ=0.2%) of W-Ni-Fe alloy as a function of temperature and strain rate. (a) 93.4% W, (b) 95% W [31].

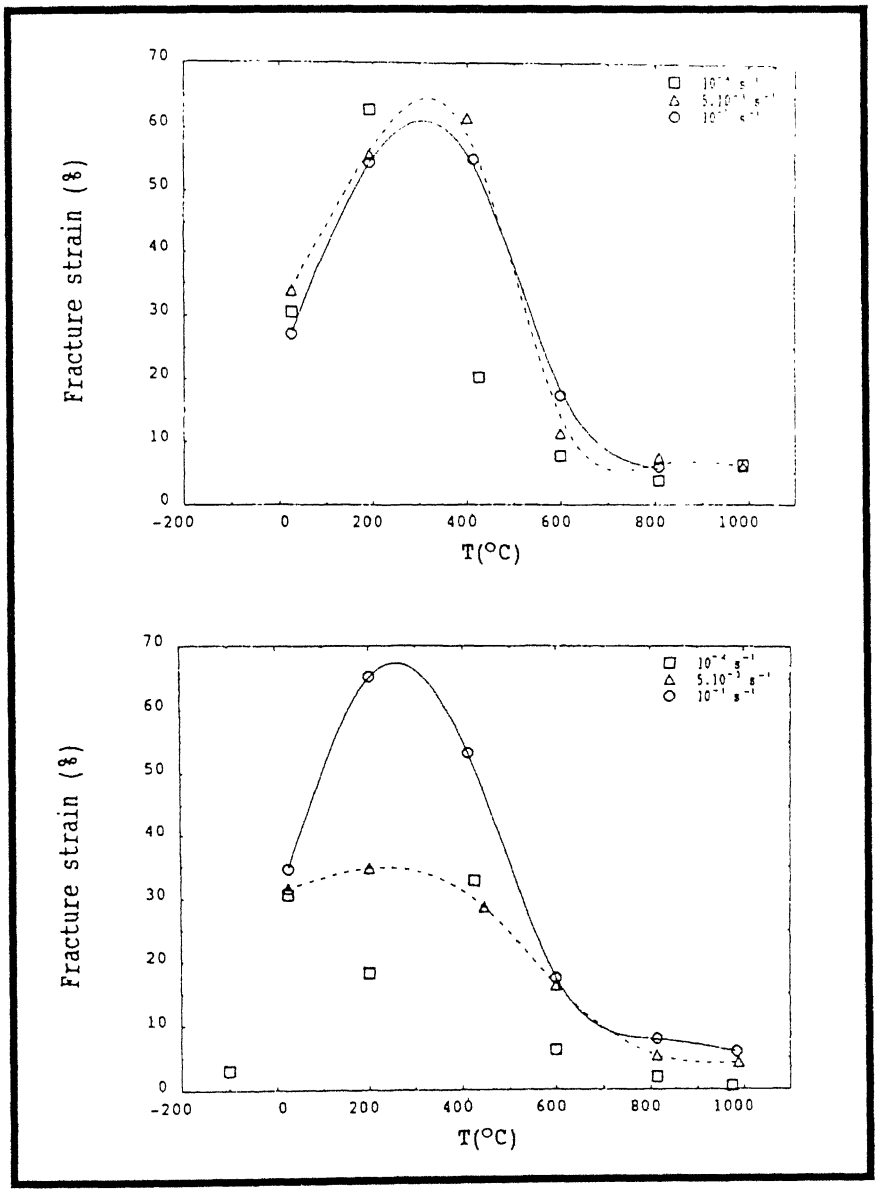

Figure 2.26. True strain at fracture in tensile test vs. deformation temperature. (a) 93.4% W (b) 95%W [31].

Aging actively superposed to the ductilizing effect of increasing temperature. When the fracture strain exceeds 30% trans granular cleavage prevails. Keeping the temperature constants at high strain rates the cleavage fracture are more prevalent than at room temperature Ductility drops dramatically beyond 600°C is associated to a dramatic loss of W-matrix adherence.

Doepker *et al* [21] also studied about the static loading of the W-Ni-Fe alloys having Ni to Fe ratio of 7, 8, and 9.

They also found that working at low temperature always preferred in order to obtain best combination of UTS and ductility. Swaging at above 600°C generally the material undergoes aging in the working temperature range of 300to 350°C, though it avoids formation of voids, but it leads embrittlement due to aging. So the best working temperature is 300 to 350°C.

2.6.2 Dynamic mechanical behaviour, of W-Ni-Fe alloys

Dynamic deformation refers to high loading rate (up to 10^6 s^{-1}) deformation. More over the ballistic performance of penetrator materials is independent of the static properties [31]. So it is essential to study the behavior of materials under high strain rate condition. The high strain rate behavior of W-Ni-Fe alloys was seldom studied until the mid-1980's, posssibly because prior to that time tungsten heavy alloys had not began to emerge as candidate materials for penetrator applications. Numerous investigators [32-34] have actively studied the behavior of tungsten heavy alloys under high strain rate condition . In these studies the material behavior is studied under a wide strain rate range. As a result of high loading rate involved special technique were involved. The most widely used technique includes: Hopkinson (kolsky) bar in tension (10^2 to 10^4 s^{-1}); and Hopkinson bar in compression (200 to $10^4 s^{-1}$); Taylor impact testing techniques (10^4 – 10^5 s^{-1}). There are two trends associated with the strain dependence of tungsten heavy alloys. The first trend is that as strain rate increases strength (yield strength and fracture strength) increases while elongation (strain to fracture) decreases which is due to strain hardening [32]. When the alloys swaged to 17% and tested under torsion by using the Hopkinson Bar technique under strain rate ranging from quasistatic (0.0001 to 0.1 s^{-1}) to strain rate ($600s^{-1}$). Their results have shown that their yield and failure strength increase while elongation decreases with increasing strain rate (Figure 2.27). On further examination it can be interpreted that the flow stress increases with increasing

shear strain for low strain rates (0.0001 to 0.1 s^{-1}) which is due to work hardening effect, where as for high strain rates ($600s^{-1}$) flow stress decreases due to softening effects. Using a strain rate range of approximately 0.0004 to 40 s^{-1} corresponding to different cross head speeds, Bose *etal* [35] studied the strain rate and temperature effects on the mechanical properties of W-7Ni-3Fe alloys. Figure 2.28. Shows that strength increases where as ductility decreases with increasing strain rate. It also shows that as temperature increases, ductility increases and strength decreases which are attributed to thermal activation of dislocation movement. The alloys (W-4.9Ni-2.1Fe) were tested under strain rates up to 7x10 $5s^{-1}$ by using pressure-shear plate impact testing technique [36] it was found that there is significant dependence on strain rate, and softening occurs at high strain rates. More over it was observed that the alloy exhibit softening at high strain rates. Ramesh et al studied a W-Ni-Fe alloy containing 91%W and Nickel to iron ratio of 7:3 under high strain rates shearing deformation conditions ($300\text{-}1200s^{-1}$). The results revealed that the alloys exhibit strain

Deformation of penetrator and armor material generates high strain rates which hardly allows any time for dissipation of heat being generated, which results adiabatic heating. Condition causing heavy plastic deformation at the penetrator head. The deformation if not controlled results in a mushroom shaped, there by penetrrator performance decreases. The shear banding results in chisel head formation, which improves the K.E penetrator performance through self-sharpening effect causes by the deformation of penetration head in such a way so as to reduce the dia of head during penetration. For better K.E penetrator performance the onset plastic instability leading to shear banding is necessary. Figure 2.29 shows the application of tungsten heavy alloy as ideal kinetic energy penetrator. Figure 2.30 shows the schematic sketch of penetration deformation behaviour of DU and WHAs. In case of WHA penetrator, the very high melting point of W causes a thermal softening and in addition to that W is also highly rate sensitive with strength, which increases with increasing the strain rate. Both these factors delay the flow softening at high strain rates. So as a result due to delayed shear stress localization. WHA develop mushroom heads during penetration. As in the conventional WHAs, the localization of deformation and discard of their material occurred only after a large mushroom head had developed on the rod [28].

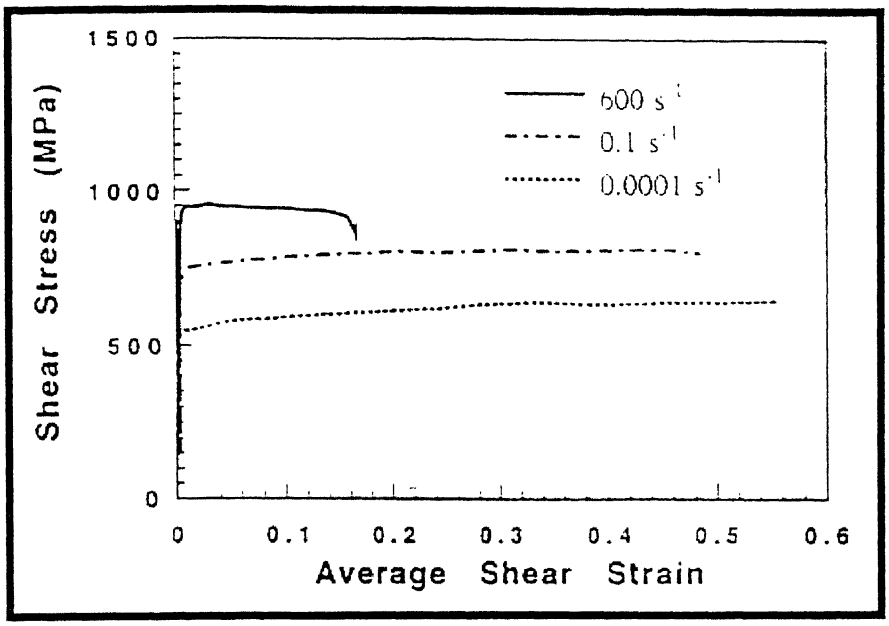

Figure 2.27. Shear stress-shear strain curves of 93W-5Ni-2Fe at different strain rates [39].

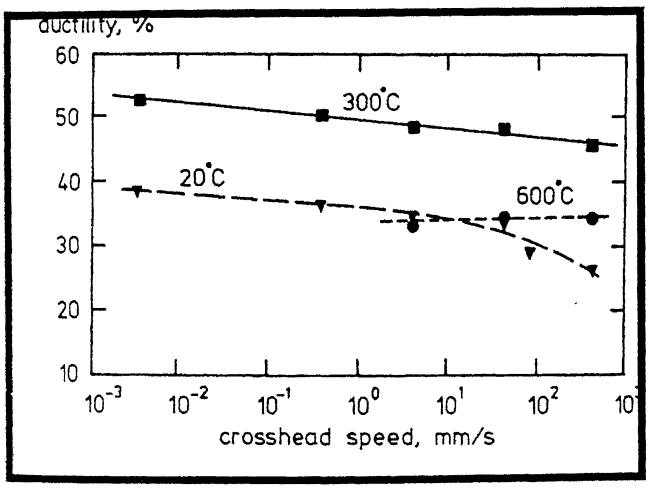

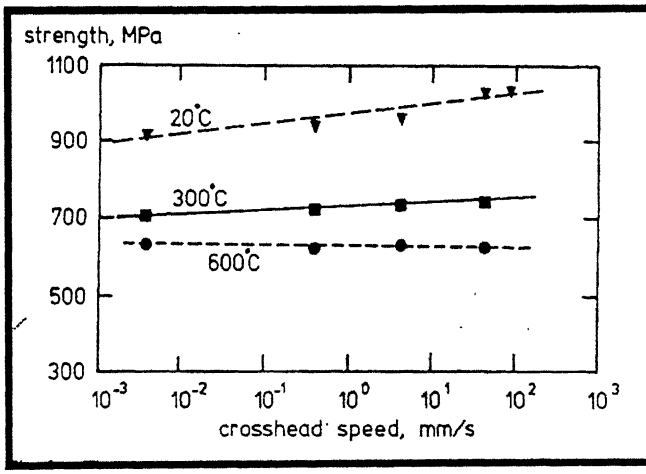

Figure 2.28. Ductility and strength variation with cross head speed and test temperature for 90W-7Ni-3Fe alloy [35].

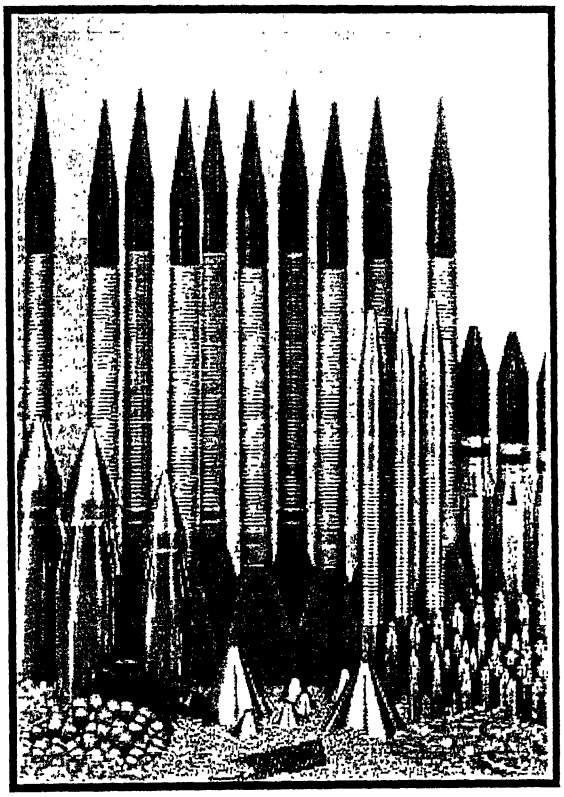

Figure 2.29. Application of tungsten heavy alloy as Kinetic energy penetrators and ammunitions [6].

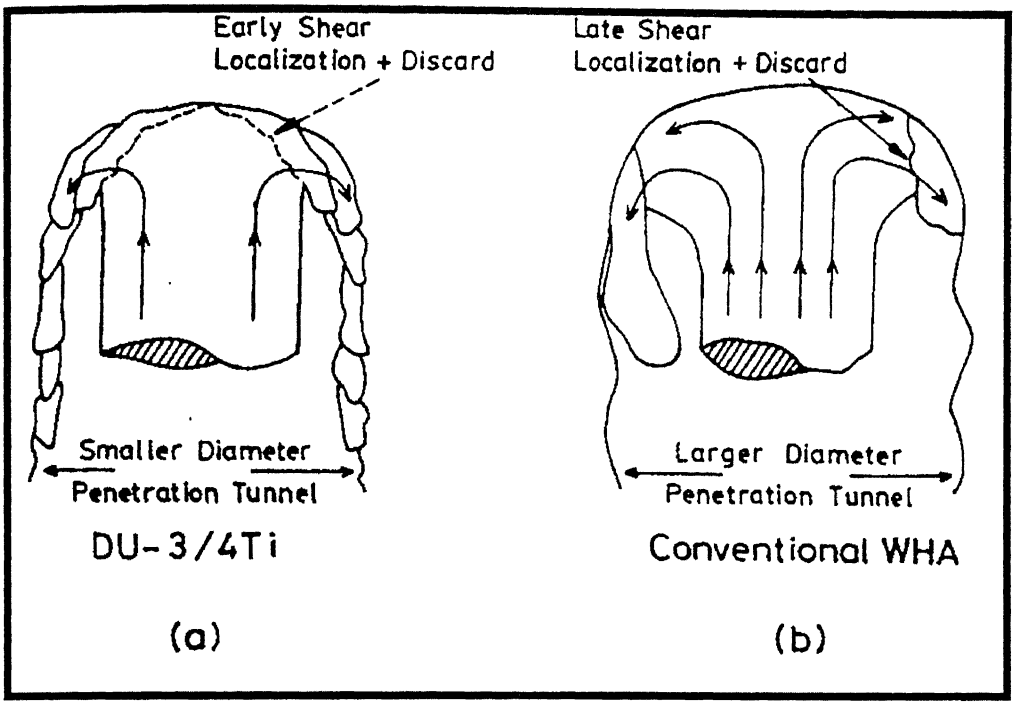

Figure 2.30. penetration deformation behavior of (a) DU and WHA penetrator [14].

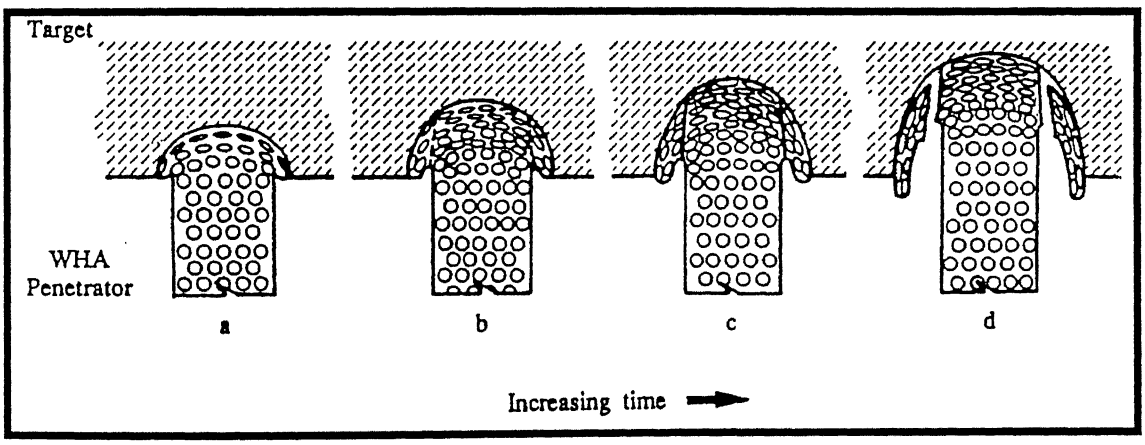

Figure 2.31. Schematic showing penetration of ideal tungsten heavy alloy Penetrator [31].

number of adjacent particles. Thus it becomes extremely difficult for the band to deform relatively large tungsten grains would create conditions unfavorable for shear localized cracking. The propensity for shear localization in tungsten heavy alloys of 90W-7Ni-3Fe decreases as the grain size increases. In case of alloy sintered for 240min, the shear induced cracks are formed, which is not found in case of 800 minutes sintered specimens. On the other hand the large matrix areas in case of 800 minutes sintered specimens probably large enough to initiate the process of shear localization, but it was found that the band was unable to propagate as it hit against the large tungsten grain size. Thus to process a tungsten heavy alloy which will have propensity for shear induced cracking during ballistic penetration which will allow easy propagation of an initiated shear band. Figure 2.32 shows the shear band formation, of 90W-7Ni-3Fe alloy at a strain rate of $5420s^{-1}$. The reason for above features has been described above.

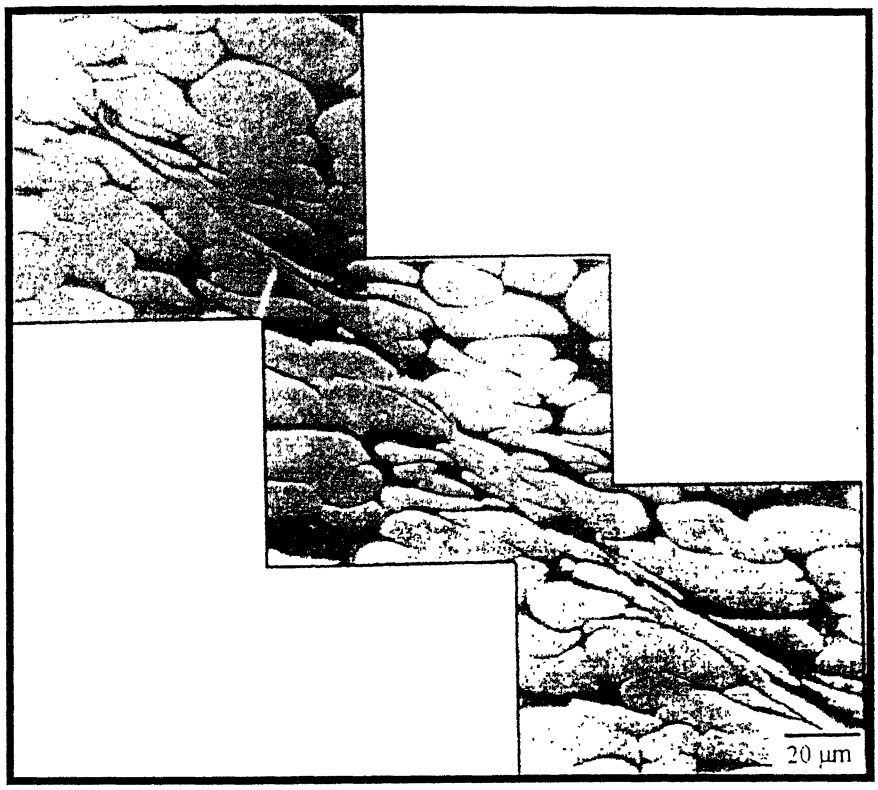

Figure 2.32. Shear band formation in the 90W-7Ni-3Fe alloy [14].

2.7 MICROSTRUCTURAL CHARACTERIZATION THROUGH STEREOLOGY.

All matter surrounding us can be described in terms of zero. One, two, three dimensions. Although the earliest work on quantitative microscopic analysis goes back to Delesse (1848), who proved mathematically that in a uniform rock the volume properties of the various minerals are equal to there area proportions, as viewed on a random sections. Microstructure basically is collection of lines, points, and surfaces, volumes in 3D. When we talk about microstructure, we are referring to the phase and constituents of material that are visible on a microscopic, rather than on an atomic or macroscopic scale,

Quantitative metallography or stereology deals with the estimation of properties of an particular material from the micro structural Parameters such as number of particles per unit volume (Nv), surface area per unit volume (Sv), volume fraction (Vv). Basically it attempts to characterize numerically the geometrical aspects of those features of microstructures, which are of interest, stereo logy relates to uniaxial viewing. Descriptive geometry, of which perspective within integral part, treats the represents of projection from objects of known three dimensional shapes if objects of similar shapes are arranged regularly in a space, many section planes or visual angles may be necessary. Whether a section plane must be place randomly through out the material or just displaced systematically parallel to itself depend upon the type of a structure orientation involved. In the case where as smaller number of similar objects of complicated sections are available, visual examination of random section are necessary. In this case projected images can be used for measurement.

So in this chapter we will deal with the microstructure characterization of thermo-mechanically treated W-Ni-Fe alloys of different compositions. The liquid phase sintered of WHA consists of features like grain coalescence (Oswald ripening), melt penetration within the grain; secondary fragments of W particle. Also it deals with isotropic and an isotropic arrangement of a microstructure. Based on the stereological measurements like putting random line in the structure, calculation of intersection of grain boundary, neck region by the line gives us an idea about the Sv, Vv of the tungsten particle. It also determines the dihedral angle; contiguity, connectivity, grain size and shape of phase, quantitative analysis of fracture failures

from typical microstructure, which is in fact, help full in determining the mechanical property like ductility, toughness, of the resulting product.

Microstructure of W-Ni-Fe Alloys.

A typical microstructure of W-Ni-Fe alloys produced by liquid phase sintering consists of spheroidized tungsten particles embedded in a Ni-Fe matrix. The particles are nearly pure tungsten with a body-centered structure (BCC). There are two discrete interfaces present in tungsten heavy alloys. The first is boundary between tungsten and matrix. The second is interface between the tungsten and tungsten.

2.7.1 2D Measurements.

Stereo logy deals with two types of properties that are metric property and topological properties. Metric property can be measured from the 2D, but topological property cannot be measured from 2D, (simplifying assumptions like all are spheres). We should distinguish among geometrical features that exists in a space, appear on the section plane or are generated by the test line or test plane. 2D measurements include calculation like Vv, Sv. P_l. The compound symbols represent fraction in which the numerator refers to the microstructure quantity and the denominator pertains to the reference quantity.

Basic Measurements

The following measurements are all performed on 2 dimensional sections on projection and involve simple point, lineal, area measurements. Mechanics of measurements are as follows:

Volume fraction

Consider the β particles embedded in α matrix, so by using "caveler's theorm" Vv of β can be calculated, which is

$$V=H.A$$

Where V= total volume

A=mean area

So finally $(Vv)_\beta = (A_A)_\beta$

Can be calculated by integrating for the whole element of the entire β particle.

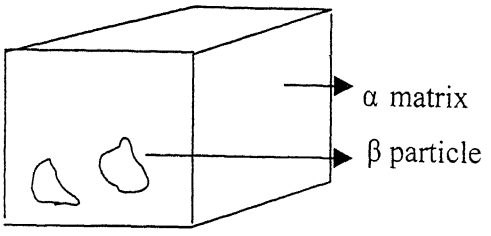

Pp measurements:

In these methods, a network of points is disposed uniformly over an ample area of all the microstructures. The number of points that falls over the areas of interest (say a phase β) is cemented for the first position of the grid. Then the grid is repositioned randomly, or translated in particular direction, and the number of points falling over the β phase is counted again. This process is repeated until a sufficient number of measurements have been obtained. The total number of points P falling over the particle is then divided by the total number of grid points Pt, to give the ratio P / Pt, denoted simply by *Pp*.

P_L Measurement:

P_L that is the number of points of intersections per unit length of test lines. A linear or circular test array is applied randomly to the microstructure in the section plane. The points usually of number of intersection made by test lines with traces of surfaces on the plane of polish. The test arrays may be applied randomly or dispersed systematically over entire microstructures. The actual length of L depends upon the magnification of the microstructures. The value of L can be determined at standard magnification with the help of a micron bar.

Statistical Analysis or Estimation of Errors.

Statistical analysis or estimation of errors is necessary for calculation of estimation of accuracy, which shows the viability of the data, measured from a given sample [39].

Errors are of three types:

1. Errors from experimental limitations: which include resolution of the microscope, etching effects, uncertainties in the length of test figure, in correct counting, and so on Improper sampling technique: During analysis it is necessary that randomisation

of process executed in truly random fashion. The test area should be selected at random fashion. The test area should be selected at random and the test figure applied at random, preferably without looking. If the observer makes a subjective decision, then some degree of bias will almost always be introduced. Bias is also introduced when the structural property being determined is not linearly related to the experimental measurements. For an example grain size numbers found by either ASTM or the intercept methods are representative of this type of bias. The magnitude of the bias is small, however and can usually be neglected.

2. A third error results from the non-representative samples, where by the areas selected for analysis is not exactly representative of the specimen as a whole. These sampling errors usually constitute the bulk of the total errors.

It is expected that the greater the number of observations involved in a measurement, the greater will be its reliability.

Sampling error also depends upon the method of measurement chosen. The choice must then be made on the relative effectiveness that is that method requires a least effort for a given accuracy.

Sampling error depends upon the type of microstructure and way of sampling. According to "central limit theorm" the sampling error can be calculated by performing N such tests. Consider β particles are embedded in a α matrix, so by putting a grid on the metallographic plane, where n_T is the total number of points and n number of points which fall on β phase then sample mean $< n >= \sum \frac{n_i}{N}$ and

$$S^2(n) = \sum \frac{(< n > - n_i)^2}{N-1}$$

where S^2 is sample variation

Mean n=<n>±2σ with 95% confidence

Increasing N decreases error. So as a whole the following basic relationships will be helpful in determining most of the 2D parameter. They are

1. $V_V = A_A = L_L = P_L$
2. $L_A = \pi / 2 \, P_L$
3. $S_V = 2P_L$

Connectivity:

Connectivity can be defined as degree of contact between two surfaces that is for an example in liquid phase sintered structures the connectivity can be measured between two surfaces (liquid solid surface, solid-solid surface) in terms of $C = S_V$ (s-s)/$S_{Vss} + S_{Vls}$. so we can know how much the surface connected.

Where C = connectivity and S_V =surface area per unit volume.

Contiguity measurements:

Srikanth and Upadhayaya [37] has cited about the variation of W spheroids of sintered Heavy Alloys. Contiguity is the measure of W-W contact area and its importance lies in understanding the mechanical behavior of W-Ni-Fe alloys. Contiguity increases with increase in the W content and maximum ductility could be obtained, where the least contiguity lies and lower the dihedral angle, the smaller is the contiguity. They found that the contiguity factor decreases with increasing binder composition, which causes formation of more melt and penetration into the W particle. Where as with increase in the sintering periods the contiguity factor for Heavy alloy composites decreases.

Bentley and Hogwood [30] reported about the characterization of material with respect to W grain size, axial ratio, contiguity, hardness and fracture morphology of two alloy containing 92.5% and 95% W which have been mechanically deformed by up to ~70% in area and aged at temperatures between 500°C to 1100°C.

In the 95 %W alloy micrographs, the W grains shape is not regular (in both cases the axial ratio =1), due to the impingement of W grains on one another, which could not grow well due to insufficient volume during liquid phase sintering. The W-W grain boundary contact area defined by the equation as follows

$$C_{aw} = \frac{a_{ww}}{a_{ww} + a_{wm}}$$

Where a_{ww} = average area of contact between adjacent grains.

a_{wm} = Average area of contact between a W-grain and the adjacent matrix.

Contiguity can also be measured metallographically by counting the number of intercepts per unit length of test line

$$C_w = \frac{2N_{ww}}{2N_{ww} + N_{wm}}$$

Where N_{ww} = Number of tungsten – tungsten grain boundaries intercepts

N_{wm} = Number W-matrix interface intercepted

The factor 2 arises because each W-W grain boundary associated with two W grains. Table 2.3 gives the contiguity for 92.5%W alloy in longitudinal direction.

Table 2.3: Contiguity for 92.5%W alloy [30].

% Amount of Deformations	Contiguity in Longitudinal Directions	Contiguity in Transverse Directions
0	0.26	0.26
32	0.32	0.33
47	0.32	0.30
73	0.24	0.27

As the deformation proceeds the W grain can not sustain all the deformation, so matrix fails, begins to deform and is forced into the gaps between the W grains (forming ribbons of matrix) decreasing contiguity. In transeverse direction the dimension of tungsten grain decreases, so microstructures are being opened up between the grains and filled with matrix phase.

Determining the topological invariants / curvatures.

Measurements of curvatures and topological properties of dual phase structures involves area, Pp, linear scans. These counts are performed on photomicrographs.

Since N_A count deals with only positive and negative loops, it cannot be supplied to parts of area boundary, such as tip of platelet, an inter-particle neck in sintered microstructures, or particular kind of interfaces containing the dual phase microstructures. So for the tungsten count must be used, because it doesn't suffer

from the edge effect problem, N_A calculation is preferred where the structure is relatively simple.

2.7.2 3D measurements

Basically this is a class of modern stereology which counts the number of particles per unit area, which can be measured by 3 techniques, those are:

- Disector
- Selector
- Nucleator

Methods of measurements

Disector technique: By taking small elements of metallographic specimens of thickness Δh and the plane of such type is called exclusion plane. As shown below this technique

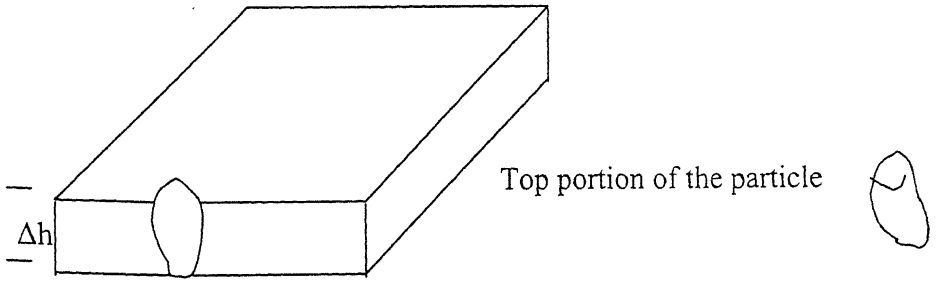

Count the heads and volumes of the particle and average them.

If N_v is the number of particles per unit volume which is defined by

N_v = number of particles with top/bottom portions/ $\Delta h\, A$

Where A= Area of the section, $N_A = D\, N_v$, Where N_v is the number of triple points per unit area and mean volume $E_N(V)$ can be calculated and that is equal to V_V / N_V and $E_N(S)$ = mean surface area $= S_V / N_v$ and $E_V(V)$ that is volume weighted (mean volume) is measured from

point sample intercept method equal to $\pi/3(\Sigma l_i^3/\Sigma i)$, where li is the random intercepts put over a particle like shown below

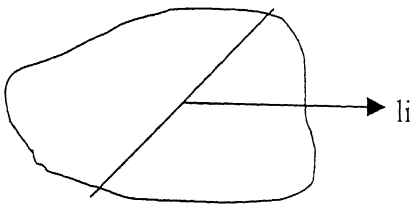

Selector: We need a stack of serial sections. If the structure is an isotropic, then we need to take sections of particles and put grids on it. Random intercepts mean random points in the particle and intercepts of random orientation through that point.

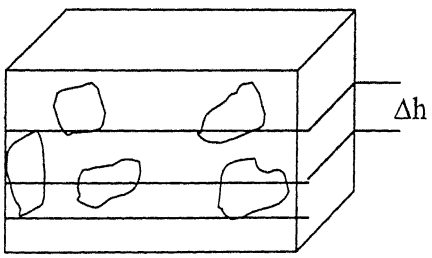

If H is the height of the cube and H> D max (maximum size of particle)

Δh< D min (minimum size of the particle)

So for this measurements consider some sample particles with respect to disector and on the sample particles perform sample intercept counts. If a point falls thrice in a particle, then consider the intercept twice, because it is the space we used to consider various sections (we can go for horizontal measurements also), for each particle we get total volume $V=\frac{\pi}{3}\left(\frac{\sum l_i^3}{N}\right)$

And $E_N(V) = V_V / N_V$

The basic advantage of this process is that we do not need to know the value of Δh and sampling is done by using number, volume, surface area and diameter. But this approach is difficult. Some of the sampling methods are shown below.

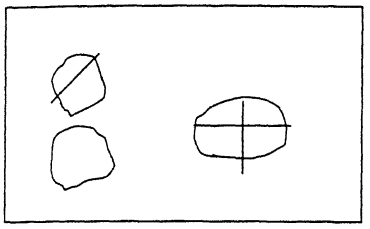

Point probe biased evaluation

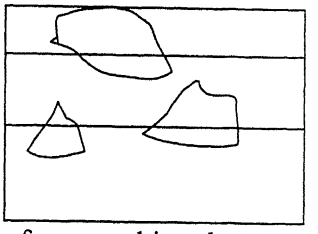

surface area biased

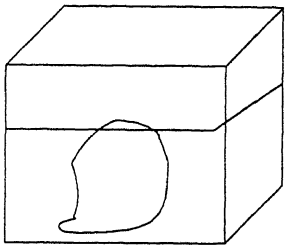

Dia based sampling

Nucleator:

For this choose any point inside the convex particle. Draw lines in all possible directions as shown below;

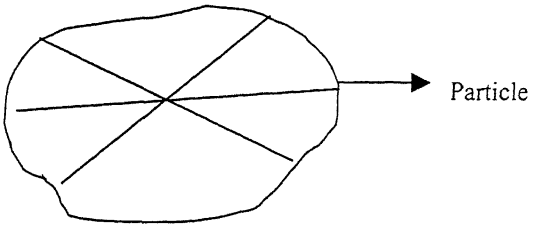

So volume of the particle V= $\frac{4\pi}{3}\left(\frac{\sum l_i^3}{N}\right)$

Where N= number of lines and l is the length of line elements measured from center.

2.8. An Overall Summary

Processing of W-Ni-Fe alloys can be done in various ways, which includes (i) Post-sintering heat treatments (ii) Cold working followed by heat treatment at high temperatures (iii) Hot working and annealing. As far as the ordance application is concerned previously depleted uranium alloys were used, but these alloys have major detrimental factor which is environmental pollution. So in order to remove these draw backs various alloys have been come into the field of materials. Among them W-Ni-Fe alloy is the most important alloy used so far. The mechanical properties of these alloys have been analysed through micro structural characterization which include volume fraction of tungsten particle and contiguity of the micro structural surfaces. So far deformation level of 45% have been achieved during cold working. Processing of W-Ni-Fe alloys lack in selection of proper composition and deformation levels up to 96% followed by heat treatment at high temperatures. So keeping the same volume fraction of the alloys and imparting deformation levels up to 96% followed by heat treatment results the better control of mechanical properties via quantitative microstructural measurements. This is the main objective of present investigation.

Chapter 3

SCOPE OF THE PRESENT WORK

From the previous chapter it is evident that the final sintered W-Ni-Fe alloys consists of nearly pure tungsten grains dispersed in ductile matrix. The combination of density, strength, conductivity, machinability and corrosion resistance makes tungsten heavy alloy composites unique in the field of materials. Due to this property combination, these alloys are used in many areas including radiation shielding, counter weights, kinetic energy penetrators, vibration damping devices and heavy-duty electrical contacts. As far as the ordnance application is concerned tungsten heavy alloys basically (W-Ni-Fe) alloys plays an important role in the manufacture of kinetic energy penetrators and fragmentation warheads. Previously depleted uranium alloys were used for these application but due to environmental hazards and and political problems of depleted uranium alloys, there has been always need for new material which can compensate the draw backs of depleted uranium alloys. So finally tungsten heavy alloys staged into the field of ordnance application. Though the penetration behavior of tungsten heavy alloys slightly less than the depleted uranium alloys but it could able to remove the environ mental pollution problem. So as a whole by seeing a better combination of all the properties it has become a new advanced emerging field for the manufacture of heavy armor materials. Though the earliest work on heavy alloys dates back to the 1930's, the linked effects of composition and processing on properties are not fully understood. Apart from the variety of properties brought about a change in composition, many other factors affect the final properties.

The present work mainly relates to processing of W-Ni-Fe alloys. Some of the research has been carried out on the cold swaging operation of W-Ni-Fe alloys, by cold working, conventionally by swaging increases the yield and UTS of the composites. But at the expense ductility. Exceeding 30% reduction in area by swaging usually results in the development of internal failures due to micro cracks and dramatic loses in ductility and toughness. Generally higher tungsten composites are less tolerance of cold working by swaging than less tungsten content alloys. As far as the anti armor application is concerned the impact of penetrators on the target gives rise to high temperatures in combination with high strain rate. So in order to have

excellent penetration affects a new processing technique have been developed. A new processing technique has been developed in this research by selecting proper combination of W-Ni-Fe alloys. This research involves the thermo-mechanical processing of 90W-7Ni-3Fe alloys with Ni to Fe ratio 7:3 in the premixes of alloy processing in order to avoid formation of intermetallic compounds, which drastically reduces the mechanical properties. The present work involves basically room temperature swaging of 90W-7Ni-3Fe alloy, which has been cold-isostatically pressed/powder forged followed by liquid phase sintering. The liquid phase sintered microstructure contains very less amount of residual pores, which does not have measure effect on properties. We have achieved % of amount of deformations up to 91% without any measure failures inside the materials by rotary swaging. This work has also achieved deformation level of 96%, which is quite a new development in the materials research of 90W-7Ni-3Fe alloys. 91to 96% reduced swaging consists of fibrous microstructures, there by increasing its chance for production of higher ductility and toughness in combination with strength. In the present work the deformation level have been achieved which are 37, 70, 91, 96% reduction in area. Further these swaged alloys heat-treated at three different temperatures that is 500, 900, 1400°C. The aim of this research is to study at which deformation level and heat treatment temperature a better combination of strength, ductility, hardness and toughness can be achieved. Quantitative micro structural analysis has been carried out which involves measurement of C_g (contiguity), S_v (surface area per unit volume) and grain size. Mechanical properties like macro and micro hardness measurements have also been studied in this research. The macro hardness results show the 91 and 96%-swaged samples achieve higher hardness as compared to 70 and 37% swaged samples in not heat-treated condition. On heat-treating the samples from 500 to 1400°C the result shows that at 1400°C the 91 and 96% reduction sample achieve good hardness levels which can be easily correlated with % of elongation of 90W-7Ni-3Fe alloys at that temperature. Quantitative analysis of C_g has been carried out for 37 and 70%-swaged sample. It has been seen that the C_g gradually decreases with heat treatment temperatures. 37% swaged sample show the C_g of 0.31 at 1400°C. On the other hand 70% swaged sample cause C_g of 0.22 at 1400°C. As we know the C_g measures the amount of W-W contact area. Higher the area more is the brittleness, there by reducing toughness on other side. So in order to achieve the better combination of toughness and strength a C_g value of 0.22 has been achieved in 70% swaged sample,

there by improving the toughness value of 90W-7Ni-3Fe in combination with hardness and strength. A lot of work has been done on the measurement of S_v of W-matrix and W-W interface with respect to orientation of test lines. The aim of measuring S_v is to study the kinetics of flow of W-matrix interface with respect to amount of reduction and heat treatment temperatures. The absolute value of S_v for 70% is more than 37% swaged samples, which confirms that 70% swaged sample is more elongated. Also grain size variation with respect to heat treatment temperatures has also been studied to analyze the change in grain size with heat treatment temperatures. The correlation of C_g, S_v and hardness value with strength and ductility is yet to be analyzed in future work.

Chapter 4

EXPERIMENTAL PROCEDURE

4.1 Material

The materials used for this investigation were obtained from Mitek Products, USA. The alloy was basically tungsten heavy alloy consisting of W, Ni and Fe with Ni to Fe ratio of 7:3. Two different techniques were used for manufacturing these composites. The specimens used along with their composition and processing techniques are shown below.

Table 4.1. Composition and Processing Techniques of W-Ni-Fe Alloys used.

Composition (by Wt%)	Processing Techniques	Sintering
90W-7Ni-3Fe	Cold Iso-statically Pressed/Powder Forged	Liquid Phase Sintering
93W-4.9Ni-2.1Fe	Cold Iso-statically Pressed/Powder Forged	Liquid Phase Sintering
97W-2.1Ni-0.9Fe	Cold Iso-statically Pressed/Powder Forged	Liquid Phase Sintering

4.2 Density Measurements

The as-received samples were in cylindrical rod form having length 10inches and diameter 0.52 inch. Samples of 5mm in length were cut by using abrasive cutter from each composition. Density Measurements for these samples were measured using Archimedes principle. Initially the weights for the samples were taken in air. Then the samples were immersed in pure distilled water and weights were taken in water. An analytical balance was used for all the measurements.

The density was calculated using the following equation:

$$\rho_S = \frac{W_{SA}}{W_{SA} - W_{SW}} \qquad (4.1)$$

Where, ρ_S is the relative density of the sample.

W_{SA} is the weight of the sample in air

W_{SW} is the weight of the sample in water.

The theoretical density of the selected composition was determined by the inverse rule of mixing. Inverse rule of mixing can be written as:

$$\frac{w}{\rho} = \frac{w_1}{\rho_1} + \frac{w_2}{\rho_2} + \frac{w_3}{\rho_3}$$

Where w_1, w_2 and w_3 are the weight fraction of compositions to be mixed. Their respective densities are represented by ρ_1, ρ_2 and ρ_3. where as ρ_{th} is the density of the respective constituent elements. In the present investigation the thermo-mechanical treatment was carried out by choosing only one composition, i.e. 90W-7Ni-3Fe.

4.3 Swaging Operation

The swaging process is used for reducing, tapering, and pointing bars and tubing. It is accomplished between two or more dies that strike the metal to be formed, reducing metal in size. The swaging operation of 90W-7Ni-3Fe (obtained in the form of rod) was carried out using rotary swaging machine obtained from Torrington, USA, which has a series of rollers that act as hammers, driving the anvil in the die towards the center of the rotary head. The article to be formed is simply hand-held in the dies. The machine is operated using 10hp motor.

The swaging machine (Figure 4.1) consists of heavy stationary rings, in which rollers are mounted at close intervals, and a moving ring, carrying two mounted dies and stationary rings. The dies are mounted facing the axis and are free to slide back and forth. The dies are blocks of hardened steel with impressions or shapes cut into them that indicate the shape the die will produce. One end of the die is flared to allow unshaped stock to be placed in the die.

The swaging action of the machine takes place when the dies that are mounted to the inner race rotate. Attached to one end of the die is anvil. As the anvil strikes the stationary rollers, it is forced towards the center of the swaging machine, squeezing or compressing the stock of material between the rollers. As the inner race of the swaging age rotates, centrifugal force further throws the die blocks towards the outer race, opening the die. When the die is opened, the anvil strikes the next set of stationary rollers and is compressed again and thrown open. The cycle is repeated, resulting in the work being rapidly hammered from all sides while being contained in the die. Results of % amount of deformation is given in Table 5.2.

4.3.1 % Amount of Deformation Measurements

The initial diameter of the as-received rod was 0.48 in after machining. The cylindrical rod was swaged stepwise to produce different deformation levels in each step. Finally the % amount of deformation was calculated by using following methods.

$$\% \text{ Amount of deformation} = \frac{D_o^2 - D_f^2}{D_o^2}$$

Where D_0 = initial diameter of rod in in.

D_f = final diameter of rod after swaging for each step in in.

4.4 Heat Treatment Procedures

Heat treatment was carried out on our own made laboratory type SiC heated horizontal tubular furnace (rating 1.5 KVA). The furnace tube was made up of doubly recrystallized alumina. The inner diameter of tube was 38mm and length 980 mm. In our present work we use commercially pure hydrogen as heat treatment atmosphere. The furnace had a heating zone of approximately 105 mm in the range of 1400-1500°C with an accuracy of ± 3°C.

In the present work three different temperatures were selected for heat treatment. The temperatures were 500, 900 and 1400°C. Requisite number of the as-received and swaged 90W-7Ni-3Fe were placed over an refractory boat and transferred to the center of the tubular furnace. Both ends of tubular furnace were sealed with SILASTIC (RTV 700) adhesive/sealant to prevent any leakage. Heating rates were 7°C/min. The samples were heated in hydrogen atmosphere to the final heat treatment temperatures without intermittent holding. Holding time was 1hr at the final heat treatment temperatures for each case. In all the cases cooling was done in prevailing atmosphere at an average rate of 2-3°C/min.

4.5 Specimen Preparation for Metallographic Observations.

Metallographic techniques used for these composites are sectioning, mounting, grinding, and polishing.

4.5.1 Sectioning

A diamond wheel was used for sectioning the specimens. The wheel was used at a very slow speed with a controlled power of 4V in order to avoid any particle pullouts or damage in the sample. During cutting lubricated oil was used time to time inside the groove of cutter in order to facilitate smooth and easy cutting. Proper care should be taken in order to avoid the distortion of diamond wheel and proper smoothening of the metallo graphic surfaces. In this research the longitudinal section of the samples have been considered for all the measurements.

4.5.2 Mounting

Specimens were hot mounted. Hot mounting was done using hot mounting machine (model: Simplimet: 2, Buehler mounting press, USA). Resin powders were used as molding compound operating within a temperature range of 130-150°C. Sufficient molding compound may be placed in the mold, so that the specimens cannot touch and damage the upper arm or mold closure during the compression cycle. Care was taken while mounting in order to maintain good gripping of samples within the mount and flatness of samples.

4.5.3 Grinding

Grinding is one of the steps, which includes considerable relief in the matrix or results in a dual plane structure. In other words, the two phases of the material being processed will be on two different levels. It also helps in proper flattening of the samples and making polishing further easier.

4.5.4 Polishing

The samples were wet polished on the Lunn Major Unit of Struers, Denmark make 220, 320, 500 and 1000 grit silicon carbide emery papers followed by fine wheel polishing with suspended 0.03 μm size alumina in distilled water. This is attributed to the fact that the emery paper used quickly grinds away the soft Ni-Fe matrix while leaving the hard tungsten particles untouched. Hence emery papers were only used for primary removal of scratch.

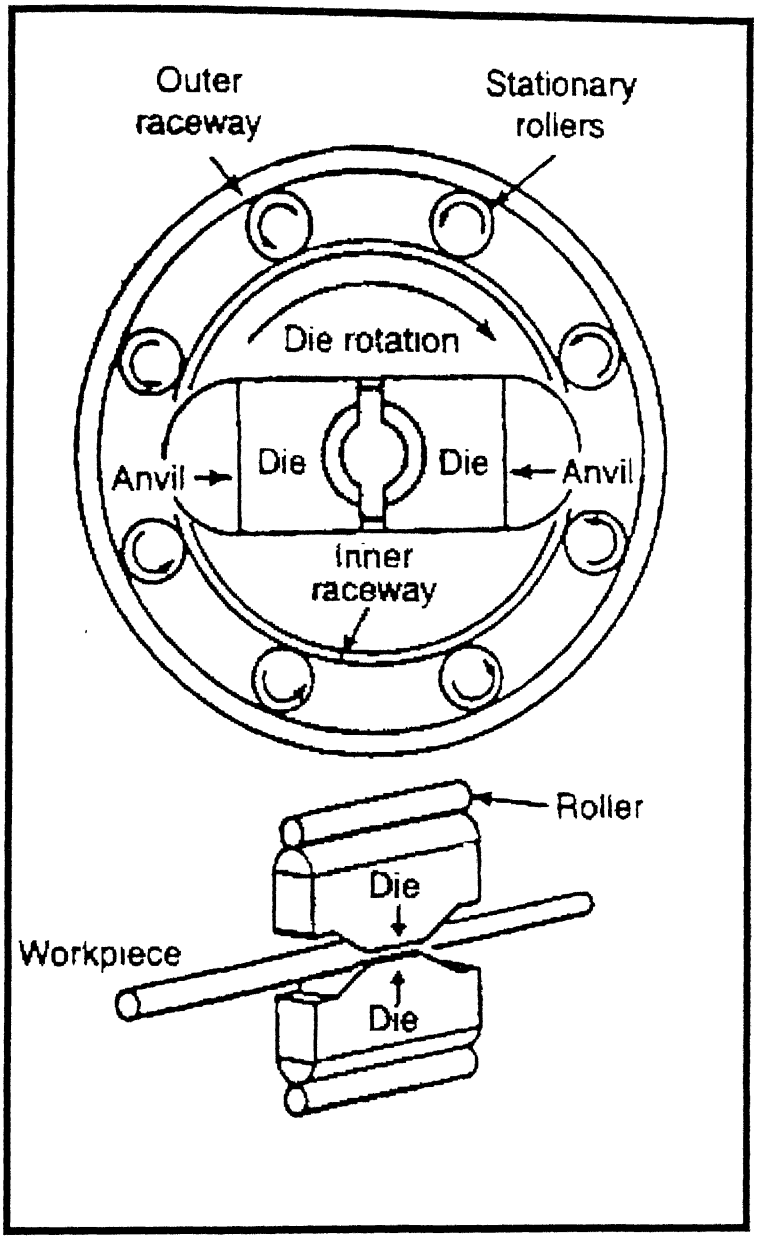

Figure 4.1. A schematic diagram of rotary swaging .

4.6 Mechanical Properties

4.6.1 Vickers Macro hardness

Vickers macro hardness of the polished specimens were measured on Leco V-100-C1, Hardness Tester, manufactured by Akashi Corporation, Japan. The machine was automatic and time for indentation was pre-programmed. Macro-hardness measurements were made using 0.3 and 5 kg load. The indentation time of 20s was maintained. The diagonal length of the impressions was measured and the hardness was obtained directly in H_v scale on the monitor.

4.6.2 Vickers Micro hardness

MHP 160 Micro-Hardness Tester was used to perform the micro-hardness tests. Micro-Hardness Test was performed on the W particle and the matrix phase. The load used for indentation was 40gms and 20gms depending upon the amount of area upon which the indentation is to be made. A diamond pyramid indenter was used. The load was applied for a short period of around 3-4 s. The indentation was square shaped. The length of the two diagonals of square indentation was measured and their mean was taken. Micro-Hardness or Vickers Hardness (VHN) was measured using the following equation:

$$\text{VHN} = 1.854\frac{P}{d^2}$$

Where, P is the load applied (in kgf), and d is the mean diagonal length of the indentation (in mm). Micro hardness of all the samples were measured except 91% and 96% swaged samples. Because in these cases the area of indentation was bigger as compared to our area of phase of interest.

4.7 Quantitative Metallography

4.7.1 Micro structure Evolution

In quantitative metallography, systematic point count analysis was carried out to evaluate the volume fraction of particles of as-received samples containing 90, 93, 97 wt%W. In systematic point count analysis a square grid with 35 grid points was superimposed on the microstructure. The number of grid points falling on the particles were counted systematically and compared with total number of grid points. If total number of points falling on the phase of interest is P_i and total number of grid points is P_a, then the point fraction

$P_p = (\frac{P_i}{P_a})$ Will give the volume fraction of the particle (Vv). The advantage of using the systematic point count analysis is that the relative error is low (10%) as compared to other methods available.

4.7.2 Contiguity of the Micro structural Surface

Contiguity is a measure of solid-solid (W-W) contact in the as received, mechanically worked and thermo-mechanically treated samples and it is given mathematically as

$$C_g = \frac{2N_{ww}}{2N_{ww} + N_{wm}}$$

Where the C_g = Contiguity of the micro structural surfaces

N_{ww} = Number of intercepts made by solid-solid contact per unit length of test line.

N_{wm} = Number of intercepts made by solid-matrix contact per unit length of test line.

4.7.3 Surface area per unit volume (Sv)

Surface area per unit volume of the W-W and W- Matrix interfaces were calculated using five lines of equal length orientated at an angle difference of 22.5°. The total angle included in between five lines is 90°. The total number of points of intersections with the solid-solid (W-W) contact and solid-liquid (W-Matrix) was calculated for 30 fields of view as shown in Figure 4.2. Finally this gave the points per unit length (P_L). Then Sv was calculated as

$$S_v = 2P_L$$

Where L = Length of line in terms of μm varies depending upon the Magnification.

4.7.4 Grain Size Measurements

The grain size was calculated from volume fraction (Vv) and surface area per unit volume of the W-W and W-Matrix interface. Grain size varies with respect to surface area per unit volume of the particle. Here as the Vv is less than 1, so the grain size is given by

$$\text{Grain size} = \frac{4V_v}{S_v}$$

Where V_v = volume fraction of the particles

S_v = total surface area per unit volume of the micro structural surfaces.

In our measurement the orientation difference does not change with respect to fields of view. As in case of swaged samples and heat-treated samples the microstructure shows an anisotropic behavior, grain size was measured with reference to one orientation.

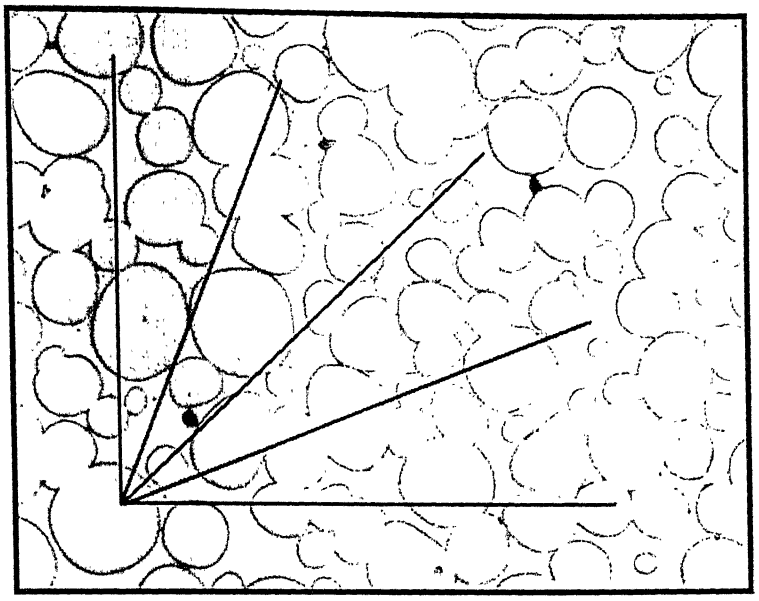

Figure 4.2. Schematic diagram showing orientation of test lines for quantitative micro structural measurements.

Chapter 5

EXPERIMENTAL RESULTS

5.1 Density Measurements

Table 5.1. Results of density measurements

Composition	Measured Density (g/cm^3) (% Theoritical)	Density (by inverse rule of mixture) (gm/cm^3)
90W-7Ni-3Fe	15.7 (91%)	17.36
93W-4.9Ni-3.1Fe	17.8 (97%)	17.8
97W-2.1Ni-0.9Fe	17.6 (94%)	18.7

The initial diameter of as-received cylindrical rod was 0.48 in (12.2 mm).

Table 5.2. Results of % amount of deformation on swaging.

Processing Step	Final Dia. of Rod (in)	% Amount of Deformation
I^{st} Step	0.38	37
2^{nd} Step	0.26	70
3^{rd} Step	0.14	91
4^{th} Step	0.10	96

5.2 Microstructure Evolution

Figures 5.1 to 5.3 shows the micrographs of the as-received samples containing 90, 93, 97 wt% W. Vv (volume fraction) of three composition have been done in order to analyze variation of *Vv* (volume fraction) of tungsten particle with respect to amount of tungsten content. But in the present research effect of swaging and heat treatment on microstructure evolution of W-Ni-Fe alloys have been analyzed for only 90wt%W. because low tungsten heavy alloys containing 90wt%W can easily cold worked to high % of deformations without any fracture. As because tungsten is brittle in nature , as we go on increasing the tungsten content from 93 to 97%, the material fails at low level of deformation even at 40% reductions. So in order to cold work heavily to high level of deformations the heavy alloy containing 90W-7Ni-3Fe alloy have been chosen in the present investigation. The tungsten heavy alloy generally processed by liquid phase sintering . so the sintered microstructure contains residual porosity as shown in Figure 5.1. Figures 5.4 to 5.7 shows the micrographs of swaged 90W-7Ni-3Fe alloys. Figures 5.8 to 5.22 shows the micrographs of heat-

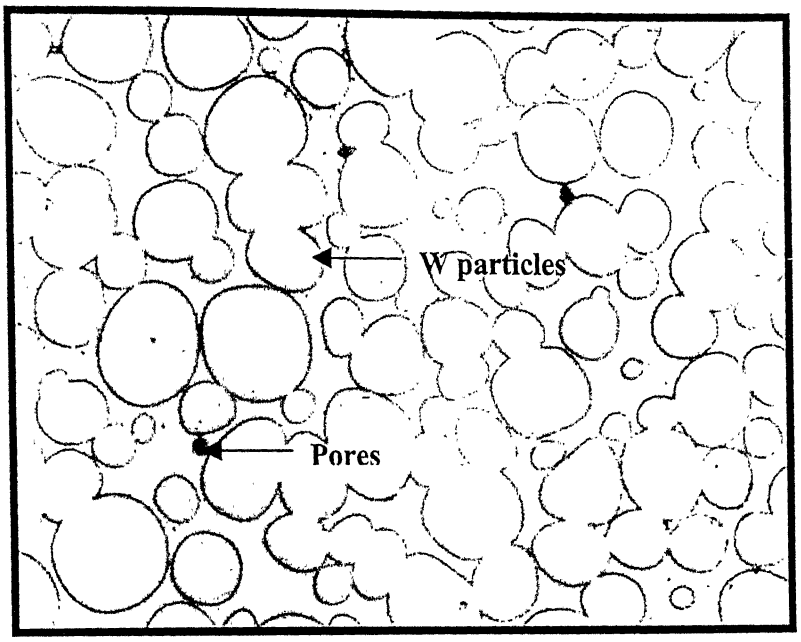

Figure 5.1. Microstructure of As-received 90W-7Ni-3Fe alloy containing residual pores.

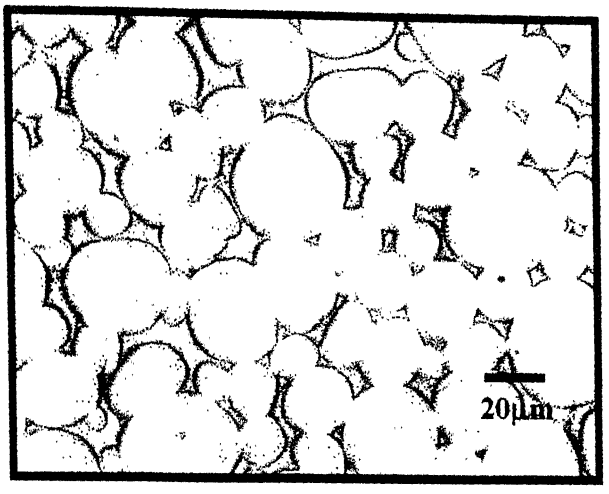

Figure 5.2. Microstructure of 93W-4.9Ni-2.1Fe alloy.

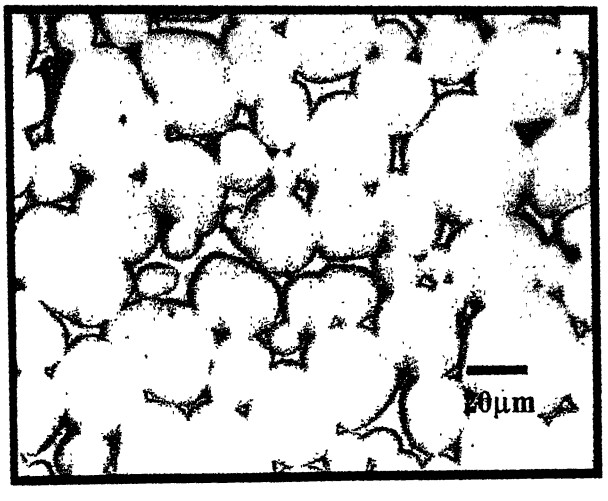

Figure 5.3. Microstructure of 97W-2.1Ni-0.9Fe alloy.

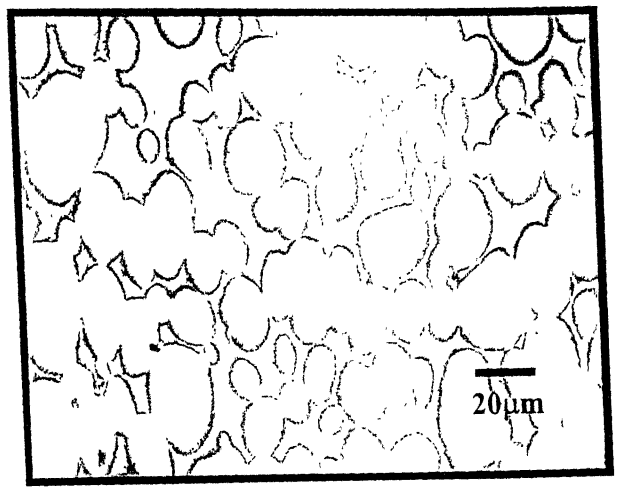

Figure 5.4. Microstructure of 37% Swaged 90W-7Ni-3Fe alloy.

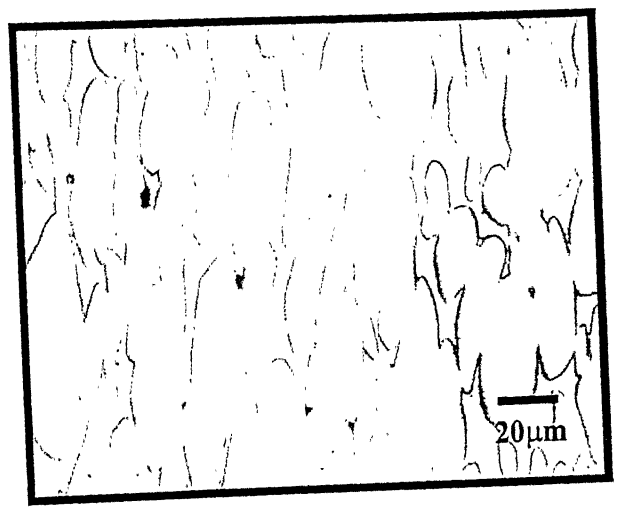

Figure 5.5. Microstructure of 70% Swaged 90W-7Ni-3Fe alloy.

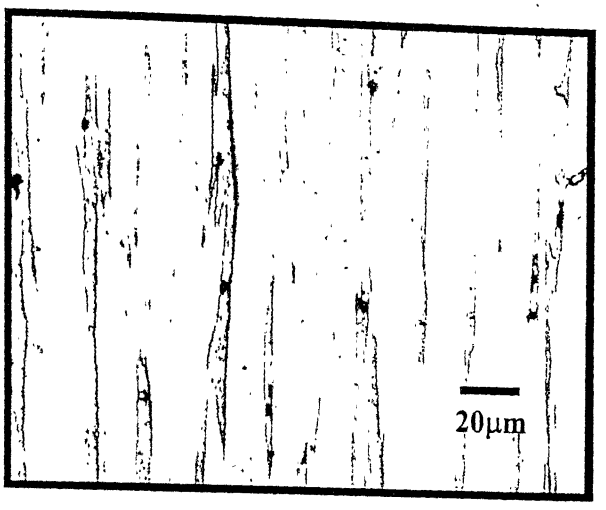

Figure 5.6. Microstructure of 91% Swaged 90W-7Ni-3Fe alloy.

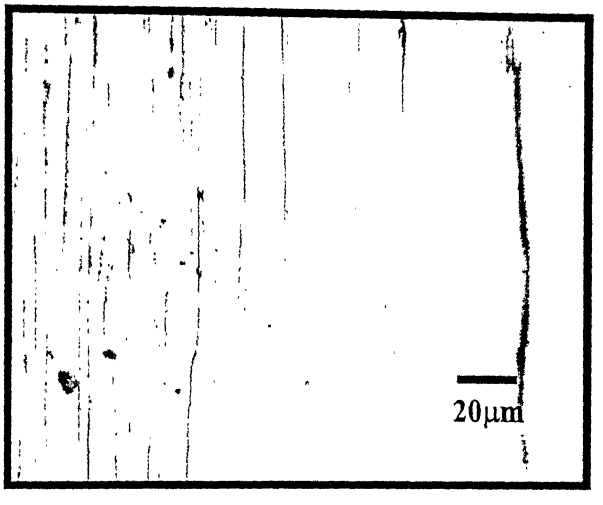

Figure 5.7. Microstructure of 96% Swaged 90W-7Ni-3Fe alloy.

Figure 5.8. Microstructure of As-received 90W-7Ni-3Fe alloy heat-treated at 500°C.

Figure 5.9. Microstructure of As-received 90W-7Ni-3Fe alloy heat-treated at 900°C.

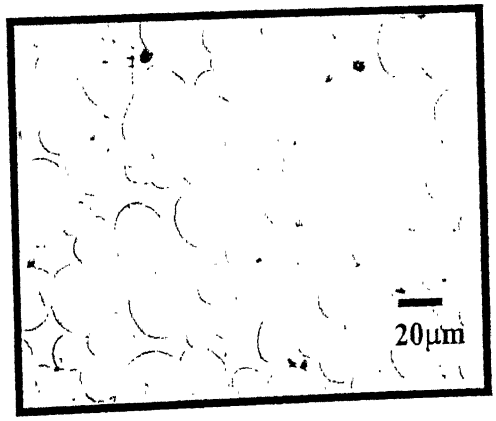

Figure 5.10. Microstructure of As-received 90W-7Ni-3Fe alloy heat-treated at 1400°C.

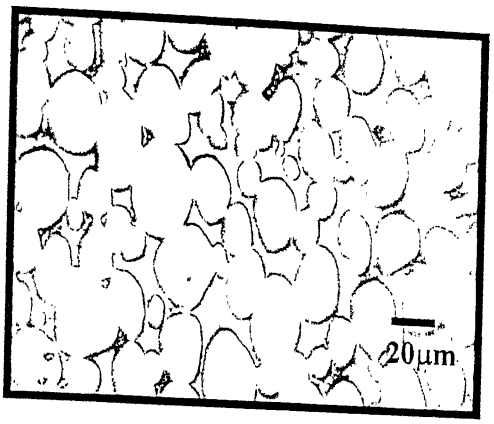

Figure 5.11. Microstructure of 37% Swaged 90W-7Ni-3Fe alloy heat-treated at 500°C.

Figure 5.12. Microstructure of 37% Swaged 90W-7Ni-3Fe alloy heat-treated at 900°C.

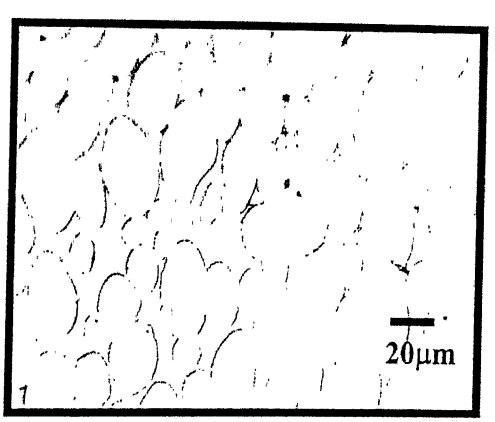

Figure 5.13. Microstructure of 37% Swaged 90W-7Ni-3Fe alloy heat-treated at 1400°C.

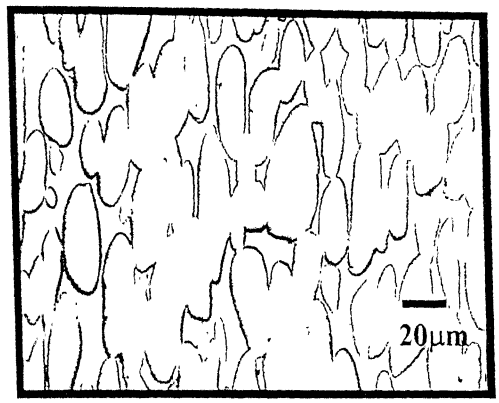

Figure 5.14. Microstructure of 70% Swaged 90W-7Ni-3Fe alloy heat-treated at 500°C.

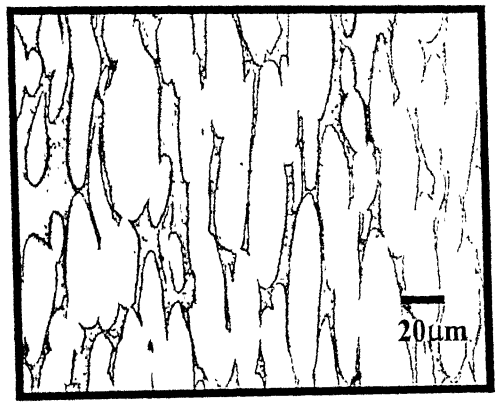

Figure 5.15. Microstructure of 70% Swaged 90W-7Ni-3Fe alloy heat-treated at 900°C.

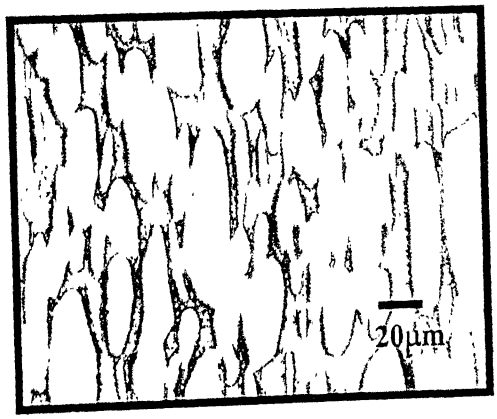

Figure 5.16. Microstructure of 70% Swaged 90W-7Ni-3Fe alloy heat-treated at 1400°C.

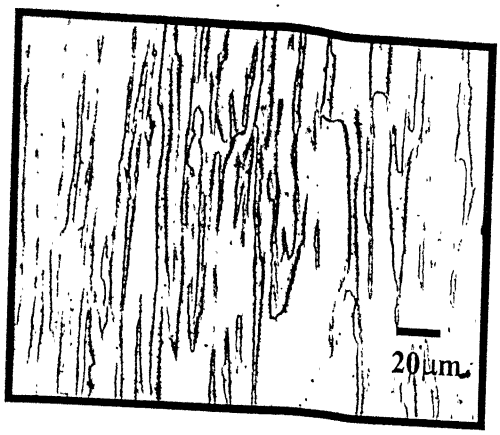

Figure 5.17. Microstructure of 91% Swaged 90W-7Ni-3Fe alloy heat-treated at 500°C.

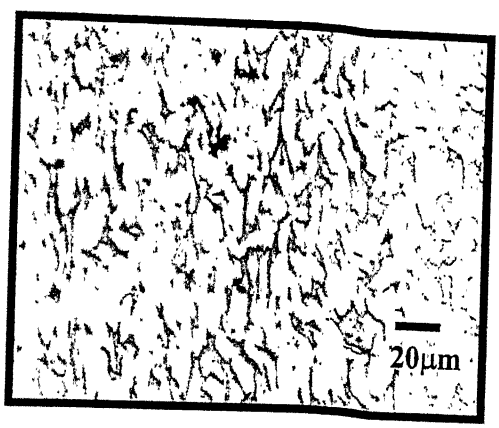

Figure 5.18. Microstructure of 91% Swaged 90W-7Ni-3Fe alloy heat-treated at 900°C.

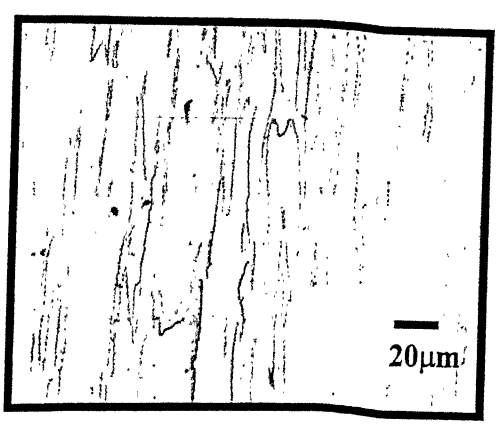

Figure 5.19. Microstructure of 91% Swaged 90W-7Ni-3Fe alloy heat-treated at 1400°C.

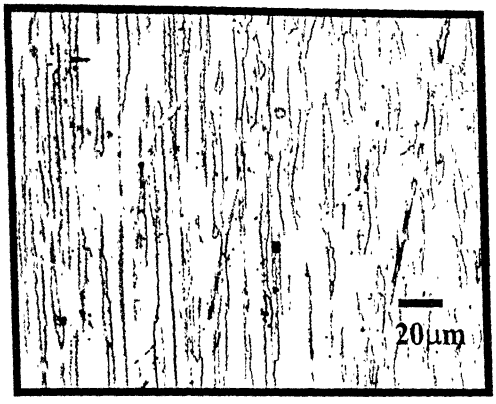

Figure 5.20. Microstructure of 96% Swaged 90W-7Ni-3Fe alloy heat-treated at 500°C.

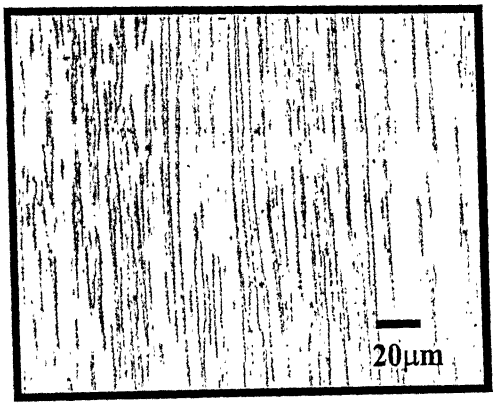

Figure 5.21. Microstructure of 96% Swaged 90W-7Ni-3Fe alloy heat-treated at 900°C.

Figure 5.22. Microstructure of 96% Swaged 90W-7Ni-3Fe alloy heat-treated at 1400°C.

treated 90W-7Ni-3Fe alloys. Quantitative analysis of these microstructures has been described in chapter 6.

5.3 Surface area per unit volume (S_v) of solid-liquid (W-matrix) interface.

The major part of this research involves determination of surface area per unit volume (S_v) of W-Matrix interface. S_v of solid-liquid (W-Matrix) interface has been determined to study the kinetics of flow of solid-liquid interface with reference to heat treatment temperatures. Tables 5.3 and 5.4 presents the S_v data for solid-liquid and solid-solid interface of as-received, 37% and 70% swaged samples. It has been seen that S_v increases with respect to orientations of test lines in all the samples measured. For as-received and not heat treated samples S_v remains almost constant with orientation of test lines (Figure 5.23). The absolute value of S_v for as received samples is seemed to decrease when heat-treated at 500°C keeps on decreasing as we go to 900 and 1400°C. On swaging the samples the W-grains gets elongated along the swaging direction. This results in an increase in intersection (P_L) count of the test lines at higher angles. The S_v is seemed to increase with angle of orientation both in case of 37% and 70% swaged samples as shown in Figures 5.24 and 5.25.

5.4 Volume fraction and Grain Size

Figure 5.26 shows the variation of volume fraction (V_v) with respect to tungsten content by wt%. The graph shows an increase in V_v with increasing tungsten content.

Grain size was measured for different processing condition by taking different test lines. Here in the present investigation one test line have been considered in order to investigate the best measurement taken, because of anisotropic behaviour of 90W-7Ni-3Fe alloys. Figures 5.27, 5.28 and 5.29 shows the variation of grain size as a function of temperature. The tungsten grain size increases with respect to heat treatment temperatures. In case of as-received and 37% swaged samples the increment of increase in W-grains is very less (Table 5.5) But in 70% swaged samples the grain size shows a rapid increase with respect to heat treatment temperatures such as 500, 900 and 1400°C.

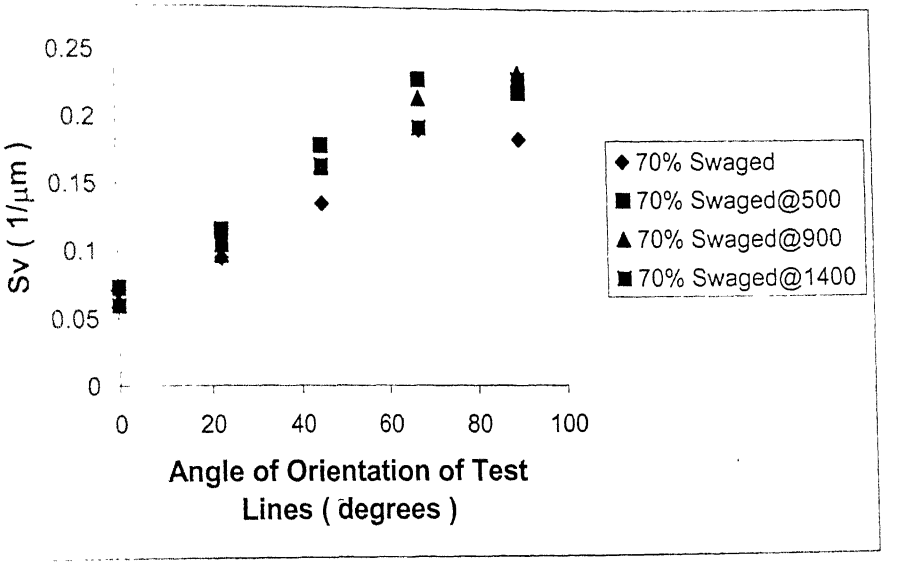

Figure 5.25. Variation of S_v with respect to orientation of test lines for 70% swaged 90W-7Ni-3Fe alloy.

Table 5.3. Results of S_v (surface area per unit volume) for W-matrix interface.

Heat Treatment Temperatures (0%Swaged)	S_v Data for W-matrix Interfaces with respect to Orientation of Test Lines				
	0°	22.5°	45°	67.5°	90°
0	0.1296	0.14827	0.14735	0.15057	0.15653
500	0.12781	0.11770	0.12735	0.12827	0.14329
900	0.11264	0.11310	0.11264	0.12229	0.10942
1400	0.11287	0.11379	0.11563	0.11402	0.12607
37%Swaged					
0	0.09057	0.11494	0.12	0.12597	0.14436
500	0.09517	0.09517	0.11954	0.12873	0.14482
900	0.10160	0.10114	0.13425	0.12919	0.14298
1400	0.10390	0.09563	0.11678	0.14528	0.14069
70%Swaged					
0	0.07034	0.09471	0.13517	0.19080	0.18936
500	0.07264	0.11540	0.17885	0.22896	0.21972
900	0.06298	0.09655	0.16229	0.21971	0.23902
1400	0.05931	0.1043	0.16367	0.19264	0.22942

Table 5.4. Results of S_v (surface area per unit volume) for W-W interface.

Heat Treatment Temperatures (0%Swaged)	S_v Data for W-W Interfaces with respect to Orientation of Test Lines				
	0°	22.5°	45°	67.5°	90°
0	0.01540	0.01885	0.01701	0.01793	0.0172
500	0.02344	0.02275	0.02574	0.02850	0.0193
900	0.03402	0.04275	0.05609	0.06804	0.0588
1400	0.03126	0.02850	0.02482	0.02712	0.0377
37%Swaged					
0	0.02298	0.02390	0.03126	0.04092	0.0441
500	0.02528	0.02850	0.03862	0.04551	0.04551
900	0.07885	0.02758	0.03586	0.04275	0.04092
1400	0.01572	0.02712	0.02666	0.0354	0.03540
70%Swaged					
0	0.1149	0.01425	0.03402	0.0331	0.04643
500	0.1103	0.01972	0.02988	0.03218	0.03908
900	0.00965	0.02160	0.02482	0.03540	0.04
1400	0.00781	0.01885	0.02712	0.02942	0.02436

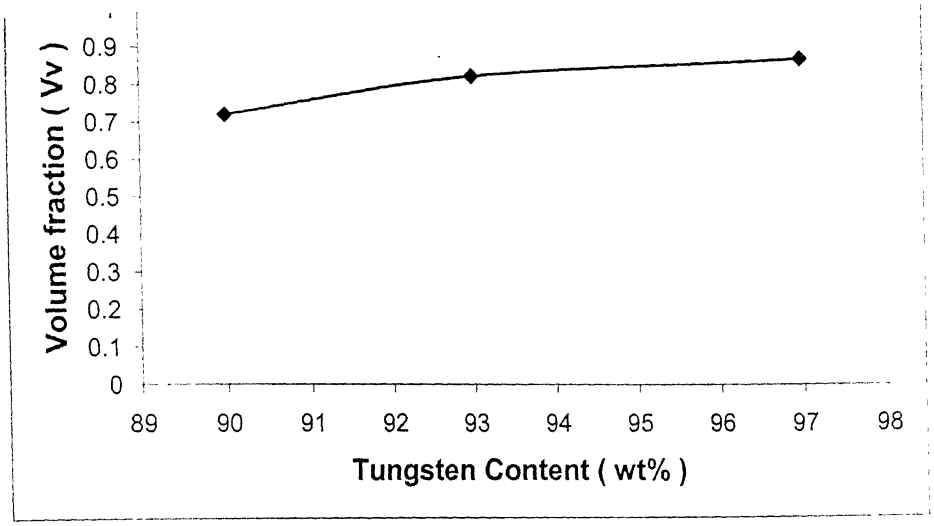

Figure 5.26. Effect of Volume fraction (V_v) of tungsten particle on amount of tungsten content.

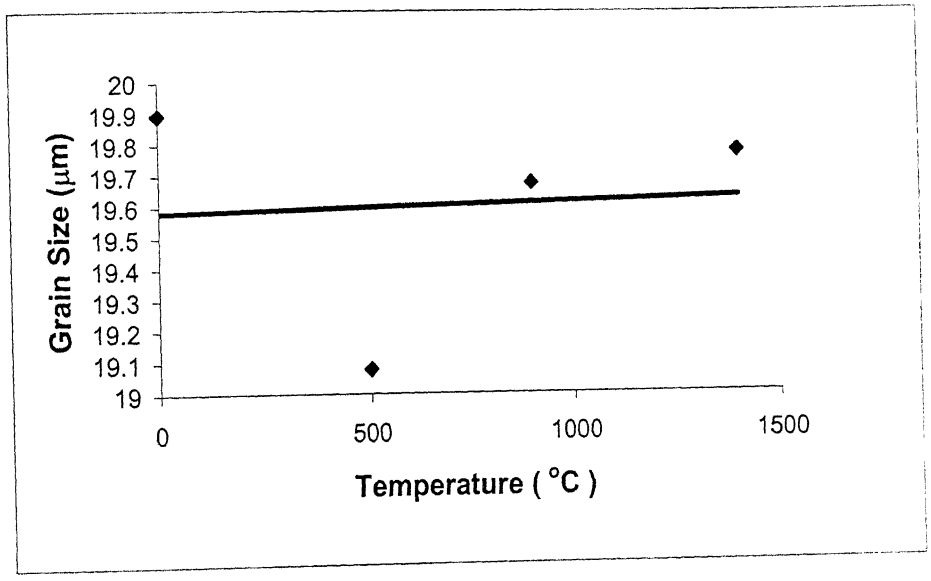

Figure 5.27. Grain size variation for As-received 90W-7Ni-3Fe alloy with heat treatment temperatures.

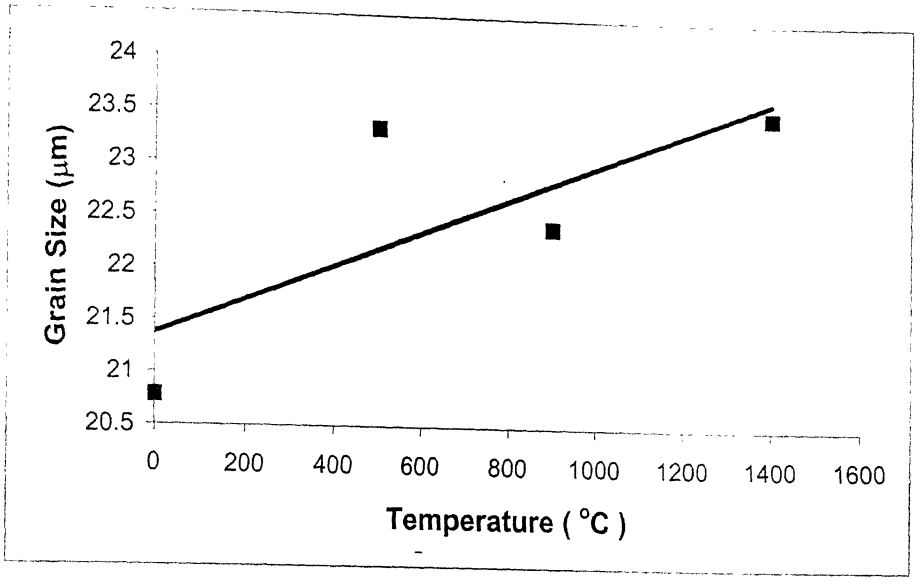

Figure 5.28. Shows the Grain size variation for 37% Swaged 90W-7Ni-3Fe alloy with heat treatment temperatures.

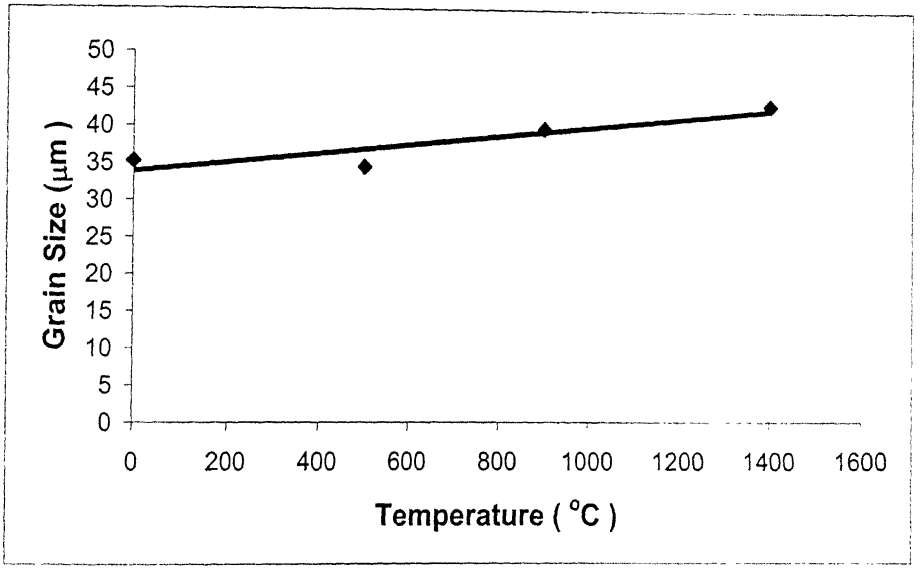

Figure 5.29. Shows the Grain size variation for 70% Swaged 90W-7Ni-3Fe alloy with heat treatment temperatures.

Table 5.5. Grain size data for not heat treated and heat treated 90W-7Ni-3Fe Alloy.

% Amount of deformations	Grain Size (μm) (Not Heat Treated)	Grain Size (μm) @500°C	Grain Size (μm) @900°C	Grain Size (μm) @1400°C
0%	19.9	19.0	19.6	19.7
37%	20.8	23.3	22.4	23.5
70%	35.2	34.4	39.7	42.9

5.5 Contiguity

Contiguity variation with respect to heat treatment temperatures has been shown in figure 5.30. The absolute value of contiguity for as-received not heat treated samples is low as compared to 37% and 70% swaged samples. Contiguity increases at 500°C and then decreases gradually for as received and 37% swaged samples as we go on increasing heat treatment temperatures to 900 and 1400°C. But the same trend is not observed in case of 70% swaged samples. From 900 to 1400°C contiguity decreases gradually in all the samples. The absolute value of contiguity for as-received, 37% and 70% swaged samples with respect to heat treatment temperatures is given in Table 5.6.

Table 5.6. Contiguity values for 90W-7Ni-3Fe Alloy.

Amount of Deformation	Contiguity (C_g) For Not heat treated	Contiguity (C_g)@500°C	Contiguity (C_g)@900°C	Contiguity (C_g)@1400°C
0%	0.19	0.56	0.47	0.27
37%	0.34	0.38	0.34	0.31
70%	0.28	0.24	0.24	0.22

In this research also variation of contiguity with respect to orientation has been analyzed for as received, 37% swaged and 70% swaged samples (Figures 5.31, 5.32, 5.33). For as-received samples heat-treated at 900°C contiguity gradually increases with respect to orientation of test lines from 0 to 90° with an angle difference of 22.5°. The same trend is not observed in case of as-received not heat-treated and as-received heat treated at 500 and 1400°C. The data shows there is an increasing and decreasing trend of contiguity with respect to orientations for 500 and 1400°C samples (Figure 5.31).

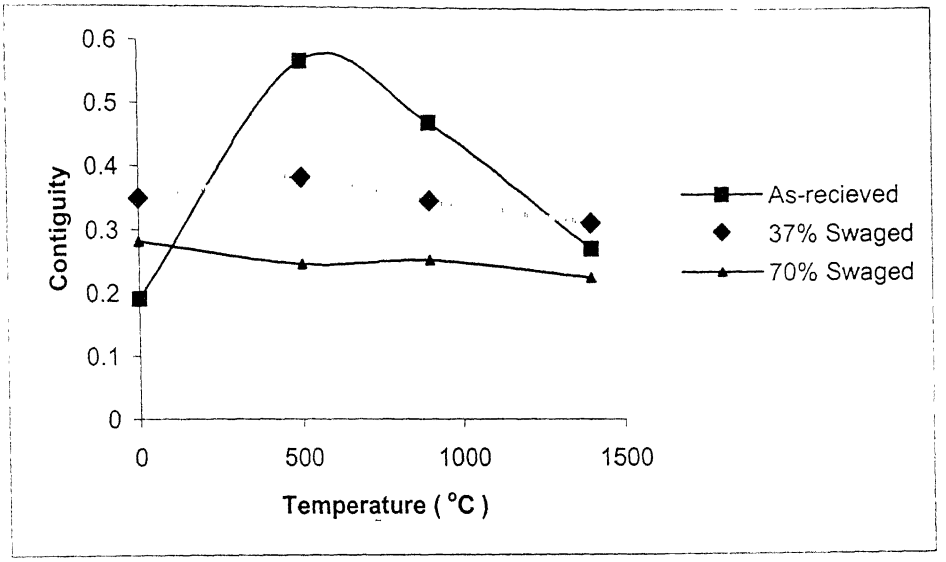

Figure 5.30. Contiguity variation with respect to heat treatment temperatures.

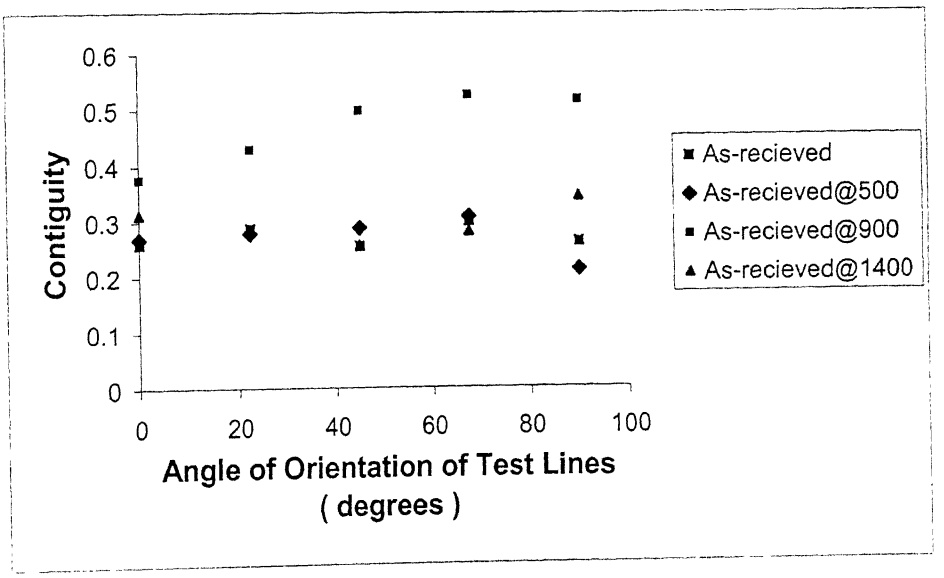

Figure 5.31. Variation of Contiguity for As-received 90W-7Ni-3Fe alloy with orientation of test lines.

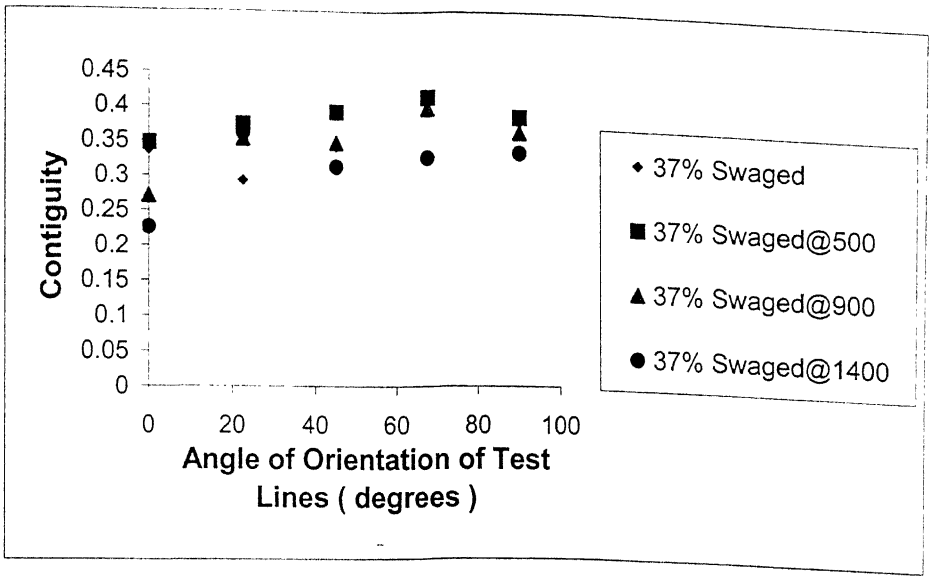

Figure 5.32. Variation of Contiguity with orientation of test lines for 37% Swaged 90W-7Ni-3Fe alloy.

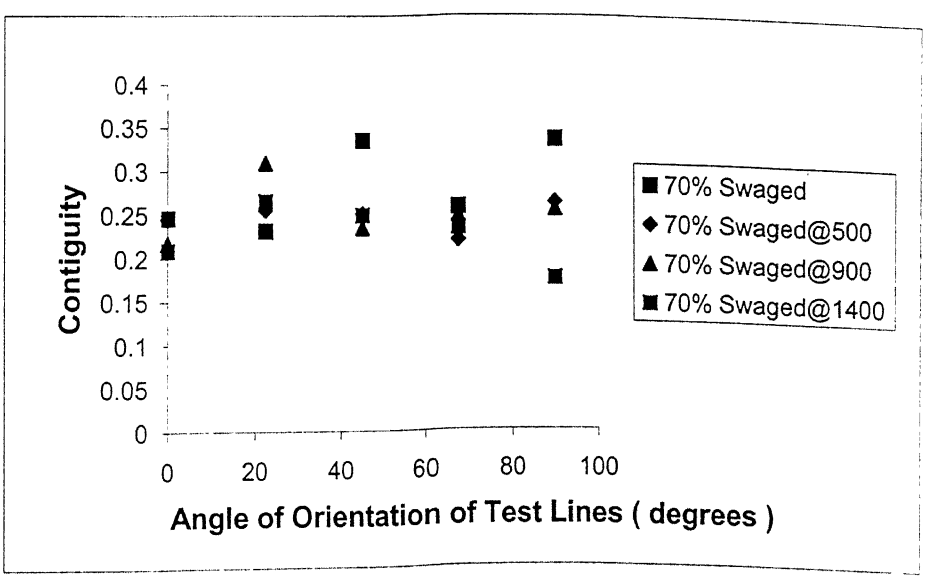

Figure 5.33. Variation of Contiguity with orientation of test lines for 70% Swaged 90W-7Ni-3Fe alloy.

The absolute value of contiguity for 37% swaged samples decreases from 500 to 900°C (Figure 5.32). On the other hand 70% swaged sample shows a random variations in contiguity measurements with respect to orientations (Figure 5.33), which keeps on decreasing as we go to 900 and 1400°C. On swaging the samples the W-grains gets elongated along the swaging direction. This is seen as there is an increase in intersection (P_L) count of the test lines at higher angles. The Sv is seemed to increase with angle of orientation both in case of 37% and 70% swaged samples.

5.6 Macro hardness

The Macro hardness value obtained from the experiments of all the samples are given in Table 5.7. Standard deviations are also calculated for all the samples. Figure 5.34 shows that as we go on increasing the reduction in area (from 37% to 96%) the hardness increases for not heat-treated samples achieving highest hardness at 96% swaged specimen. For as-received samples the hardness does not varies (remains almost constant) with respect to heat treatment. On swaging the grains become elongated forming highly deformed grains at 96% reduction in area. It has been seen that in all the samples the hardness keeps on decreasing with increase in heat treatment temperatures from 500 to 900 and 1400°C. At 500°C the 96% swaged samples achieve highest hardness as compared 91, 70, 37% swaged alloys.

5.7 Micro hardness

In this research the micro hardness measurements has been done for W-particle as well as matrix also for as-received, 37% and 70% swaged samples. All the hardness values have been tabulated in Table 5.8. It is seen that the W-particle hardness does not varies that much (almost remains constant) with increase in heat-treatment temperatures. In case of 37% swaged samples the hardness is more as compared to 70% and as received alloys in not heat-treated condition. But as we go on increasing swaging from 37% to 70% reduction in area the W-particle hardness decreases. Further when the swaged samples are heat-treated the micro-hardness of W-particle keeps on decreasing as we go on from 500 to 1400°C (Figure 5.35).

On the other hand micro-hardness of matrix for as-received alloys shows almost constant behavior with heat treatment temperatures. But 70% swaged samples shows highest matrix hardness as compared to 37% swaged samples in not heat

treated condition and goes on decreasing with increase in heat treatment temperatures (Figure 5.36). It has been seen that the variation of micro hardness value for 37% and 70% swaged sample are almost similar.

Table 5.7. Macro hardness values for 90W-7Ni-3Fe alloy.

Condition	No. Of Observ.	D1	D2	Hardness (VHN)	Average Hardness (VHN)	Standard Deviation	
						σ_n	σ_{n-1}
0%Swaged (Not Heat Treated)	1	175.6	181.4	291	293	5	5
	2	178.2	182.2	285			
	3	179.4	175	295			
	4	183.2	170.3	297			
	5	177	176.3	297			
0%Swaged@500°C	1	174.5	178.9	297	293	6	7
	2	180.1	177.5	290			
	3	178.3	176	295			
	4	179.9	183.5	281			
	5	180.7	171.3	299			
0%Swaged@900°C	1	177.9	177.9	293	294	6	7
	2	177.8	181.5	287			
	3	176.7	179.7	292			
	4	177.4	177.1	295			
	5	171.1	177.5	305			
0%Swaged@1400°C	1	176.7	182.3	288	286	5	6
	2	173	181.6	295			
	3	180.7	180.1	285			
	4	180.5	184.5	278			
	5	178.3	182.1	285			
37%Swaged (Not Heat Treated)	1	145.4	150.1	425	426	8	9
	2	148.7	149.3	418			
	3	145.5	144.2	442			
	4	148.5	146.6	426			
	5	148.7	149.3	418			
37%Swaged @500°C	1	144.6	145.7	440	444	9	10
	2	146.3	145.6	435			
	3	147.2	144.8	435			
	4	142.3	142.1	458			
	5	142.7	144	451			
37%Swaged @900°C	1	146.2	148.6	427	423	5	5
	2	147.9	148.5	422			
	3	147.3	150.6	418			
	4	149.2	148.8	418			
	5	146	147.8	430			
37%Swaged @1400°C	1	172.7	178.3	301	303	2	2
	2	174.9	176.7	301			
	3	172.8	175.8	305			
	4	173.2	175.5	305			
	5	174.9	176.7	301			
70%Swaged (Not Heat Treated)	1	140.7	144	457	461	5	6
	2	142.4	139.7	466			

	3	146.3	139.1	455			
	4	142.7	139.1	467			
	5	142.2	142.2	458			
70%Swaged @500°C	1	137.4	133.5	505	503	6	7
	2	134.1	136.1	508			
	3	136	139	490			
	4	136.6	139	508			
	5	133.4	137.4	506			
70%Swaged @900°C	1	139.7	148.7	446	439	9	10
	2	143.8	148.9	433			
	3	145.5	140.5	453			
	4	149.6	144.2	430			
	5	143.8	14.9	433			
70%Swaged @1400°C	1	175.3	171.4	308	307	7	8
	2	174.3	175.4	303			
	3	177.7	173.1	301			
	4	173.6	166.9	320			
	5	174.3	175.4	303			
91%Swaged (Not Heat Treated)	1	134	46.7	471	484	12	13
	2	135.6	140.8	485			
	3	138.3	135.7	494			
	4	140.5	140.5	470			
	5	136	136.7	499			
91%Swaged @500°C	1	138.3	134	500	508	5	6
	2	137.2	132.7	509			
	3	134.6	136	506			
	4	134.3	135.2	511			
	5	131.9	136.3	515			
91%Swaged @900°C	1	139.1	137.8	484	489	12	14
	2	138.8	134.6	496			
	3	138	142.5	471			
	4	137.1	139.3	485			
	5	132.2	137.9	508			
91%Swaged @1400°C	1	169.3	169.9	322	320	4	5
	2	171.2	171.7	315			
	3	169.9	168.1	325			
	4	167.4	171.2	323			
	5	171.2	171.7	315			
96%Swaged (Not Heat Treated)	1	133.1	140.2	496	476	12	13
	2	136	145.8	467			
	3	136.3	140.7	483			
	4	138.5	143.3	467			
	5	136	145.8	467			
96%Swaged @500°C	1	130.3	133.1	534	553	12	13
	2	125.1	132.5	559			
	3	123.5	132.3	567			
	4	133.7	127.1	545			
	5	128.6	129	559			

96%Swaged @900°C	1	135.8	136.9	499	494	2	3
	2	132.4	141.2	495			
	3	133.3	141.2	492			
	4	133.4	140.5	494			
96%Swaged @1400°C	1	167.7	167.3	330	334	4	5
	2	164.8	167.9	335			
	3	163.7	165.4	342			
	4	167.7	167.3	330			
	5	164.8	167.9	335			

Table 5.8. Micro hardness values for 90W-7Ni-3Fe alloy.

Condition	Micro hardness Values (H_v)	
	W-Particle	Matrix
As-received (Not Heat Treated)	358	270
As-received@500°C	402	263
As-received@900°C	370	295
As-received@1400°C	402	263
37%Swaged (Not Heat Treated)	559	394
37%Swaged@500°C	472	369
37%Swaged@900°C	461	343
37%Swaged@1400°C	235	299
70%Swaged (Not Heat Treated)	460	420
70%Swaged@500°C	410	360
70%Swaged@900°C	370	354
70%Swaged@1400°C	305	320

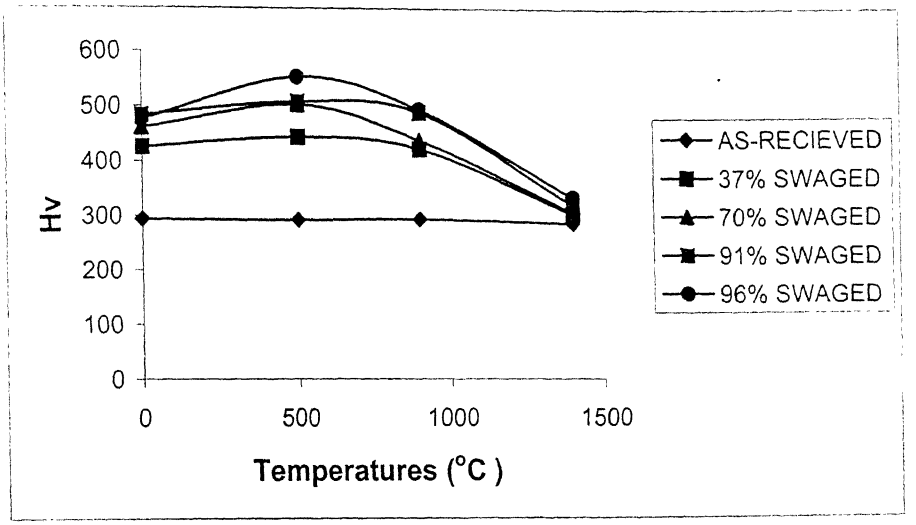

Figure 5.34. Shows the macro hardness 90W-7Ni-3Fe alloy with heat treatment temperatures.

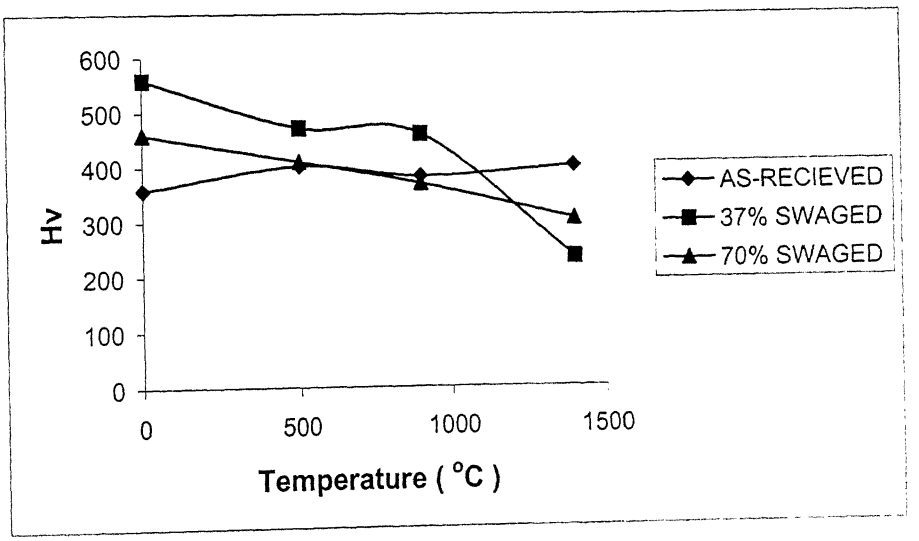

Figure 5.35. Micro hardness variation of tungsten particle with heat treatment temperatures.

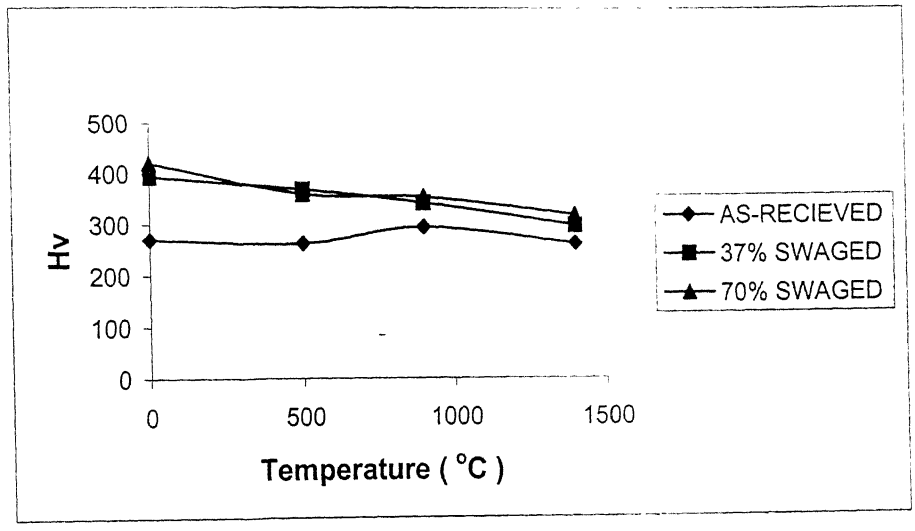

Figure 5.36. Micro hardness variation of Matrix with heat treatment temperatures.

Chapter 6

DISCUSSION

6.1 Quantitative Analysis of Microstructures

As we know the liquid phase sintering is the best method for consolidation of the tungsten heavy alloys in order to achieve high density and high strength. As we can see in Figure 5.1 that the microstructure contain rounded tungsten grain embedded in Ni-Fe-W matrix for 90W-7Ni-3Fe alloys. Considering the same field of view, as we go on increasing the amount of tungsten content from 90 to 97wt% W, the volume fraction of tungsten particle increases gradually (Figure 5.26). As because these alloys are liquid phase sintered, they contains small amount of residual porosity in the sintered microstructures, which is clearly seen in the as-received micrographs of 90W-7Ni-3Fe alloys. On room temperature swaging the tungsten grains become elongated in longitudinal directions. Figures 5.4 and 5.5 shows the micrographs of 37% swaged and 70% swaged sample. In 70% swaged sample the tungsten grains are more elongated and the elongated grains are impinged on one another but when the deformation levels are increased the tungsten grains as well as matrix become more and more elongated and there by creating space for matrix to entrap into elongated tungsten grains. Finally the microstructures result in to fibrous structures, as can be seen in case of 91 and 96% reduced samples (Figures 5.6 and 5.7).

In this research the 90W-7Ni-3Fe alloys have been heat-treated to 500, 900, 1400°C. When the as-received samples are heat-treated from 500°C to 1400°C the size of tungsten grains increases, which means that at high temperatures coarser grains are formed for as –received samples. This is driven by the phenomenon known as Ostwald-ripening. The similar case of grain growth have been observed for 37, 70, 91, 96% reduced heat-treated samples. The analysis of microstructures for as-received, 37% and 70% swaged samples have been discussed in detail in quantitative analysis of S_v measurements.

6.2 Analysis of Surface area per unit volume (S_v) of W-Matrix Interface

Figures 5.23 to5.25 describes about the variation of S_v for W-Matrix interface with respect to orientation of test lines for as received, 37% swaged and 70% swaged samples. It is clear that in all the cases the S_v increases with increase in heat treatment temperatures. From Figure 5.23 it is seen that the S_v for W-matrix interface is constant with the orientation of test lines. This means that W-matrix interfaces are iso-tropically oriented (or the W-grains are equiaxed). The absolute value of S_v is seemed to be decreasing when heat-treated at 500°C and keeps on decreasing as we go to 900 and 1400°C. This implies that the W-grains are increasing in size (coarsening). This is expected due to the thermodynamic driving force requiring decreasing the interfacial surface area. This is driven by the phenomenon known as Ostwald ripening. As S_v increases the number of tungsten grains is expected to decrease because of same volume fraction of tungsten content, though this was not measured in this study. This also implies that the phenomenon of precipitation of tungsten when cooled from high temperatures is not pre-dominant, because that would result in a fine W-grain size and higher S_v (which is not seen).

Figures 5.24 and 5.25 reveals that on swaging the samples, the tungsten grains get elongated along the swaging direction. This results in higher fraction of surfaces parallel to direction of swaging. This is seen as an increase in intersection (P_L) count of the test lines at higher angles (the S_v is seem to increase with angle of orientation both in Figures 5.24 and 5.25). The absolute increase in Sv with angle of orientation is more for 70% swaged samples as compared to 37%, which means that the tungsten grain in 70% swaged samples, are more elongated.

The general trend of variation of S_v with temperature of heat treatment for 37% and 70% swaged samples could not be established, because of scattered in the data. It would be expected that S_v should decrease with increase in temperature of heat treatment, unless precipitation during cooling is pre-dominant. It is yet to be established that the scattered in the data is due to lack of sampling or because of the phenomenon of reprecipitation during cooling. More detailed stereological results are yet to be determined.

6.3 Macro hardness Measurements

For as-received samples hardness does not varies that much (showing the curve almost flat) with heat treatment temperatures. This can be explained on the basis of the fact that as-received samples are not subjected to any types of deformations. So whatever hardness change occurs they are generally due to change in grain shape. It is seen that the 96% and 91% swaged samples have almost same hardness and is the highest hardness achieved among all the samples in not heat-treated condition. It is attributed to the fact that when the alloys are subjected to room temperature swaging the plastic deformation produces an increase in number of dislocations, which is by virtue of their interaction results in a higher state of internal stress. As the deformation proceeds cross-slip takes place and multiplication process operate. As a result of which the cold worked structure forms high dislocation density regions or tangles, which soon develop into tangled networks. So as we go on increasing reduction in area the W-grains become more and more elongated and 96% reduced sample produces fibrous microstructures with high strain hardening having high hardness value, but when the samples are heat treated at 500, 900, 1400°C the thermodynamic driving force requiring to decrease interfacial surface area causes an increase in tungsten grain i.e. coarsening. Also on increasing temperature it lowers the strain hardening by dislocation rearrangement, there by releasing dislocation pileups. So hardness decreases as we go on increasing the heat treatment temperatures for swaged samples. It is also expected that swaging also causes decrease in the amount of W-W grain boundary de cohesion as the grains work harden.

6.4 Micro-hardness Measurements

In micro hardness measurement curves the hardness of W-particle for as-received sample does not show much variation with heat treatment temperatures. 37% swaged sample shows higher W-particle hardness, as compared to 70% swaged samples in not heat-treated condition (Figure 5.35). As we know hardness depends upon the resistance to plastic deformation of material. So at 37% the resistance to plastic deformation of W particle is more. Also at 70% the tungsten grains are more elongated as compared to 37% swaged sample. So we can say that the highly elongated grain could not with stand properly to the load of indentation, there by causing low hardness in 70% swaged sample. On the other hand when the swaged

samples are heat-treated the W-particle hardness decreases due to grain coarsening at higher temperatures and lowering of strain hardening by dislocation rearrangements. The general trends of variation of hardness of tungsten particle with heat treatment temperatures for as-received samples could not be established because of the scattered in the data. It would be expected that hardness of tungsten particle should decrease with heat treatment temperatures due to grain coarsening. But the graph shows that at 1400°C there is an increase in hardness of tungsten particle, which may be due to precipitation of tungsten grains when cooled from higher temperatures.

Micro hardness measurements of matrix for 37% and 70% swaged sample shows a decreasing trend with heat treatment temperatures. The reason for this is same as described for W-particle micro hardness measurements.

6.5 Contiguity and Grain Size Measurements

Contiguity graph (Figure 5.30) shows that on swaging from 0% to 37% there is an increase in contiguity in longitudinal direction in not heat-treated condition. A possible explanation for this behavior is that this increase in W-W grain boundary contact area in longitudinal direction occurs due to the fact that as the tungsten grains are deformed into an ellipsoidal shape they are forced together and increasingly impinge on one another. As a result of which the contiguity increases due to increase in W-W contact area. On the other hand 70% swaged sample shows lower contiguity as compared to 37% swaged sample. As discussed earlier when the amount of deformation is increased further the tungsten grains cannot sustain all the applied deformations and hence the matrix phase begins to deform and is forced into the gaps between tungsten grain producing very thin ribbons of matrix between the grains. This cause a decrease in contiguity for 70% swaged sample in longitudinal direction.

Contiguity variation with heat treatment temperatures has also been discussed in this work. Contiguity of as received sample is more at 500 and 900°C, as compared to 37% and 70% swaged samples. This means that there may be precipitation of tungsten grain in case of as-received samples when cooled from high temperatures resulting finer W grains. But this can not be confirmed, because at 1400°C the contiguity decreases drastically even below the 37% swaged samples. The reason for this is yet to be established. When the samples are heat-treated the contiguity

decreases. The explanation for this behavior is that on increasing temperature the grain size increases forming bigger grains, there by decreasing the W-W contact area and this phenomenon is basically driven by Ostwald ripening. The graph also shows that the contiguity variation for 70% swaged sample is not that much as compared to as-received and 37% swaged sample. As we know at high deformations like 70% some of the matrix phase have been forced into the gap between W-grains. So on heat-treating the material at temperatures like 500, 900°C the growth of tungsten grain is some what hindered by entrapped matrix. There by causing less variation in contiguity of W grains with heat treatment temperatures for 70% swaged sample.

In this research contiguity variation with respect to orientation of test lines at an angle difference of 22.5° have been analyzed. The 37% swaged sample shows higher contiguity at 500°C as compared to 900 and 1400°C. This means at 500°C the grains are smaller as compared to 900 and 1400°C, which results into an increase in W-W contact area. But the graph for as-received and 37% swaged sample show a complete random variation of contiguity with respect to orientations. It would be expected that the contiguity should decrease with respect to orientations and increase in heat treatment temperatures (which is not seen). The general trend of variation of contiguity with orientation of test line could not be established because of scattered in the data.

In this research grain size variation have been analyzed by taking three test lines in order to achieve the best result with less amount of error. A series of grain size data have been shown with reference to heat treatment temperatures. As-received samples show an increase in grain size at 900°C and keeps on increasing up to 1400°C. But the exact trend of increase in grain size for as-received sample could not be established. This may be due to high % of error in measurement of P_L count (points per unit length) while measuring *Sv*. As grain size varies inversely with *Sv*. For 37 and 70% swaged sample the data shows an increasing trend with temperatures for a concerned test line. This implies that grain size is increasing with increase in heat treatment temperatures. From *Sv* data analysis it has been predicted that the absolute value of *Sv* is more for 37% swaged sample as compared to 70% swaged sample taking 0° orientation. So from this result it is obvious that the grain size for 70% swaged sample is more as compared to 37%, which has been shown in the graph (Figure 5.29)

Chapter 7

CONCLUSIONS

Considering results and discussions of the present investigation, the following conclusions can be drawn:

1. A new processing route has been developed for production of fibrous microstructures in 90W-7Ni-3Fe alloys.
2. This is the first time ever in research that by selecting proper composition in W-Ni-Fe alloys, a deformation level of 96% has been achieved.
3. V_v (volume fraction) of tungsten particle increases with increase in amount tungsten content.
4. Contiguity decreases with increase in heat treatment temperatures from 500 to 1400°C.
5. Average grain size increases for as-received sample with heat treatment temperatures.
6. In not heat-treated condition macro hardness of alloy increases with amount of deformation through room temperature swaging achieving highest hardness at 91% reductions.
7. Macro hardness decreases with heat treatment temperatures.
8. In micro hardness measurements the hardness of W particle is more for 37% swaged sample as compared to 70% swaged sample.
9. Micro hardness of W particle as well as matrix decreases with increase in heat treatment temperatures.
10. Total S_v (surface area per unit volume of W-matrix interface) increases with angle of orientation of test lines.
11. Total S_v decreases with increase in temperatures.
12. S_v is constant with orientation of test lines for not swaged samples.
13. The absolute increase in S_v with angle of orientation is more for 70% swaged sample as compared to 37% swaged sample.

REFERENCES

1. S. G. Caldwell, "Tungsten Heavy Alloys," ASM Hand Book, P.W. Lee and R. Lacocca (eds.), Powder Metal Technologies and Applications, Materials Park, Ohio, USA, 1998, v. 7, pp. 914 –921.
2. I. Massalski, T.B., "Binary Alloy Phase Diagrams," ASM International, Materials Park, Ohio, USA, 1990.
3. G.V. Raynor and V.G. Rivlin, "Phase Equilibria in Iron Ternary Alloys," Institute of Metals, London, n. 4, 1988.
4. S.G. Caldwell, "Variation of Ni to Fe Ratio in W-Ni-Fe Alloys: A current Perspective," Tungsten and Tungsten Alloys –1992, A. Bose and R.J. Dowding (eds.), Metal Powder Industries Federation, NJ, USA, 1992, PP. 89-96.
5. J.R. Spencer, "The Effect of Nickel:Iron Ratios on the mechanical properties, Microstructure and Processing of W-Ni-Fe Alloys," Tungsten and Tungsten Alloys –1992, A. Bose and R.J. Dowding (eds.), Metal Powder Industries Federation, NJ, USA, 1992, PP. 111-117.
6. E. Lassner and W.D. Schubert, Tungsten, Plenum Publishers, New York, NY, USA, 1999.
7. G.S. Upadhyaya, Powder Metallurgy Technology, Cambridge International Science Publishing, Cambridge, UK, 1999.
8. E. Klar, Powder Metallurgy:Applications, Advantages and Limitations, American Society of Metals, Metals Park, OH, USA, 1983.
9. D.J. Williams, S. Clyens, and W. Johnson, "Production of Tungsten-Iron-Nickel Alloys by Mechanical Alloying Technique," *Powder Metallurgy*, 1980, n. 2, pp. 92-94.
10. J.S. Hirschhorn, "Sintering," Introduction to Powder Metallurgy, American Powder Metallurgy Institute, Princeton, NJ, USA, pp. 155-244.
11. W.D. Jones, Fundamental Principles of Powder Metallurgy, Edward Arnold Ltd, London, England, 1960.

12. R.M. German, Sintering Theory and Practice, John Wiley & Sons, New York, NY, USA, 1998.

13. R.M. German, "Sintering," Powder Metallurgy Science, Metal Powder Industries Federation, Princeton, NJ, USA, 1994, pp. 241-296.

14. A. Upadhyaya, "Processing Strategy for Consolidating Tungsten Heavy Alloys for Ordnance Application," *Materials Chemistry and Physics*, 2001, n. 67, pp.101-110.

15. L.L. Bourguignon and R.M German, "Sintering Temperature Effects on a Tungsten Heavy Alloy," *The International Journal of Powder Metallurgy*, 1988, v. 2, n. 2, pp. 115-121.

16. R.M German, A. Bose and S.S. Mani, "Sintering time and Atmosphere influences on the Microstructure and Mechanical Properties of Tungsten Heavy Alloy," *Metallurgical Transaction A*, 1992, v. 23, pp. 211-219.

17. K.S. Churn and R.M. German, "Fracture Behavior of W-Ni-Fe Heavy Alloys," *Metallurgical Transactions A*, 1984, v. 15, pp. 331-338.

18. R.M. German and K.S. Churn, "Sintering Atmosphere Effects on the Ductility of W-Ni-Fe Heavy Metals," *Metallurgical Transaction A*, 1984, v. 15, pp. 747-754.

19. C. Lea, B.C. Muddle and D.V. Edmonds, "Segregation to Inter Phase Boundaries in Liquid Phase Sintered Tungsten Alloys," *Metallurgical Transaction*, 1983, v. 14, pp. 667-677.

20. T. Kohno and O. Mayama, "Effects of Sintering and Post Sintering Heat treatment on the Mechanical Properties of W-Ni-Fe Heavy Alloys," International Conference on Powder Metallurgy, Institute of Metals, London, 1990, v. 1, pp. 324-331.

21. S.P Doepker, J.A. Mullendore and J.R. Spencer, "A Comparison of W- Ni-Fe and W-Ni-Co Alloys," Tungsten and Tungsten Alloys –1992, A. Bose and R.J. Dowding (eds.), Metal Powder Industries Federation, Princeton, NJ, USA, 1992, pp. 273-281.

22. V. Srikanth and G.S. Upadhyaya, "Effect of Cold Work and Annealing on the Mechanical Properties of 90W-7Ni-3Fe Heavy Alloy," *Journal of Materials Science Letters*, 1988, v. 7, pp. 195-197.

23. H.K. Yoon, S.H. Lee, S.J.L. Kang, D.N. Yoon, "Effect of Vacuum Treatment on Mechanical Properties of W-Ni-Fe Heavy Alloy," *Journal of Materials Science*, 1983, v. 18, pp. 1374-1380.

24. Y.V. Milman, "The Influence of Thermo-Plastic Deformation on the Structure and Mechanical Properties of Powder Metallurgy Materials," Advanced Science and Technology of Sintering, Stojanovic *et al* (eds.), Plenum Publisher, New York, 1999.

25. M.C. Hogwood and A.R. Bentley, "The Development of High Strength and Toughness Fibrous Microstructures in Tungsten-Nickel-Iron Alloys for Kinetic Energy Penetrator Application," Tungsten and Refractory Metals, A. Bose and R.J. Dowding (eds.), Defence Research Agency, Kent, England, 1994, pp. 37-45.

26. M. Mitkov and W. A. Kaysser, "Influence of Sintering and Thermo-mechanical Treatment on Microstructure and Properties of W-Ni-Fe Alloys," Modern Developments in Powder Metallurgy, 1985

27. G.R. Goren-Muginstein and A. Rosen, "Recrystallization of Heavy Metals After Cold Deformation," Tungsten and Refractory Metals, A. Bose and R.J. Dowding (eds.), Metal Powder industries Federation, Princeton, NJ, USA, 1995, pp. 193-200.

28. W. Leonard and L. Magness jr, "Improving Mechanical properties of Tungsten Heavy Alloy Composites through Thermo-Mechanical Processing," Tungsten and Tungsten Alloys -1992, A. Bose and R.J. Dowding (eds.), Metal Powder Industries Federation, Princeton, NJ, 1992, pp. 127-135.

29. M.H Hong, S. Lee, J.N. Noh and Y.W. Kim, "The Effect of Thermo-Mechanical Treatment on the Microstructure and Failure Behavior of Sintered Tungsten Heavy Alloy," Advances in Powder Metallurgy and Particulate Materials-1994, A. Lawley and A. Swanson (eds.), Metal Powder Industries Federation, Princeton, NJ, USA, 1994, v. 5, pp. 279-288.

30. A.R. Bentley and M.C. Hogood, "The Effect of Mechanical Deformation and Heat-Treatment on the Microstructure Characteristics of Two Tungsten Alloy," Tungsten and Tungsten Alloys –1992, A. Bose and R.J. Dowding (eds.), Metal Powder Industries Federation, NJ, USA, 1992, PP. 419-431.

31. K.O. Zamora, J.G. Sevillano and M.F. Perez, "Flow Stress and Ductility of Tungsten Heavy Metal Alloys," Tungsten and Tungsten Alloys –1992, A. Bose and R.J. Dowding (eds.), Metal Powder Industries Federation, Princeton, NJ, 1992, PP. 281-288.

32. A. Bose, J. Lankford jr and H. Couque, "Dynamic Compressive Properties of Tungsten Heavy Alloys with varying Grain Sizes," Advances in Powder Metallurgy and Particulate Materials –1994, A. Lawley and A. Swanson (eds.), Metal Powder Industries Federation, Princeton, NJ, USA, 1994, v. 4, pp. 227-238.

33. R.C. Woodward, N.J. Baldwin, I. Burch and B. Baxter, "Effect of Strain Rate on the Flow Stress of Three Liquid Phase Sintered Tungsten Alloys," *Metallurgical Transactions A*, 1985, v. 11, n. 11, pp. 2031-2037.

34. M.C. Hogwood and A.R. Benteley, "The Behaviour of a Tungsten-Nickel-Iron Alloy Over a Range of Strain Rates," Tungsten and Tungsten Alloys – 1992, A. Bose and R.J. Dowding (eds.), Metal Powder Industries Federation, NJ, USA, 1992, PP. 325-334.

35. K.T. Ramesh, S. Yadav and J.A. Davis, "Shear Localization in a Tungsten Heavy Alloy," Tungsten and Tungsten Alloys-1992, A. Bose and R.J. Dowding (eds.), Metal Powder Industries Federation, NJ, USA, 1992, PP. 299-306.

36. A. Bose, D. Sims and R.M. German, "Test Temperature and Strain Rate Effects on the Properties of a Tungsten Heavy Alloy," *Metallurgical Transaction A*, 1988, v. 19, pp. 487-494.

37. M. Zohu, R.J. Clifton and A. Needleman, "Shear Band Formation in a W-Ni-Fe Alloy under Plate Impact," Tungsten and Tungsten Alloys-1992, A. Bose and R.J. Dowding (eds.), Metal Powder Industries Federation, NJ, USA, 1992, PP. 343-350.

38. V. Srikanth and G.S. Upadhyaya, "Contiguity Variation in Tungsten Spheroids of Sintered Heavy Alloys," *Metallography*, 1986, v. 19, pp. 437-445.

39. E.E. Underwood, Quantitative Stereology, Addison-Wesley, London, UK, 1970.

40. T. Weerasooriya and P.A. Beaulieu, "Deformation and Failure Behaviour of 93W-5Ni-2Fe at Different Shear Strain Rate Loading," Tungsten and Tungsten Alloys-1992, A. Bose and R.J. Dowding (eds.), Metal Powder Industries Federation, NJ, USA, 1992, PP. 317-324.